# FERMI EDGE POLARITONS FORMED BY ELECTRON-HOLE PAIRS INTERACTING WITH CAVITY-CONFINED PHOTONS

YOSSI MICHAELI

Master of Science in Physics

Physics

Physics

Technion - Israel Institute of Technology

March 2009

Yossi Michaeli: *Fermi edge polaritons formed by electron-hole pairs interacting with cavity-confined photons,* Master of Science in Physics, © March 2009

ABSTRACT

Short summary of the contents in English...

*We have seen that computer programming is an art,*
*because it applies accumulated knowledge to the world,*
*because it requires skill and ingenuity, and especially*
*because it produces objects of beauty.*

— **?** [**?** ]

# ACKNOWLEDGMENTS

Put your acknowledgments here.

# CONTENTS

# LIST OF TABLES

# 1 INTRODUCTION

# Part I

# THEORY REVIEW

# 2 ELECTRONIC PROPERTIES OF SEMICONDUCTORS

The optical properties of nanostructures are intimately connected to the electronic states, the response of electrons within the atomic lattice to external perturbations. As such, a precise knowledge of the electronic properties is required for a proper device analysis. In bulk semiconductors, the lattice periodicity and its symmetry leads to the formation of electronic bands, continuously (within the band) relating the crystal momentum$\mathbf{k}$ of an electron to its energy $E_n(\mathbf{k})$. The combination of different materials within a nanostructure breaks the symmetry of the semiconductor crystal, leading to *quantization effects*, i.e. modifications of the electronic properties from their bulk properties. These modifications have a pronounced impact on the electronic and optical properties of nanostructures. The present chapter covers the theory of the calculation of the electronic states in nanostructures using the *envelope function method* (EFM).

The first section contains an extensive introduction to the Schrödinger equation within a semiconductor crystal, which will later also serve as the basis for the analysis of optical effects covered in Chapter 3 and the many body effects in optical spectra in Chapter 4.

After introducing certain approximations to the crystal Schrödinger equation, the concept of solving the resulting single-particle Schrödinger equation using the bulk $\mathbf{k}\cdot\mathbf{p}$ method is presented. The subsequent section derives the equations of the $\mathbf{k}\cdot\mathbf{p}$ envelope function method used in nanostructures and simultaneously introduces the $\mathbf{k}\cdot\mathbf{p}$ model for zinc-blende crystals, with an emphasis on the two-band model . Note that the presented discusion doesn't include the influance of strain effects on the electronic properties.

Finally, we present the Schrödinger-Poisson model of the electronic bands structure where the electrostatics of the system of relevance.

## 2.1 CRYSTAL SCHRÖDINGER EQUATION

### 2.1.1 *Introduction*

The total Hamiltonian of all electrons, atoms and the electro-magnetic field of a solid state crystal is given by

$$H = \sum_i \frac{1}{2m_i}\left(\mathbf{p}_i - ez_i\mathbf{A}(\mathbf{r}_i)\right)^2 + \frac{\epsilon_0}{2}\int\left(\mathbf{E}^2 + c_0^2\mathbf{B}^2\right)d\mathbf{r} \tag{2.1}$$

In the second term $\mathbf{E}$ denotes the electric- and $\mathbf{B}$ the magnetic field. These fields are related to the vector potential $\mathbf{A}$ and the scalar potential $\phi$ via Jackson [30]

$$\mathbf{E} = -\frac{\partial\mathbf{A}}{\partial t} - \nabla\phi \tag{2.2}$$

$$\mathbf{B} = \nabla\times\mathbf{A}. \tag{2.3}$$

In the first term of 2.1, $e$ is the elementrary charge, $z_i$ is the charge of particle $i$ in units of $e$ (-1 for electrons) and $m_i$ denotes the particle

mass. The term $\mathbf{p}_i - ez_i\mathbf{A}(\mathbf{r}_i)$ is the mechanical momentum of particle $i$, which is invariant to our gauge choise (see below) for $\mathbf{A}$ and $\phi$. The electrical field term $\mathbf{A}^2$ holds both transverse and longitudinal contributions. In the following discussion we assume a Coulomb gauge for the vector potential, i.e. $\nabla \cdot \mathbf{A} = 0$ Jackson [30]. In this gauge the term $\frac{\partial \mathbf{A}}{\partial t}\nabla\phi$ in $\mathbf{E}^2$ vanishes, and so we can split this term to the transverse and longitudinal contributions $\mathbf{E}^2 = \mathbf{E}_l^2 + \mathbf{E}_t^2$. Using Poisson's equation, the longitudinal contribution can be written in terms of the charge density

$$\int \mathbf{E}_l^2 d\mathbf{r} = \int (\nabla\phi)^2 \, d\mathbf{r} = \langle \phi \nabla\phi \rangle - \int \phi \nabla^2 \phi d\mathbf{r} = \int \phi \frac{\rho}{\epsilon_0} d\mathbf{r}. \tag{2.4}$$

Next, the contributions to $\phi$ are distinguished between internal $\phi_{int}$ and external $\phi_{ext}$, where the internal contributions are created by the crystal electrons and atomic cores. The internal contributions are given by the longitudinal Coulomb interaction between the charged particles $i$ and $j$

$$V_{i,j} = \frac{e^2 z_i z_j}{4\pi\epsilon_0 |\mathbf{r}_i - \mathbf{r}_j|}, \tag{2.5}$$

with unit charges $z_i$ and $z_j$. The external contribution are

$$V_{ext} = \sum_i z_i e \phi_{ext}(\mathbf{r}_i). \tag{2.6}$$

The crystal Hamiltonian for electrons $i, j$ and atoms $I, J$ then reads

$$\begin{aligned} H &= \underbrace{\sum_i \frac{(\mathbf{p}_i + e\mathbf{A})^2}{2m_0}}_{T_e} + \underbrace{\sum_I \frac{(\mathbf{p}_I + ez_I\mathbf{A})^2}{2m_I}}_{T_a} + \underbrace{\frac{1}{2}\sum_{i,j} \frac{e^2}{4\pi\epsilon_0 |\mathbf{r}_i - \mathbf{r}_j|}}_{V_{ee}} \\ &+ \underbrace{\frac{1}{2}\sum_{I,J} \frac{e^2 z_I z_J}{4\pi\epsilon_0 |\mathbf{r}_I - \mathbf{r}_J|}}_{V_{aa}} - \underbrace{\frac{1}{2}\sum_{i,J} \frac{e^2 z_J}{4\pi\epsilon_0 |\mathbf{r}_i - \mathbf{r}_J|}}_{V_{ea}} + V_{ext} \\ &+ \underbrace{\frac{\epsilon_0}{2}\int \left(\mathbf{E}_t^2 + c_0 \mathbf{B}^2\right) d\mathbf{r}}_{H_{EM}}, \end{aligned} \tag{2.7}$$

where $T$ is the kinetic energy part of the Hamiltonian, and $V$ the potential energy one. As the atoms have a much higher mass than the electrons, the Born-Oppenheimer approximation Yu and Cardona [47] can be used to separate the motion of electrons and atoms. The electrons will react on movements of the atoms instantaneously. Therefore, the interaction between ion cores and between electrons and ion cores can be concentrated into a potential $U(\mathbf{x})$, leading to the final crystal electron Hamiltonian

$$\begin{aligned} H &= \sum_i \left( \frac{(\mathbf{p}_i + e\mathbf{A}(\mathbf{r}_i))^2}{2m_0} + U(\mathbf{r}_i) \right) \\ &+ \frac{1}{2}\sum_{i,j} \frac{e^2}{4\pi\epsilon_0 |\mathbf{r}_i - \mathbf{r}_j|} + V_{ext} + H_{EM}. \end{aligned} \tag{2.8}$$

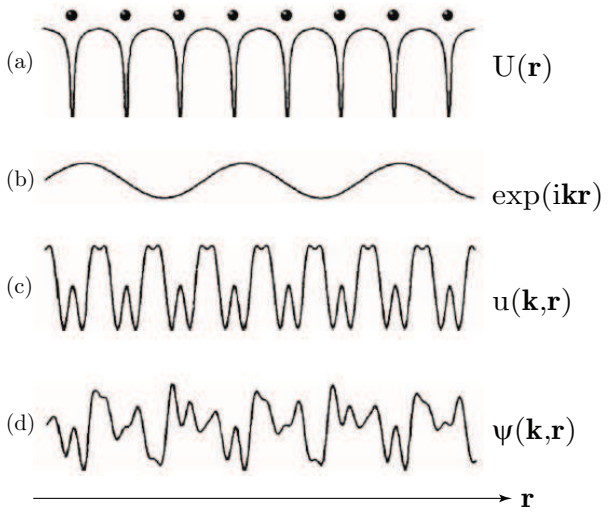


Figure 1: Schematic representation of electronic functions in a crystal (a) potential plotted along a row of atoms, (b) free electron wave function, (c) amplitude factor of Bloch function having the periodicity of the lattice, and (d) Bloch function $\psi$ (after Piprek [42])

The next step is to perform the *single electron approximation* or *mean field approximation* by assuming that the electron-electron interaction $V_{ee}$ with the core- and valence electrons can also be concentrated into the potential $U(\mathbf{r})$. This step is necessary as solving the equation for $10^{23}$ explicitly considered electrons is an impossible task. The equation reduces to a single electron equation, where an electron experiences the mean-field potential $U(\mathbf{r})$. Within this step, the vector potential $\mathbf{A}$ is restricted to external excitations, where the local oscillations within the crystal lattice are averaged out. Overall, the effect of the external electromagnetic field on the atoms has been excluded. This approximation is usually justified in the case of weak fields and heavy atomic masses. The interaction between electrons and atoms is restricted to a frozen lattice. The interaction between the movement of the atoms and the electrons can be reintroduced using *phonons* Yu and Cardona [47], but this will be omitted throughout the thesis.

### 2.1.2 *Bloch's Theorem*

Assuming no external field, the time independent single electron Schrödinger equation to solve is given by

$$\left(-\frac{\hbar^2}{2m_0}\nabla^2 + U(\mathbf{r})\right)\psi = E\psi. \tag{2.9}$$

For the moment, the crystal is assumed to be homogeneous and perfect. The potential $U(\mathbf{r})$ is periodic within the lattice (see Figure 1). For any translation vector $\mathbf{R}$ mapping the infinite crystal lattice to itself, the potential obeys

$$U(\mathbf{r}) = U(\mathbf{r}+\mathbf{R}) \tag{2.10}$$

and the wavefunction $\psi_{n\mathbf{k}}$ can be expressed in the form known as *Bloch function*

$$\psi_{n\mathbf{k}} = u_{n\mathbf{k}}(\mathbf{r})e^{i\mathbf{k}\cdot\mathbf{r}}, \tag{2.11}$$

where $u_{n\mathbf{k}}(\mathbf{r})$ denotes the lattice periodic path with

$$u_{n\mathbf{k}}(\mathbf{r}) = u_{n\mathbf{k}}(\mathbf{r}+\mathbf{R}) \tag{2.12}$$

and the plane wave is the slowly modulating envelope. The $n\mathbf{k}$ are the quantum numbers indexing the solutions. Applying the differential operators to the plane wave and multiplying the equation on both sides from the left with $e^{=i\mathbf{k}\cdot\mathbf{r}}$ gives the equation for the lattice periodic functions as

$$\begin{aligned} H_{\mathbf{k}\cdot\mathbf{p}}(\mathbf{k})u_{n\mathbf{k}}(\mathbf{r}) &= \left(-\frac{\hbar^2}{2m_0}\nabla^2 + \frac{\hbar}{m_0}\mathbf{k}\cdot\mathbf{p} + \frac{\hbar^2k^2}{2m_0} + U(\mathbf{r})\right) u_{n\mathbf{k}}(\mathbf{r}) \\ &= E_n(\mathbf{k})u_{n\mathbf{k}}(\mathbf{r}). \end{aligned} \tag{2.13}$$

An important consequence of the Bloch theorem is the fact that wavefunctions with different $\mathbf{k}$ values are not coupled together (due to the slowly varying plane wave) and therefore 2.13 has a parametric dependence on the crystal momentum $\mathbf{k}$.

### 2.1.3 *The* $\mathbf{k}\cdot\mathbf{p}$ *Method*

#### 2.1.3.1 *Introduction*

There is a vast number of methods to obtain solutions to Eq. 2.13. One of the most frequently used is the semi-empirical $\mathbf{k}\cdot\mathbf{p}$ method that serves to derive analytical expressions for the band structure, using symmetry arguments and experimental observations. The method was initially introduced by Bardeen and Seitz (see references in Chuang [19]) and applied by many researchers. It is particularly useful to describe the band structure for direct semiconductors used in optoelectronic devices at the $\Gamma$ point of the Brillouin zone with a high precision.

Hereafter a short introduction of the general concepts will be given. These concepts will later reappear within the Envelope Fucntion Methods (EFM). This introduction is mainly based on Yu and Cardona [47].

The basic idea within the $\mathbf{k}\cdot\mathbf{p}$ theory Kane [32] is to solve 2.13 for an extremal point with high symmetry of the band structure, usually the $\Gamma$ point at $\mathbf{k} = 0$. There, 2.13 reduces to

$$\left(-\frac{\hbar^2}{2m_0}\nabla^2 + U(\mathbf{r})\right) u_{n0}(\mathbf{r}) = E_n(0)u_{n0}(\mathbf{r}). \tag{2.14}$$

The solutions $u_{n0}(\mathbf{r})$ are denoted as *zone-center* functions and span the complete Hilbert space of all solutions to 2.13. Therefore, one may express the lattice periodic functions $u_{n\mathbf{k}}(\mathbf{r})$ away from the $\Gamma$ point in terms of the zone-center functions

$$u_{m\mathbf{k}}(\mathbf{r}) = \sum_{n'} a_{m\mathbf{k},n'}u_{n'0}(\mathbf{r}). \tag{2.15}$$

To obtain the coefficients $a_{\mathbf{mk},n'}$, the expansion 2.15 is inserted into 2.13, multiplied from the left by $u_{n0}(\mathbf{r})$ and integrated over the crystal unit-cell to obtain

$$\sum_{n'} \left( \left( E_{n'}(0) + \frac{\hbar^2 k^2}{2m_0} \right) \delta_{nn'} + \frac{\hbar}{m_0} \mathbf{k} \cdot \mathbf{p}_{nn'} \right) a_{\mathbf{mk},n'} = E_m(\mathbf{k}) a_{\mathbf{mk},n'}, \tag{2.16}$$

where

$$\mathbf{p}_{nn'} = \int u^*_{n0}(\mathbf{r}) \mathbf{p} u_{n'0}(\mathbf{r}) d\mathbf{r} \tag{2.17}$$

is used to express the momentum matrix element between two zone-center Bloch functions. The above equation can obviously be written in matrix form, where a matrix entry is given by

$$h_{ij} = \left( E_j(0) + \frac{\hbar^2 k^2}{2m_0} \right) \delta_{ij} + \frac{\hbar}{m_0} \mathbf{k} \cdot \mathbf{p}_{ij} \tag{2.18}$$

and a diagonalization of the$\mathbf{k}$ dependent, infinite matrix would lead to the exact coefficients and energies $E_m(\mathbf{k})$. As the matrix is continuous in $\mathbf{k}$, is is clear that the dispersion $E_m(\mathbf{k})$ will also be continuous.

As a remark, we can point out that 2.14 is not solved explicitly and no closed expression for $u_{n0}(\mathbf{r})$ is needed. Instead, the matrix 2.18 is constructed by using group theory to derive symmetry properties of the zone-center functions $u_{n0}(\mathbf{r})$. Using these symmetry properties, similarities and equivalences for the momentum matrix elements $\mathbf{p}_{ij}$ can be deduced. A profound introduction into the group theory for semiconductors is beyond the current scope. A rough guideline illustrating the essence required by the $\mathbf{k} \cdot \mathbf{p}$ theory is presented in Appendix C. An extensive presentation can be found in Yu and Cardona [47] and Bir et al. [7].

#### 2.1.3.2 *Löwdin-Renormalization*

While the matrix $h_{ij}$ 2.18 is infinite, leading to an infinite number of bands, the assessment of light emission in optoelectronic devices usually requires only the knowledge of the lowest conduction and highest valence bands. For the relevant III-V semiconductors, the conduction and the valence bands lie at the $\Gamma$ point energetically close together. Other bands can be regarded as being remote, so the interaction in-between these bands can be considered to dominate for the band structure of interest. In the model developed by Kane Kane [31], therefore a submatrix $h_{ij}$ of the conduction- and valence band at the $\Gamma$ point is extracted out of 2.18 and diagonalized. Although the primary interest of Kane's model was to include spinorbit interaction, the missing interaction with remote bands resulted in a heavy-hole band structure, given by the free-electron dispersion, bending for a hole into the wrong direction. Luttinger and Kohn Luttinger and Kohn [38] included the interaction of remote states onto the selected set of bands, using Löwdin's perturbation theory Lowdin [36]. The idea of Löwdin perturbation theory is to divide the bands in two classes S and R (see Fig. 2). Bands in class S are considered explicitly, i.e. the respective rows and columns of the matrix $h_{ij}$ are kept. The bands R are considered being remote and their effect on the bands in class S are included in the

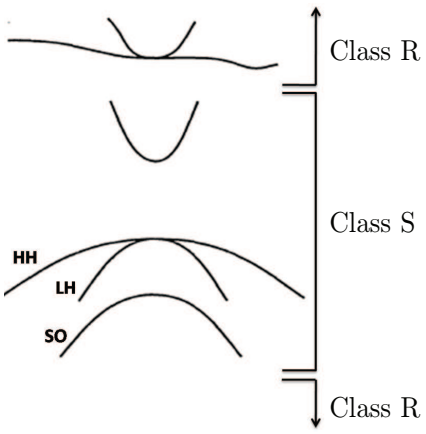


Figure 2: Schematic band structure classification in the Löwdin perturbation theory.

submatrix of $h_{ij}$ using perturbation theory. Hereby, the renormalized matrix elements are given by

$$h'_{ij} = h_{ij} + \sum_{\nu}^{R} \frac{h_{i\nu} h_{\nu j}}{E_i - h_{\nu\nu}}, \tag{2.19}$$

where $i$ and $j$ are in class S and $\nu$ is in R. Group theory and symmetry arguments are then used to derive similarities and vanishing terms and reduce the perturbation expressions to a few constants. By analytically diagonalizing the remaining matrix, the few remaining constants can be determined by comparing analytical dispersion expressions to experimentally determined effective masses. An important note here is that $E_i$ denotes the energy of band $i$ such that the renormalization of the matrix element depends on the result of the eigenvalue calculation, actually requiring self-consistency. In practice, the energies $E_i$ are approximated by the zone-center energy $E_i(0)$, given by the matrix element $h_{ii}$, which is fine close the zone-center. By keeping only one single band in class S, one obtains the single band effective mass dispersion for band $i$ as

$$E_i(0) + \left( \frac{\hbar^2 k^2}{2m_0} + \frac{\hbar}{m_0} \sum_{\nu}^{R} \frac{\mathbf{k} \cdot \mathbf{p}_{s\nu} \mathbf{p}_{\nu s} \cdot \mathbf{k}}{E_i - h_{\nu\nu}} \right) = E_i(0) + \frac{\hbar^2}{2} \mathbf{k}^T \frac{1}{\mathbf{m}^*} \mathbf{k}. \tag{2.20}$$

In the case of several bands within the class S, the resulting matrix can be written, ordered by the dependence on the wavenumber $\mathbf{k}$, as

$$\sum_{i,j=x,y,z} \mathbf{H}^{(2)}_{i,j} k_i k_j + \sum_{i=x,y,z} \mathbf{H}^{(1)}_{i,j} k_i + \mathbf{H}^{(0)}. \tag{2.21}$$

To summarize, the second order terms $\mathbf{H}^{(2)}_{i,j}$ are a result of the combination of the free carrier dispersion and the perturbation treatment of remote states in class R, while first order terms $\mathbf{H}^{(1)}_{i,j}$ stem from the direct treatment of the $\mathbf{k} \cdot \mathbf{p}$ interaction (and later from linear spin-orbit terms), while zero order terms $\mathbf{H}^{(0)}$, contain zone-center energies (and possible terms if the zone-center basis is not orthogonal).

## 2.2 THE $\mathbf{k}\cdot\mathbf{p}$ ENVELOPE FUNCTION METHOD

### 2.2.1 *Introduction*

In previous sections, the crystal was assumed to be homogeneous and infinitely extended. In nanostructures, this assumption is no longer valid and the translational symmetry is broken in certain directions. As a consequence, a carrier might be energetically confined within a lower-bandgap material, but still free to propagate within the translational invariant direction. In the case of a quantum well, the symmetry is broken by the atoms of the other species in one direction, for a quantum wire, it is broken in two directions and for a quantum dot in all three directions. Consequently, the number of translational invariant directions is reduced from two for a quantum well to zero for a quantum dot. As a result, the Bloch function employing the plane wave ansatz has to be modified

$$\varphi_{m\mathbf{k}_t}(\mathbf{r},z) = \sum_n u_n(\mathbf{r},z)e^{i\mathbf{k}_t\cdot\mathbf{r}}F_{n\mathbf{k},m}(z). \tag{2.22}$$

Here, $\mathbf{r}$ denotes the coordinate of translational invariant direction(s), $z$ is the coordinate of the direction(s) where the crystal symmetry is broken and $u_n(\mathbf{r},z)$ is a lattice-periodic function. The crystal momentum $\mathbf{k}$ is only defined within the translational invariant direction. The expression $F_{n\mathbf{k},m}(z)$ is referred to as slowly-varying envelope and denotes at every position in the symmetry broken direction $z$, how the lattice-periodic functions are mixed together. In the bulk crystal, the plane wave term decouples the wavefunctions with different crystal momenta $\mathbf{k}$. In a nanostructure, this decoupling is only true for the translational invariant direction, while in the symmetry broken direction, the states are now mixed together.

As a result of the symmetry breaking, the bands are split into *subbands*, depending on the transversal crystal momentum $\mathbf{k}_t$. The task of the envelope function method is now to select a suitable set of lattice periodic functions $u_n(\mathbf{r},z)$ for 2.22 and derive a proper equation to determine the envelopes $F_{n\mathbf{k},m}(z)$.

### 2.2.2 $\mathbf{k}\cdot\mathbf{p}$ *Envelope Function Ansatz*

The traditional ansatz is to use the zone-center $\mathbf{k}\cdot\mathbf{p}$ lattice periodic functions $u_{n0}(\mathbf{r})$ for the expansion 2.22, together with a set of matching conditions. The equation for the envelopes is obtained by replacing the wave number $k_i$ by the corresponding operator $=i\partial_i$. As in the nanostructure, different materials are involved, the wavefunction is in each material expanded into the materials zone-center functions. The result is that the effective mass like parameters from the perturbation interaction with remote states and the zone-center energies are position dependent. For the single-band effective mass approximation for e.g. the conduction band in a quantum well for $\mathbf{k}_t = 0$, the envelope equation is given by

$$\left(-\frac{\hbar^2}{2m^*(z)}\frac{\partial^2}{\partial z^2} + E_c(z)\right)F_s(z) = E(0)F_s(z). \tag{2.23}$$

$E_c(z)$ denotes the position dependent bulk band edge, corresponding in the direct band gap semiconductors to the conduction band energy at $\Gamma$. Once the eigenvalues $E_m(0)$ and normalized eigenfunctions $F_{s,m}(z)$ (indexed by the subband quantum number $m$) of 2.23 are obtained, the in-plane dispersion is usually approximated using the dominant effective mass of the quantum well material

$$E_m(\mathbf{k}) = E_m(0) + \frac{\hbar^2 k^2}{2m_c^*}. \tag{2.24}$$

The way the equation is written, it is in the presence of a material interface not Hermitian and therefore unexpected imaginary eigenvalues for the energy would result. The usual ad-hoc fix, justified by the requirement of a continuous probability flow, is to rewrite the second order differential operator Chuang [19]

$$-\frac{\hbar^2}{2m^*(z)}\nabla^2 \to -\nabla\frac{\hbar^2}{2m^*(z)}\nabla. \tag{2.25}$$

The particular order of the coefficient and the differential operators is commonly referred to as operator ordering. The form of 2.25 is denoted as Ben-Daniel and Duke ordering BenDaniel and Duke [5], but within the single-band effective mass theory, other orderings are suggested too (see Morrow and Brownstein [41] and references therein). The ordering is irrelevant within bulk materials, but plays a substantial role at a material interface: it is equivalent to the matching conditions for the bulk Bloch functions. In the case of a multi-band equation, where not only one, but several lattice periodic functions are included, one obtains in analogy to 2.25 for all envelopes involved $\mathbf{F}(z) = (F_1(z), F_2(z), ..., F_M(z))^T$ a system of coupled partial differential equations

$$\mathbf{H}_{\mathbf{k}\cdot\mathbf{p}}(z)\mathbf{F}(z) = E\mathbf{F}(z), \tag{2.26}$$

where the $\mathbf{k}\cdot\mathbf{p}$ differential operator is given by

$$\begin{aligned}\mathbf{H}_{\mathbf{k}\cdot\mathbf{p}}(z) \quad = \quad & -\sum_{i,j}\partial_i \mathbf{H}^{(2)}_{i,j}(\mathbf{r};\mathbf{k}_t)\partial_j \\ & +\sum_i \left(\mathbf{H}^{(1)}_{i;L}(\mathbf{r};\mathbf{k}_t)\partial_i + \partial_i \mathbf{H}^{(1)}_{i;R}(\mathbf{r};\mathbf{k}_t)\right) \\ & +\mathbf{H}^{(0)}(\mathbf{r};\mathbf{k}_t).\end{aligned} \tag{2.27}$$

Here the Hermitian operator ordering has already been introduced. The problem is that within the bulk $\mathbf{k}\cdot\mathbf{p}$ Hamiltonian, terms of the type $Nk_ik_j$ with $i \neq j$ can appear, for which the operator ordering is not clear. The usual fix is to split the contribution symmetrically

$$Nk_ik_j \to \partial_i\frac{N}{2}\partial_j - \partial_j\frac{N}{2}\partial_i. \tag{2.28}$$

It can be shown that this particular choice, which is called *symmetrized operator ordering*, may lead to erroneous results. The traditional envelope equations for one and several bands are widely applied and used in a variety of numerical calculations of quantum wells (and superlattices) Altarelli [1], Bastard [3, 4], Eppenga et al. [23], Chuang [18].

Beside its successful application to some material systems, the traditional way of deriving the envelope equations contains several ad hoc fixes, which are required within the presence of material interfaces. The operator ordering is crucial at a material interface, where the material parameters change and therefore the ad-hoc operator ordering involves unknown approximations made to the effect of the interface. In order to analyze the involved approximations, Burt Burt [13, 15, 11, 10] derived the operator ordering 2.25 from the nanostructure's Schrödinger equation and demonstrated that the symmetrization approach for the terms 2.28 in the multi-band envelope equation is incorrect. The derived multi-band Hamiltonian is Hermitian, but not necessarily symmetric. The derivation focusing on operator ordering is not summarized here, but the reader is reffered to reviews Burt [11, 15] and for the numerical estimates of the introduced errors to Burt [13]. In essence, Burt's theory clearly demonstrated the existence and omission of interface terms and showed that exact envelope equations could be derived from the original Schrödinger equation. But Burt's theory is not widely applied. The issue of operator ordering attracts growing interest and it is crucial for the mathematical stability of the envelope equations Veprek et al. [46**?** ]. Foreman Foreman [24] derived the correct operator ordering for zinc-blende crystals and therefore the derived operator ordering is commonly referred to as Burt-Foreman operator ordering. Beside the operator ordering, the theory regarding the omitted interface terms in the traditional model is only used rarely Foreman [26, 25]. The effect of the interface terms is to perturb the system and create an additional mixing of the bands. In the traditional envelope equations, the effect of the interface was introduced using phenomenological models (see e.g. Krebs and Voisin [35] and references therein) or by a variational least action principle Rodina and Alekseev [44]. The reason of the fundamental popularity of the traditional envelope function method over Burt's method is given by its simple form, which allows to write quantum well solvers within days, and the fact that mostly known, bulk input parameters can be used, which is not the case for the interface terms within the exact envelope function theory.

### 2.2.3 *The Zinc-blende Models*

#### 2.2.3.1 *Direct Interaction*

To apply the envelope equations 2.26 to direct-bandgap semiconductor nanostructures, the exact form of the $\mathbf{k}\cdot\mathbf{p}$ Hamiltonian at the $\Gamma$ point is required. Ignoring spin, the top of the valence band at $\Gamma$ is triply degenerate, corresponding to the $\Gamma_{15}$ representation with p-type basis functions $x, y$ and $z$, while the lowest-lying conduction band is of s-type symmetry, corresponding to $\Gamma_1$. The direct interaction terms 2.18 of the $\mathbf{k}\cdot\mathbf{p}$ matrix for $s, x, y$ and $z$ are given by Kane [32]

$$\mathbf{H}_d^{4\times4} = \left(\begin{array}{c|cccc} & |s\rangle & |x\rangle & |y\rangle & |z\rangle \\ \hline |s\rangle & E_c + \frac{\hbar^2}{2m_0} & iPk_x & iPk_y & iPk_z \\ |x\rangle & -ik_xP & E_v + \frac{\hbar^2}{2m_0} & 0 & 0 \\ |y\rangle & -ik_yP & 0 & E_v + \frac{\hbar^2}{2m_0} & 0 \\ |z\rangle & -ik_zP & 0 & 0 & E_v + \frac{\hbar^2}{2m_0} \end{array}\right).$$

(2.29)

Here, $E_c$ and $E_v$ correspond to the zone-center energies

$$E_c = \langle s|H|s\rangle \tag{2.30}$$
$$E_v = \langle x|H|x\rangle \tag{2.31}$$
$$P = -\frac{i\hbar}{m_0}\langle s|p_x|s\rangle \tag{2.32}$$

and $P$ the nonzero interband momentum matrix element from the direct $\mathbf{k}\cdot\mathbf{p}$ interaction between the conduction- and the valence band. The momentum matrix element is often given as an energy parameter $E_p$ , the *optical matrix parameter*, related to $P$ by

$$E_p = \frac{2m_0}{\hbar^2}P^2. \tag{2.33}$$

For the $\Gamma_{15}$ states, the nonzero momentum matrix element is of the type $\langle x|p_y|z\rangle$, where no coordinate appears twice Yu and Cardona [47] (the crystal is invariant under a rotation of 180° around one of the axes like Ren et al. [43]). Therefore, one would expect the direct interaction within the valence band $\mathbf{k}\cdot\langle x|\mathbf{p}|y\rangle$ resulting into a linear term in $\mathbf{k}$ given explicitly by $k_z\langle x|p_z|y\rangle$. In fact, the first order matrix elements within $\Gamma_{15}$ vanish due to time reversal symmetry of the Hamiltonian Dresselhaus [20]. For example, a reflection in the (110) plane for $\langle x^a|p_z|y^b\rangle$ results in $\langle y^a|p_z|x^b\rangle$, while integration by parts gives $\langle x^a|p_z|y^b\rangle = -\langle y^b|p_z|x^a\rangle$. Here $a$ and $b$ index the degenerate level. If the states are from the same degenerate level, then $a = b$ and the matrix elements vanish. If the states are not from the same degenerate level, the interaction is nonzero.

The operator ordering in the first order terms, e.g. $H_{sx} = iPk_x$ and $H_{xs} = -ik_xP$ is an ad hoc fix. If $P$ is allowed to vary, the here chosen ordering is required to ensure the Hamiltonians Hermiticity.

#### 2.2.3.2 *Remote Contributions*

The next step is to include the interaction between the remote states and keep track of the correct operator ordering. It is clear from table 1 that the remote contributions to the conduction band stem from remote $\Gamma_{15}$ states, while the valence band states have contributions from all except the $\Gamma_2$ states. The corresponding terms are given by the matrix $\mathbf{H}_r^{4\times4}$ 2.39 and the coefficients 2.40. In deriving these terms, the energy for the energy-dependent renormalization has been replaced by the according band edge energies $E_v$ and $E_c$. Although the approximation might be reasonable for very remote bands $v$, it remains crude. The derivation of the terms tese terms involves only symmetry arguments similar to the already used arguments within this chapter. The bar in $\bar{A_c}$, $\bar{L}$ and $\bar{M}$ indicates the close relationship to the parameters $\tilde{A_c}$,$\tilde{L}'$ and $\tilde{M}$ , which include the free-electron dispersion

$$\tilde{A_c} = \bar{A_c} + \frac{\hbar^2}{2m_0},\ \tilde{L}' = \bar{L} + \frac{\hbar^2}{2m_0},\ \tilde{M} = \bar{M} + \frac{\hbar^2}{2m_0}, \tag{2.34}$$

whereas in this case the free electron dispersion is still contained in the direct interaction matrix 2.29. The operator ordering in the offdiagonal terms $k_y\tilde{N}_+k_x + k_x\tilde{N}_-k_y$ has been derived by Foreman 25. The term

$\tilde{N}_+$ contains the contribution from $\Gamma_1$ (F) and $\Gamma_{12}$ (G) bands, while $\tilde{N}_-$ contains the contributions from $\Gamma_{15}$ ($H_1$) and $\Gamma_{25}$ ($H_2$) bands. In the bulk $\mathbf{k}\cdot\mathbf{p}$ theory, the ordering is irrelevant and the terms are summed together into the Kane's parameter $\tilde{N}'$

$$\tilde{N}' = \tilde{N}_+ + \tilde{N}_-. \tag{2.35}$$

Within the traditional $\mathbf{k}\cdot\mathbf{p}$ envelope function method applied to heterostructure, the symmetrized operator ordering 2.28 simply uses

$$\tilde{N}_+ = \tilde{N}_- = \frac{\tilde{N}'}{2}. \tag{2.36}$$

The parameters $\tilde{L}'$, $\tilde{M}$ and $\tilde{N}$ are usually determined by calculating analytical expressions for the dispersion and relating them to measured effective masses. The detailed splitting of $\tilde{N}'$ into $\tilde{N}_+$ and $\tilde{N}_-$ is not directly accessible from experiment, but can be estimated Foreman [24] using the following arguments: The term $\tilde{N}_-$ contains contributions of $\Gamma_{15}$ and $\Gamma_{25}$ bands. The $\Gamma_{25}$ bands can only be formed by f-type and higher atomic orbitals, while $\Gamma_{15}$ bands can be formed by p-,d-,f- and higher type orbitals Foreman [25]. Within the usual semiconductors, the influence of f orbitals is insignificant. Therefore, neglecting the influence of the $\Gamma_{25}$ bands ($H_2 = 0$) and using **??**, the value for $\tilde{N}_-$ is given by

$$\tilde{N}_- = \bar{M} = \tilde{M} - \frac{\hbar^2}{2m_o}. \tag{2.37}$$

$\tilde{N}_+$ can be deduced using 2.35 and the experimentally determined value for $\tilde{N}'$. In a usual zinc-blende semiconductor such as GaAs, $\tilde{M}$ = −2.65 and $\tilde{N}'$ = −17.4 (in units of $\frac{\hbar^2}{2m_0}$). The symmetric operator ordering would therefore use $\tilde{N}_{+/-}$ = −8.7, while the Burt-Foreman ordering gives strongly asymmetric values $\tilde{N}_+$= −13.75 and $\tilde{N}_-$ = −3.65. In contrast to the operator ordering within the valence band, the ordering in the off-diagonal terms between the conduction and valence bands, given by the terms $k_y C k_z + k_z C k_y$, is required to be symmetric. Only remote $\Gamma_{15}$ type bands mix into the s-type conduction band, and therefore, the non-vanishing elements from the perturbation are

$$k_y \langle s \mid p_y \mid y^r \rangle \langle y^r \mid p_z \mid x \rangle k_z + k_z \langle s \mid p_z \mid y^r \rangle \langle z^r \mid p_y \mid x \rangle k_y. \tag{2.38}$$

By crystal symmetry, these terms are equal. The term C is related to the common Kane parameter $B = 2C$. As B is usually small, it is commonly neglected, i.e. $C = 0$.

$$\mathbf{H}_r^{4\times4} = \left(\begin{array}{c|cccc} & |s\rangle & |x\rangle & |y\rangle & |z\rangle \\ \hline |s\rangle & k\bar{A}_c k & k_y C k_z + k_z C k_y & k_x C k_z + k_z C k_x & k_y C k_x + k_x C k_y \\ |x\rangle & k_z C k_y + k_y C k_z & k_x \bar{L} k_x + k_y \bar{M} k_y + k_z \bar{M} k_z & k_x \tilde{N}_+ k_y + k_y \tilde{N}_- k_x & k_x \tilde{N}_+ k_z + k_z \tilde{N}_- k_x \\ |y\rangle & k_z C k_x + k_x C k_z & k_y \tilde{N}_+ k_x + k_x \tilde{N}_- k_y & k_y \bar{L} k_y + k_x \bar{M} k_x + k_z \bar{M} k_z & k_y \tilde{N}_+ k_z + k_z \tilde{N}_- k_y \\ |z\rangle & k_x C k_y + k_y C k_x & k_z \tilde{N}_+ k_x + k_x \tilde{N}_- k_z & k_z \tilde{N}_+ k_y + k_y \tilde{N}_- k_z & k_z \bar{L} k_z + k_x \bar{M} k_x + k_y \bar{M} k_y \end{array}\right), \tag{2.39}$$

$$\begin{aligned} &\bar{L} = F + 2G, \qquad \bar{M} = H_1 + H_2, \\ &\tilde{N}_+ = F - G, \qquad \tilde{N}_- = H_1 - H_2, \\ &F = \frac{\hbar^2}{m_0^2} \sum_{\nu}^{\Gamma_1} \frac{|\langle x \mid p_x \mid u_\nu \rangle|^2}{(E_\nu - E_\nu)}, \quad G = \frac{\hbar^2}{m_0^2} \sum_{\nu}^{\Gamma_{12}} \frac{|\langle x \mid p_x \mid u_\nu \rangle|^2}{(E_\nu - E_\nu)}, \\ &H_1 = \frac{\hbar^2}{m_0^2} \sum_{\nu}^{\Gamma_{15}} \frac{|\langle s \mid p_x \mid u_\nu \rangle|^2}{(E_c - E_\nu)}, \quad H_2 = \frac{\hbar^2}{m_0^2} \sum_{\nu}^{\Gamma_{25}} \frac{|\langle x \mid p_x \mid u_\nu \rangle|^2}{(E_\nu - E_\nu)}, \\ &\bar{A}_c = \frac{\hbar^2}{m_0^2} \sum_{\nu}^{\Gamma_{15}} \frac{|\langle s \mid p_x \mid u_\nu \rangle|^2}{(E_c - E_\nu)}, \quad C = \frac{\hbar^2}{m_0^2} \sum_{\nu}^{\Gamma_{15}} \frac{\langle s \mid p_x \mid u_\nu \rangle \langle u_\nu \mid p_x \mid z \rangle}{\left(\frac{1}{2}(E_c + E_\nu) - E_\nu\right)}. \end{aligned} \tag{2.40}$$

#### 2.2.3.3 *Spin-Orbit Interaction*

Up to this point, the electron spin has been omitted. Within the semiconductors involving heavier atoms, the spin-orbit interaction has a large impact on the electron dispersions. The spin-orbit energy leads to additional terms in the equation 2.23 for the zone-center functions, namely

$$H_{SO,\mathbf{p}} = \frac{\hbar}{4m_0^2c^2}(\nabla V \times \mathbf{p})\cdot\boldsymbol{\sigma}, \tag{2.41}$$

$$H_{SO,\mathbf{k}} = \frac{\hbar}{4m_0^2c^2}(\nabla V \times \mathbf{k})\cdot\boldsymbol{\sigma}, \tag{2.42}$$

where $c$ is the vacuum speed of light and $\boldsymbol{\sigma}$ are the *Pauli operators* acting on the electoron-spin variable

$$\sigma_x = \begin{pmatrix} 0 & 1 \\ 1 & 0 \end{pmatrix}, \ \sigma_y = \begin{pmatrix} 0 & -i \\ i & 0 \end{pmatrix}, \ \sigma_z = \begin{pmatrix} 1 & 0 \\ 0 & -1 \end{pmatrix}.$$

The Bloch basis functions have to be extended to include the spin degree of freedom, which is done by giving the spin $z$-component, which can be either up $|\uparrow\rangle$ or down $|\downarrow\rangle$. The spin variable is diagonal, meaning that $\langle\uparrow|\uparrow\rangle = \langle\downarrow|\downarrow\rangle = 1$ and $\langle\uparrow|\downarrow\rangle = 0$. Using the spin, the initial basis of four states describing the lowest conduction band and the top valence bands is doubled to eight states

$$|s\uparrow\rangle, |x\uparrow\rangle, |y\uparrow\rangle, |z\uparrow\rangle, |s\downarrow\rangle, |x\downarrow\rangle, |y\downarrow\rangle, |z\downarrow\rangle. \tag{2.43}$$

All operators in the zone-center Hamiltonian 2.14 do not act on the spin variable. Therefore, the Hamiltonian is diagonal in the spin variable. Within the basis 2.43, the Hamiltonian is given by

$$\mathbf{H}_{rd}^{8\times8} = \begin{pmatrix} \mathbf{H}_d^{4\times4} + \mathbf{H}_r^{4\times4} & 0 \\ 0 & \mathbf{H}_d^{4\times4} + \mathbf{H}_r^{4\times4} \end{pmatrix}. \tag{2.44}$$

In contrast to this Hamiltonian, the spin-orbit interaction 2.41 and 2.42 is not diagonal in the basis 2.43. The reason to this lies in the symmetry of the spin. The crystal potential $V(\mathbf{r})$ without spin terms is invariant under any rotation around an angle of $2p$, denoted here as $\hat{E}$. Under such a rotation, the wavefunction including the spin switches sign and is only invariant under the rotation of $4p$. Therefore, if the point group of the crystal neglecting spin is given by $\mathcal{G}$, then the point group including spin will be given by the elements of $\mathcal{G}$ and $\hat{E}\mathcal{G}$, leading to the definition of the *double-group* $\tilde{\mathcal{G}}$ of $\mathcal{G}$ defined as

$$\tilde{\mathcal{G}} = \{g, \tilde{g} = -g\} \ \ \forall g \in \mathcal{G}. \tag{2.45}$$

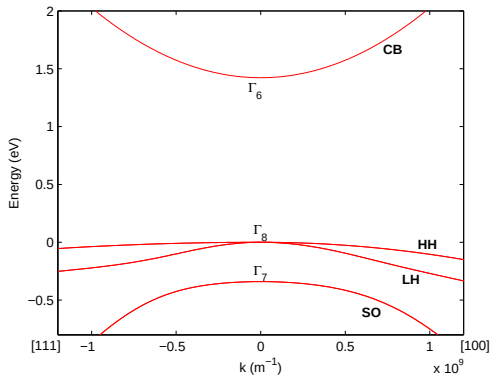


Figure 3: Band structure of bulk GaAs around the Γ point at room temperature, calculated using the $8 \times 8$ $\mathbf{k} \cdot \mathbf{p}$ for two crystal directions.

The spin-orbit interaction for $H_{SO,\mathbf{p}}$of 2.41 leads, for the basis in 2.43, to Enders et al. [22]

$$\mathbf{H}_{SO,\mathbf{p}} = \frac{\Delta}{3} \begin{pmatrix} 0 & 0 & 0 & 0 & 0 & 0 & 0 & 0 \\ 0 & 0 & -i & 0 & 0 & 0 & 0 & 1 \\ 0 & i & 0 & 0 & 0 & 0 & 0 & -i \\ 0 & 0 & 0 & 0 & 0 & -1 & i & 0 \\ 0 & 0 & 0 & 0 & 0 & 0 & 0 & 0 \\ 0 & 0 & 0 & -1 & 0 & 0 & i & 0 \\ 0 & 0 & 0 & -i & 0 & -i & 0 & 0 \\ 0 & 1 & i & 0 & 0 & 0 & 0 & 0 \end{pmatrix}. \tag{2.46}$$

Here, the spin-orbit energy $\Delta$ is defiend as

$$\Delta = -3i\frac{\hbar}{4m_0^2c^2}\left\langle x \mid (\nabla V \times \mathbf{p})_y \mid z \right\rangle. \tag{2.47}$$

The k-dependent spin-orbit interaction $H_{SO,\mathbf{k}}$ of 2.42 is small and therefore commonly neglected Kane [32]. The result of $H_{SO,\mathbf{k}}$ are terms linear in k, leading to an off-diagonal coupling between the conduction and the valence band. Further, the spin-orbit interaction $H_{SO,\mathbf{p}}$ is usually only included in the direct interaction, while perturbative contributions from remote bands are in general neglected. The effect of the spin-orbit interaction is to split the six-fold (threefold without spin) degeneracy of the valence band at Γ into a fourfold degeneracy with eigenvalue $\frac{\Delta}{3}$ and a two-fold degeneracy with an eigenvalue of $-\frac{2\Delta}{3}$ . In other words, the states are separated by $\Delta$. The four-fold degenerate states corresponds to the irreducible representation $\Gamma_8$ of the double group of $T_d$. Away from Γ, these states create the *heavy-hole* (HH) and the *light-hole* (LH) bands. The two-fold degenerate states correspond to the $\Gamma_7$ representation and lie below the $\Gamma_8$ states by $-\Delta$. The $\Gamma_7$ band is referred to as *spin-orbit split off band* (SO). The lowest conduction band (CB) states finally correspond to $\Gamma_6$ states. The situation is illustrated in Fig. 3, where the band structure of GaAs calculated using the here presented $\mathbf{k} \cdot \mathbf{p}$ model is plotted around $\mathbf{k} = 0$. The experimental accessible bandgap is given by the difference between the $\Gamma_6$ and the $\Gamma_8$ states. Therefore, the valence band edge $E_v$ in 2.31, needs to be shifted by $-\frac{\Delta}{3}$.

The here elaborated model, including the CB, HH, LH and SO band, is commonly referred to as the $8\times 8$ $\mathbf{k}\cdot\mathbf{p}$ model. For large band gap materials, the coupling between the conduction and valence bands is weak and therefore the $8\times 8$ $\mathbf{k}\cdot\mathbf{p}$ model can be divided into to a $6\times 6$ model, including only the valence bands and a single band model for the spin degenerate conduction band. This division is achieved by perturbatively folding the conduction band onto the valence bands and vice versa. The $6\times 6$ $\mathbf{k}\cdot\mathbf{p}$ is therefore obtained by using only the valence band part of $\mathbf{H}_{rd}^{8\times 8}+\mathbf{H}_{SO,\mathbf{p}}$ with modified parameters $L'$ and $N'$ given by

$$L' = \tilde{L}' + \frac{P^2}{E_g}, \quad N_+ = \tilde{N}_+ + \frac{P^2}{E_g} \tag{2.48}$$

instead of $\tilde{L}'$ and $\tilde{N}_+$. The parameter $\tilde{M}$, and consequently $\tilde{N}_-$, remain unchnged. Thereby, the correct operator ordering is conserved. The conduction band parameter is obtained using

$$A_c = \tilde{A}_c + \frac{P^2}{E_g}, \tag{2.49}$$

which is then equal to the common conduction band effective mass. For some semiconductors, the spin-orbit splitting is large and the SO band has only little influence on the top of the valence band. Then, the $6\times 6$ $\mathbf{k}\cdot\mathbf{p}$ model can be further reduced to only include the HH and LH bands. The reduction is performed by choosing a combination of basis functions 2.43 effectively diagonalizing the spin-orbit interaction $\mathbf{H}_{SO,\mathbf{p}}$. The new basis is labelled according to its total angular momentum $J$ and the angular momentum around the $z$-axis, $J_z$. A possible choice, using $|J,J_z\rangle$ as notation, is given by

$$\begin{aligned}
u_{hh} &= \left|\frac{3}{2},\frac{3}{2}\right\rangle &&= -\frac{1}{\sqrt{2}}\left(|x\uparrow\rangle + i\,|y\uparrow\rangle\right),\\
u_{lh} &= \left|\frac{3}{2},\frac{1}{2}\right\rangle &&= -\frac{1}{\sqrt{6}}\left(|x\downarrow\rangle + i\,|y\uparrow\rangle\right) + \sqrt{\frac{2}{3}}\,|z\uparrow\rangle,\\
\bar{u}_{lh} &= \left|\frac{3}{2},-\frac{1}{2}\right\rangle &&= \frac{1}{\sqrt{6}}\left(|x\uparrow\rangle - i\,|y\uparrow\rangle\right) + \sqrt{\frac{2}{3}}\,|z\downarrow\rangle,\\
\bar{u}_{hh} &= \left|\frac{3}{2},-\frac{3}{2}\right\rangle &&= \frac{1}{\sqrt{2}}\left(|x\downarrow\rangle - i\,|y\downarrow\rangle\right),\\
u_{SO} &= \left|\frac{1}{2},\frac{1}{2}\right\rangle &&= \frac{1}{\sqrt{3}}\left(|x\downarrow\rangle + i\,|y\downarrow\rangle + |z\uparrow\rangle\right),\\
\bar{u}_{SO} &= \left|\frac{1}{2},-\frac{1}{2}\right\rangle &&= \frac{1}{\sqrt{3}}\left(|x\uparrow\rangle - i\,|y\uparrow\rangle - |z\downarrow\rangle\right).
\end{aligned} \tag{2.50}$$

The four states with total angular momentum of $\frac{3}{2}$ belong to $\Gamma_8$ and the two states with an angular momentum of $\frac{1}{2}$ form the $\Gamma_7$ (or SO) bands. Transforming the Hamiltonian into the basis 2.50 and neglecting the $\Gamma_7$ rows and columns finally results in the $4\times 4$ $\mathbf{k}\cdot\mathbf{p}$ model. Within the $4\times 4$ $\mathbf{k}\cdot\mathbf{p}$ model, it is common to use the Luttinger parameters $\gamma_1,\gamma_2$ and $\gamma_3$[1]Luttinger [37] instead of the Kane's parameters of the

1 The full listing of these parameters is given is Appendix XXX .

$6\times 6$ model L′, M and N′. The Luttinger parameters are usually those given in literature. The parameters are related to each other via

$$\begin{aligned} L' &= -\frac{\hbar^2}{2m_0}(\gamma_1+4\gamma_2) \\ M &= -\frac{\hbar^2}{2m_0}(\gamma_1-2\gamma_2) \\ N' &= -\frac{\hbar^2}{2m_0}6\gamma_3. \end{aligned} \tag{2.51}$$

From 2.51, the parameters for $8\times 8$ model can be calculated using the renormalization 2.48.

In terms of the Luttinger parameters the full $8\times 8$ Hamiltonian can be written explicitly as Chuang [19], Luttinger and Kohn [38], Luttinger [37]

$$\mathbf{H}^{8\times 8} = \begin{pmatrix} E_c & P_z & \sqrt{2}P_z & -\sqrt{3}P_+ & 0 & \sqrt{2}P_- & P_- & 0 \\ P_z^\dagger & P+\Delta & \sqrt{2}Q^\dagger & -S^\dagger/\sqrt{2} & -\sqrt{2}P_+^\dagger & 0 & -\sqrt{3/2}S & -\sqrt{2}R \\ \sqrt{2}P_z^\dagger & \sqrt{2}Q & P-Q & -S^\dagger & -P_+^\dagger & \sqrt{3/2}S & 0 & R \\ -\sqrt{3}P_+^\dagger & -S/\sqrt{2} & -S & P+Q & 0 & \sqrt{2}R & R & 0 \\ 0 & -\sqrt{2}P_+ & -P_+ & 0 & E_c & P_z & -\sqrt{2}P_z & -\sqrt{3}P_- \\ \sqrt{2}P_-^\dagger & 0 & \sqrt{3/2}S^\dagger & \sqrt{2}R^\dagger & P_z^\dagger & P+\Delta & \sqrt{2}Q^\dagger & -S/\sqrt{2} \\ P_-^\dagger & -\sqrt{3/2}S^\dagger & 0 & R^\dagger & -\sqrt{2}P_z^\dagger & \sqrt{2}Q & P-Q & S \\ 0 & -\sqrt{2}R^\dagger & R^\dagger & 0 & -\sqrt{3}P_-^\dagger & -S^\dagger/\sqrt{2} & S^\dagger & P+Q \end{pmatrix} \tag{2.52}$$

where

$$E_c = E_g + \frac{\hbar^2}{2m_0}\left(k_x^2+k_y^2+k_z^2\right), \tag{2.53}$$

$$P = \frac{\hbar^2}{2m_0}\gamma_1\left(k_x^2+k_y^2+k_z^2\right), \tag{2.54}$$

$$P_\pm = \sqrt{\frac{1}{6}}\left[i\mathcal{P}\left(k_x\pm ik_y\right)+\mathcal{B}k_z\left(k_y\pm ik_x\right)\right] \tag{2.55}$$

$$P_z = \sqrt{\frac{1}{3}}\left(i\mathcal{P}k_z+\mathcal{B}k_xk_y\right), \tag{2.56}$$

$$Q = \frac{\hbar^2}{2m_0}\gamma_2\left(k_x^2+k_y^2-2k_z^2\right), \tag{2.57}$$

$$R = \frac{\hbar^2}{2m_0}\left[-\sqrt{3}\gamma_2\left(k_x^2-k_y^2\right)+i2\sqrt{3}\gamma_3k_xk_y\right], \tag{2.58}$$

$$S = \frac{\hbar^2}{2m_0}\gamma_3\left(k_x-ik_y\right)k_z. \tag{2.59}$$

The parameter $\Delta$ is, as before, the spin-orbit splitting energy. The coupling between the $\Gamma$ conduction band edge state $|s\rangle$ and the $\Gamma$ valence band edge state $|z\rangle$ is given by

$$\mathcal{P} = -\frac{\hbar^2}{m_0}\int_{V_c}\varphi_s\frac{\partial}{\partial z}\varphi_z. \tag{2.60}$$

The Kane parameter $\mathcal{B}$ describes the inversion asymmetry. In most practical calculations, this parameter is neglected. The parameters $\gamma_1,\gamma_2,\gamma_3$

and $\mathcal{P}$ can ne determined from effective masses at the $\Gamma$ point of the bulk semiconductor Chuang [19]

$$\frac{m_0}{m_{hh}(001)} = \gamma_1 - 2\gamma_2, \tag{2.61}$$

$$\frac{m_0}{m_{lh}(001)} = \gamma_1 + 2\gamma_2 + \lambda, \tag{2.62}$$

$$\frac{m_0}{m_{SO}(001)} = \gamma_1 + \frac{1}{2}\lambda r, \tag{2.63}$$

$$\frac{m_0}{m_{hh}(111)} = \gamma_1 - 2\gamma_3, \tag{2.64}$$

where the dimensionless parameters $\lambda$ and $r$ are given by

$$\lambda = \frac{4m_0\mathcal{P}^2}{3\hbar^2 E_g}, \tag{2.65}$$

$$r = \frac{E_g}{E_g + \Delta}. \tag{2.66}$$

Put here the 6X6 and 4X4 Hamiltonians

### 2.2.4 *Two Band Model*

The conduction band can be modeled quite easily if we assume that the interaction with the other bands is weak enough for it to be treated perturbatively, i.e. use a simple effective mass model. In the case of the valence band, however, the strong interaction between the degenerate light and heavy hole bands (near the band edge) requires that these bands are taken into account explicitly. Only when we consider energy levels deep into the valence bands (close to the SO splitting energy, about 300 $meV$ in $GaAs$) do the coupling terms to the SO and conduction bands (1.5 $eV$ splitting) can be introduced through the effective mass.

The degeneracy of the light and heavy hole bands near the band edge generates a coupling term (as in the Luttinger Hamiltonian). Including spin degeneracy, this yeilds a set of four coupled effective mass equations Chuang [19], Andreani et al. [2], Broido and Sham [9].

Fortunately, this set of coupled equations can be greatly simplified by a method described in Broido and Sham [9]. Here a unitary transformation of the four basis Bloch functions in 2.50 into a new set $u_A, u_B, u_C, u_D$ to decouple the set of four coupled equations into two coupled ones. The Bloch functions $u_i$ are given by

$$u_A = \frac{1}{\sqrt{2}}\left(u_{hh} - \bar{u}_{hh}\right), \tag{2.67}$$

$$u_B = \frac{1}{\sqrt{2}}\left(-u_{lh} - \bar{u}_{lh}\right), \tag{2.68}$$

$$u_C = \frac{1}{\sqrt{2}}\left(u_{lh} + \bar{u}_{lh}\right), \tag{2.69}$$

$$u_D = \frac{1}{\sqrt{2}}\left(u_{hh} + \bar{u}_{hh}\right). \tag{2.70}$$

Consequently, the $4 \times 4$ $\mathbf{k} \cdot \mathbf{p}$ Hamiltonian

$$\mathbf{H}^{4\times4} = \begin{pmatrix} P-Q & -S^{\dagger} & 0 & R \\ -S & P+Q & R & 0 \\ 0 & R^{\dagger} & P-Q & S \\ R^{\dagger} & 0 & S^{\dagger} & P+Q \end{pmatrix}. \tag{2.71}$$

In terms of the the new base propesed above, it can be diagonalized into two $2 \times 2$ block matrices, upper $H^{U}$ and lower $H^{L}$, given by

$$H^{\sigma} = \begin{pmatrix} P \pm Q & W \\ W^{\dagger} & P \mp Q \end{pmatrix}, \tag{2.72}$$

where $W = |R| - i\,|S|$. The index $\sigma = U(L)$ refers to the upper (lower) $\pm$ signs. The upper and lower blocks are quivalent, showing the double degeneracy of the heavy and light hole bands. It is therefore sufficient to solve the upper block and obtain its solutions. The solutions of the lower block can easily be determined from the latter.

We can identify $P-Q$ and $P+Q$ with the light hole energy (operator) $\hat{H}_{lh}$ and the heavy hole energy $\hat{H}_{hh}$, respectively. Similarly to the conduction band case, the Schrödinger equation with the Hamiltonian 2.72 can be simplified into an effective-mass formalism with

$$\hat{H}_{lh} = -(\gamma_1 + 2\gamma_2)\frac{\partial^2}{\partial z^2} + (\gamma_1 - \gamma_2)\,k_t^2, \tag{2.73}$$

$$\hat{H}_{hh} = -(\gamma_1 - 2\gamma_2)\frac{\partial^2}{\partial z^2} + (\gamma_1 + \gamma_2)\,k_t^2, \tag{2.74}$$

$$\hat{W} = \begin{cases} \sqrt{3}k_t\left(\gamma_2 k_t - 2\gamma_3 \frac{\partial}{\partial z}\right) & \text{for } [100] \\ \sqrt{3}k_t\left(\gamma_3 k_t - 2\gamma_3 \frac{\partial}{\partial z}\right) & \text{for } [110] \end{cases} \tag{2.75}$$

Finally, we take into account the potential $V(z)$, which represents the (bulk) valence-band-edge offset with respect to an arbitrary reference energy. This allows us write the effective mass equation as

$$\begin{pmatrix} \hat{H}_{hh} + V & \hat{W} \\ \hat{W}^{\dagger} & \hat{H}_{lh} + V \end{pmatrix} \begin{pmatrix} F_{hh} \\ F_{lh} \end{pmatrix} = E(\mathbf{k}) \begin{pmatrix} F_{hh} \\ F_{lh} \end{pmatrix}, \tag{2.76}$$

where $F_{hh}$ and $F_{lh}$ are the envelope fucntions corresponding to $u_A$ and $u_B$ respectively. Note that in this formalism, hole energies are taken to be positive.

The first step in solving the quantum well problem, is finding the solution in bulk material, where we take $V$ to be a constant $V_0$. The value of $V_0$ will be different in well material and barriersm reflecting the different valence band edge offsets. We can now easily solve for the eigenenergies $E(\mathbf{k})$, yeilding the bulk energy dispersion relations for the heavy and light hole subbands. We consider the case of a $[100]$ plane, writing the in-plane $\mathbf{k}$ component as $k_t$

$$E(\mathbf{k}) - V_0 = \gamma_1\left(k_z^2 + k_t^2\right) \pm \sqrt{4\gamma_2^2\left(k_z^2 + k_t^2\right) + 12\left(\gamma_3^2 - \gamma_2^2\right)k_z^2 k_t^2}, \tag{2.77}$$

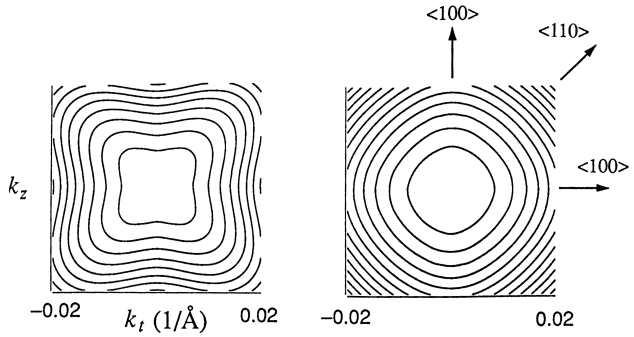


Figure 4: Contours of constant energy within any [100] plane of k-space for the heavy (right) and light (left) hole subbands in bulk GaAs. The energy spacing between each contour level is 0.5 meV for the HH band and 3 meV for the LH band. The effective HH mass is much larger along the[110] direction than along the [100] direction, as indicated by the larger contour spacing. The effective LH mass is seen to be much more isotropic (after Zory et al. [48]).

where the plus sign referes to the light hole solution, and the minus to the heavy hole one. This expression can be rewritten to

$$E(\mathbf{k}) = V_0 + \left[\gamma_1 \pm \gamma_2\sqrt{1+3\frac{\gamma_3^2-\gamma_2^2}{\gamma_2^2}\frac{k_z^2k_t^2}{\left(k_z^2+k_t^2\right)^2}}\right]\left(k_z^2+k_t^2\right). \quad (2.78)$$

A similar derivation can be formulated for the [110] crystal planes.

Constant energy contours are shown in Fig. 4, illustrating that $\gamma_3$can be related to the mass anisotropy along the [100] and [110] directions. If $k_t$ small compared to $k_z$, we can expand the square root in 2.77

$$E(\mathbf{k}) = V_0 + (\gamma_1 \pm \gamma_2)\left(k_z^2+k_t^2\right) \pm 3\frac{\gamma_3^2-\gamma_2^2}{\gamma_2}k_t^2. \quad (2.79)$$

The Energy term accounting for anisotropy for a given $k_t$ and $k_z$ is equal fot the HH and LH subbands. However, due to the lower energy of the HH bands the anisotropy term is relatively more important for HH than for LH, resulting in a clearly anisotropic HH band and a quasi isotropic LH band.

Still, we see that in bulk material, the effective masses along the z-axis [001] and x- and y- axes [100] and [010] are identical (as expected), as the dispersion realtion is given by $E(\mathbf{k}) = V_0 + (\gamma_1 \pm 2\gamma_2)\,k^2$.We can easily find this from 2.77 with $k_t = 0$ for [001], and $k_z = 0$ for the x- and y- directions.

The eigenvectors of 2.76 are found to be, apart from a normalization constant

$$\varphi_1(\mathbf{k},\mathbf{r}) = \begin{pmatrix} F_{hh,1} \\ F_{lh,1}\end{pmatrix} = e^{i\mathbf{k}\cdot\mathbf{r}}\begin{pmatrix} H_{lh}+V_0-E_{hh} \\ -W^\dagger\end{pmatrix}, \quad (2.80)$$

$$\varphi_2(\mathbf{k},\mathbf{r}) = \begin{pmatrix} F_{hh,2} \\ F_{lh,2}\end{pmatrix} = e^{i\mathbf{k}\cdot\mathbf{r}}\begin{pmatrix} H_{lh}+V_0-E_{lh} \\ -W^\dagger\end{pmatrix}, \quad (2.81)$$

where the matrix notation implies

$$\varphi = F_{hh}u_A + F_{lh}u_B. \quad (2.82)$$

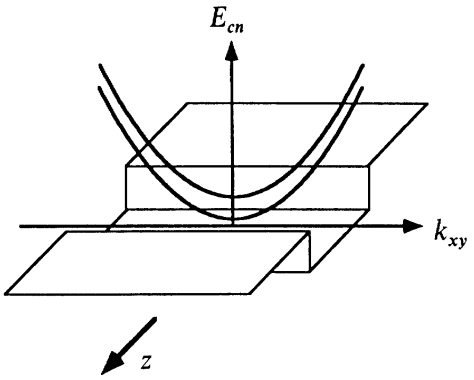


Figure 5: The "in-plane" subband structure of the quantum well in the conduction band. Within the plane of the well, the electron still behaves like a "free" electron. Thus, for each quantized level, a parabolic energy subband exist (after Zory et al. [48]).

To solve the quantum well problem, we choose the well growth direction (direction of confinment) along the $z$-axis. The $xy$-plane is the plane of the well, as in Fig. 5. We can construct a confined solution from the bulk plane wave solutions by imposing boundary conditions along the confinement axis. In the plane of the well, there is no confinment and hence we retain the bulk plane wave solution. By taking a linear combination of the bulk solutions in each material, a general solution can be cinstructed. As illustrated in Fig. 6, four plane wave solutions exist at a given energy, yielding a general solution $\Phi$ of the form

$$\Phi = \sum A_{\pm}\varphi_1(\pm k_{z1}, k_t, \mathbf{r}) + \sum B_{\pm}\varphi_2(\pm k_{z2}, k_t, \mathbf{r}). \tag{2.83}$$

The four coefficients $A_{\pm}$ and $B_{\pm}$ are unknown constants. Both $\varphi_1$ and $\varphi_2$ are two-component vectors as seen in 2.80 and 2.81. We can write the components of $\Phi$, $F_{hh}$ and $F_{lh}$, as

$$F_{hh} = e^{i\mathbf{k}_t\cdot\mathbf{r}_t}\left[\sum A_{\pm}F_{hh,1}(\pm k_{z1}, k_t)e^{\pm ik_{hh}z} + \sum B_{\pm}F_{hh,2}(\pm k_{z2}, k_t)e^{\pm ik_{hh}z}\right] \tag{2.84}$$

$$F_{lh} = e^{i\mathbf{k}_t\cdot\mathbf{r}_t}\left[\sum A_{\pm}F_{lh,1}(\pm k_{z1}, k_t)e^{\pm ik_{lh}z} + \sum B_{\pm}F_{lh,2}(\pm k_{z2}, k_t)e^{\pm ik_{lh}z}\right] \tag{2.85}$$

Thus we have four unknown constants in each region, making a total of 12 unknowns over the three regions. The boundary conditions at the interfaces between the regions and the demand that the solutions be confined in the quantum well provide the necessary relations to solve the problem. In order to symmetr The following quantities have to be matched across the interfaces

$$F_{hh} \text{ and } (\gamma_1 - 2\gamma_2)\frac{dF_{hh}}{dz} + \sqrt{3}\gamma_3 k_t F_{lh}, \tag{2.86}$$

$$F_{lh} \text{ and } (\gamma_1 - 2\gamma_2)\frac{dF_{lh}}{dz} - \sqrt{3}\gamma_3 k_t F_{hh}. \tag{2.87}$$

These boundary conditions were obtained by symmettrizing the Hamiltonian 2.72. Caution should be issued however that the above boundary conditions only apply when the Bloch functions in both well materials and are similar, as is the case for the $GaAs - AlGaAs$ system used throughout this thesis. The boundary conditions boil down to the continuity of the wave function and "generalized" continuity of its derivative, corresponding to current across the interface. The numerical

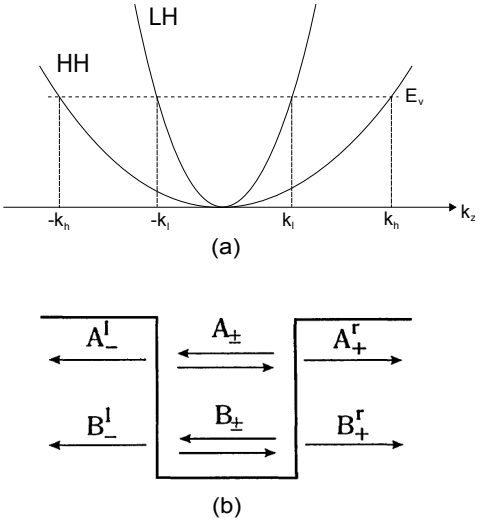


Figure 6: At any one enrgy on a bulk material, we can find four wavevectors corresponding to the heavy and light hole bands. An eigenstate of the Hamiltonian in a quantum well is then madde of a linear combination of the bulk plane waves corresponding to those wave vectors. The amplitudes $A_\pm$ and $B_\pm$ in (a) correspond, respectively, to $\pm k_{z1}$(light hole) and $\pm k_{z2}$ in (b) for the well layer of the quantum well (GaAs throughout this thesis). In the barriers (AlGaAs) a similar mechanism is employed. The boundary conditions at the interfaces then determine the energy eigenvalues and the coefficients.

implementation details of the two bands model is given in Appendix B.

As an illustration, we present in Fig. 7(a) the valence subband structure of a 100Å $GaAs/Al_{0.3}Ga_{0.7}As$ quantum well. The light and heavy holes are very heavily coupled, giving rise to highly non-parabolic subbands.

Particularly important is the *density of states* (DOS), which can be found from

$$\rho(E) = \frac{1}{\pi}\frac{dk}{dE}, \tag{2.88}$$

assuming the dispersion relationship is isotropic (using the axial approximation, see Appendix B). As an illustration, we plot in Fig. 7(b) the calculated ratio between the DOS of the valence subbands from 7(a) and the DOS of the first conduction subband. The spikes in the DOS are sue to the band extrema away from the zone center.

## 2.3 SCHRÖDINGER-POISSON MODEL

All of the theoretical methods and examples described so far have concentrated solely on solving systems for a single charge carrier. In many devices such models would be inadequate as large numbers of charge carriers, e.g. electrons, can be present in the conduction band. In order to decide whether or not typical carrier densities would give rise to a *significant* additional potential on top of the usual band-edge potential terms (which will be labelled specifically as $V_{CB}$ or $V_{VB}$), it then becomes necessary to solve the electrostatics describing the system.

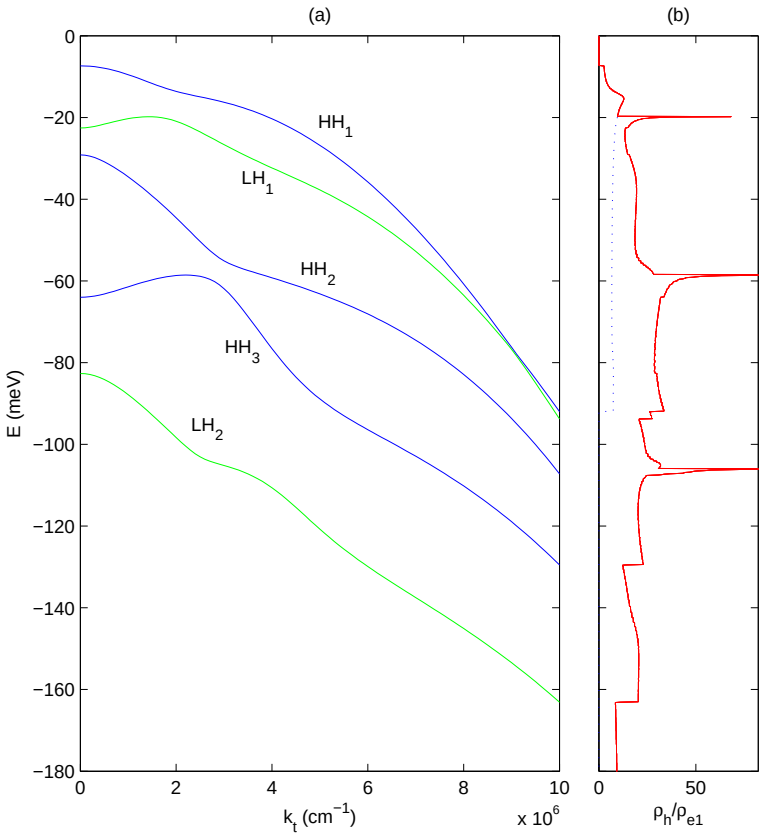


Figure 7: (a) Valence subbands dispersion relations calculated for a 100Å wide $GaAs/Al_{0.3}Ga_{0.7}As$ quantum well, for [100] crystal plane. The subbands are named after their dominant character at the zone center ($k_t = 0$). (b) The ratio between the density of states of the valence subbands and the first conduction subband, calculated for the same structure.

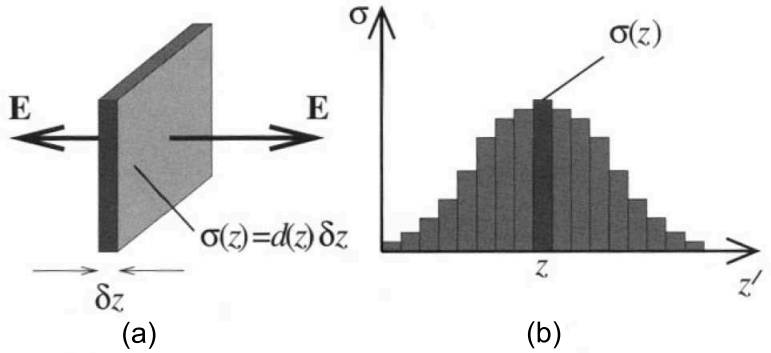


Figure 8: Electric field strength from an infinite plane of charge of volume density $d(z)$ and thickness $\delta z$ (after Harrison [28]).

When considering the case of an n-type material, then (although obvious) it is worth stating that the number of "free" electrons in the conduction band is equal to the number of positively charged ionised donors in the heterostructure. As an example, we can point out the modulation doped system, where the doping is located in a position wher the free carriers it produces will become spatially separated from the ion. The additional potential term $V_\rho(z)$ arising from this, or any other charge distribution $\rho$, can be expressed by using Poisson's equation

$$\nabla^2 V_\rho = -\frac{\rho}{\epsilon} \tag{2.89}$$

where $\epsilon$ is the permittivity of the material, i.e. $\epsilon = \epsilon_r \epsilon_0$. The solution is generally obtianed via the electric field strength $\mathbf{E}$. Recalling that

$$\mathbf{E} = -\nabla V \tag{2.90}$$

the potential then follow in the usual way Jackson [30]

$$V_\rho(z) = -\int_{-\infty}^{\mathbf{r}} \mathbf{E} \cdot d\mathbf{r}. \tag{2.91}$$

Given that the potential profiles, $V_{CB}(Z)$ for example, are one-dimensional, then they will also produce a one-dimensional charge distribution. In addition, remembering that the quantum wells are assumed infinite in the $x-y$ plane then any charge density $\rho(z)$ can be thought of as an infinite plane, i.e. a sheet, with areal charge density $\sigma(z)$ and thickness $\delta z$, as shown in Fig. 8(a). Such an infinite plane of charge produces an electric field perpendicular to it, and with a strength

$$\mathbf{E} = \frac{\sigma}{2\epsilon}. \tag{2.92}$$

Note that as the sheet is infinite in the plane, then the field strength is constant for all distances from the plane. The total electric field strength due to many of these planes of charge, as shown in Fig. 8(b), is then the sum of the individual contributions as follows

$$\mathbf{E}(z) = \sum_{z'=-\infty}^{\infty} \frac{\sigma(z')}{2\epsilon} \text{sign}\left(z - z'\right) \tag{2.93}$$

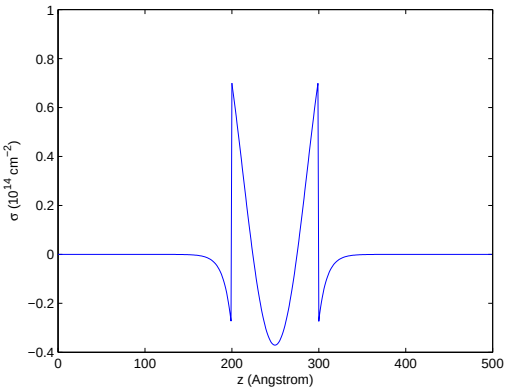


Figure 9: Areal charge density a for a 100 Å GaAs well, n-type doped to $2 \times 10^{18} cm^{-3}$, surrounded by undoped $Ga_{0.8}Al_{0.2}As$ 4 meVbarriers.

where the function sign is defined as

$$\text{sign}(z) = \begin{cases} 1, & z \geqslant 0 \\ -1, & z \leqslant 0 \end{cases} \tag{2.94}$$

and has been introduced to account for the vector nature of **E**, i.e. if a single sheet of charge is at a position $z'$, then for $z > z'$, $\mathbf{E}(z) = +\sigma/2\epsilon$, whereas for $z < z'$, $\mathbf{E}(z) = -\sigma/2\epsilon$. Note further that it is only the charge neutrality, there are as many ionised donors (or acceptors) in the system as there are electrons (or holes), or expressed mathematically

$$\sum_{z=-\infty}^{\infty} \sigma(z) = 0, \tag{2.95}$$

which ensures that the electric field, and hence the potential, go to zero at large distances from the charge distribution. For the case of a doped semiconductor, there would be two contributions to the charge density $\sigma(z)$, where the first would be the ionised impurities and the second the free charge carriers themselves. While the former would be known from the doping density in each semiconductor layer, as defined at growth time, the latter would be calculated from the probability distributions of the carriers in the heterostructure. Thus if $d(z)$ defines the volume density of the dopants at position $z$, where the planes are separated by the usual step length $\delta z$, then the total number of carriers, per unit cross-sectional area, introduced into the heterostructure is given by

$$N = \int_{-\infty}^{\infty} d(z)dz. \tag{2.96}$$

The net charge density in any of the planes follows as

$$\sigma(z) = q\left[N\psi^*(z)\psi(z) - d(z)\right]\delta z \tag{2.97}$$

where q us the charge on the extrinsic carriers. The step length $\delta z$ selects the proportion of the carriers that are within that slab and converts the volume density of dopant, $d(z)$, into an areal density.

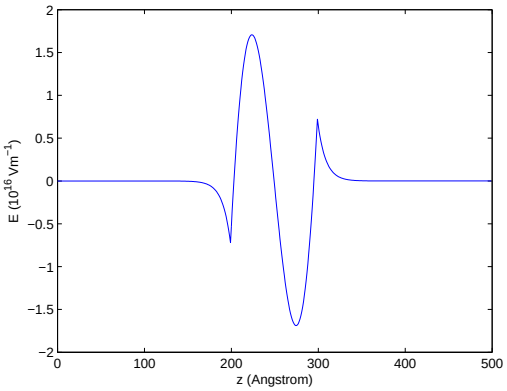


Figure 10: The electric field strength **E** due to the charge distribution shown in Fig. 9.

If the charge carriers are distributed over more than one subband, then the contribution to the charge density $\sigma(z)$ would have to be summed over the relevant subbands

$$\sigma(z) = q\left[\sum_{i=1}^{n} N_i \psi_i^*(z)\psi_i(z) - d(z)\right]\delta z, \tag{2.98}$$

where $\sum_{i=1}^{n} N_i = N$.

Fig. 9 shows the areal charge density along the growth axis for a 100 Å GaAs well, n-type doped to $2\times10^{18}cm^{-3}$, surrounded by undoped $Ga_{0.8}Al_{0.2}As$ barriers. The ionized donors yield a constant contributions to $\sigma$ within the well of $d(z)\delta z = 2\times10^{24}m^{-3}\times 1Å = 2\times10^{14}m^{-2}$, in each of the 1 Å thick slabs. Hence, the total number N of electrons in the quantum well is $100\times2\times10^{14}m^{-2} = 2\times10^{12}cm^{-2}$. By assuming that the electrons introduced by such doping all occupy the ground state of the quantum well, then the curve on top of the ionised impurity background clearly resembles $-\psi^*\psi$, as expected from the mathematics. The discontinuities in a occur at the edges of the doping profiles and are of magnitude $2\times10^{14}m^{-2}$, again as expected.

There are a number of points to note about Fig. 10, which plots the electric field strength **E** due to the charge distribution (as defined in equation 2.93) along the growth axis of the heterostructure. First, the field does reach zero at either end of the structure, which implies charge neutrality. In addition, the zero field point at the centre of the structure reflects the symmetry of the charge distribution. The electric field strength itself is not an observable, merely an intermediate quantity which can be useful to plot from time to time; the quantity which is significant is, of course, the potential due to this charge distribution. Fig. 11 plots the potential as calculated from equation 2.91, as usual defining the origin, in this case for the potential, at the effective infinity u at the left-hand edge of the barrier-well-barrier structure. Again, the symmetry of the original heterostructure and doping profiles are reflected in the symmetric potential. The potential is positive at the centre of the well since the system under consideration consists of electrons in the conduction band, so any test charge used to probe the potential is also an electron which would be repelled by the existing charge. The carrier density in this single quantum well is reasonably

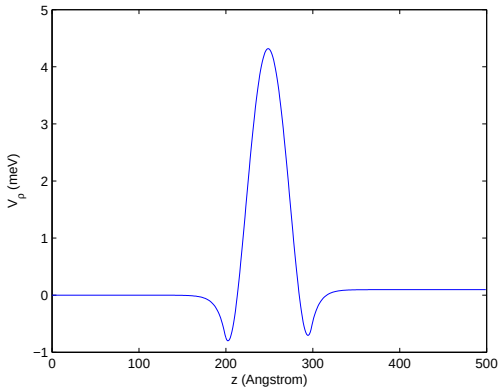


Figure 11: The potential due to the ionised donor/electron charge distribution.

high at $2 \times 10^{12} cm^{-2}$, and this produces a potential of up to $4\,meV$; while this is small compared to the conduction band offset, which is usually of the order of one or two hundred meV or more, it could still have a measurable effect on the energy eigenvalues of the quantum well.

The energy eigenvalues are calculated by considering the introduction of a further test electron into the system and incorporating the potential due to the carrier density already present into the standard Schrödinger equation, i.e. the potential term $V(z)$ in equations 2.76 becomes

$$V(z) \rightarrow V(z) + V_\rho(z), \tag{2.99}$$

where $V$ represents the band edge potential at zero doping and the potential due to the non-zero number of carriers, the charge density $\rho$, represented by the function $V_\rho$.

The numerical shooting method, described in detail earlier in this chapter, can be used without alteration to solve for this new potential, which will thus yield new energies and wave functions. The latter is an important point since the potential due to the charge distribution is itself dependent on the wave functions. Therefore, it is necessary to form a closed loop solving Schrodinger's equation, calculating the potential due to the resulting charge distribution, adding it to the original bandedge potential, solving Schrödinger's equation again, and so on - a process illustrated schematically in Fig. 12. The process is repeated until the energy eigenvalues converge; at this point the wave functions are simultaneously solutions to both Schrodinger's and Poisson's equations—the solutions are described as *self-consistent.* The numerical implementation details of the self-consistent Schrödinger-Poisson model is presented in Appendix C.

Figure 13 shows the result of adding the potential due to the charge distribution $V_\rho$, as displayed in Fig. 11, to the original band-edge potential for the single quantum well. The perturbation, even at this relatively high carrier density of $2 \times 10^{12} cm^{-2}$, is rather small compared to the barrier height, for instance. Nonetheless it is important to calculate the effect of this perturbation on the electron energy levels by continuing with the iterative process and looking for convergence of the resulting energy solutions.

Although mention has been made of quantum well systems in which doping in the barriers leads to a spatial separations of the ions and

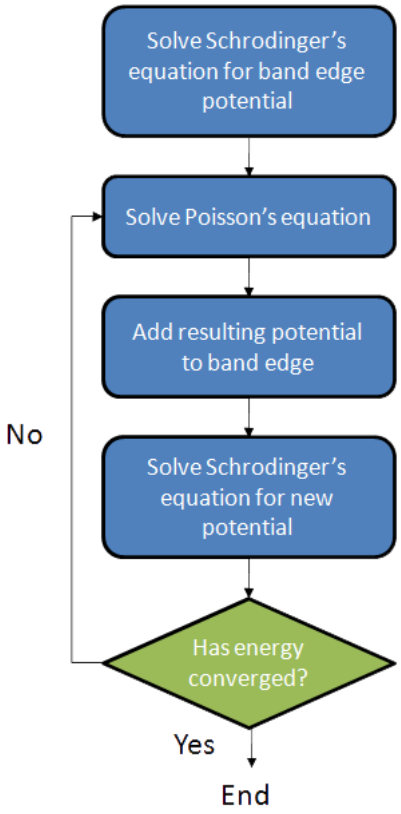


Figure 12: Block diagram illustrating the process of self-consistent iteration.

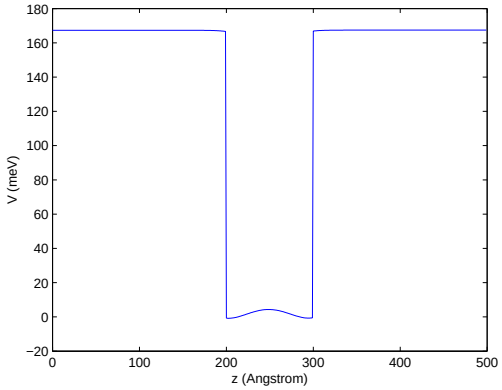


Figure 13: The sum of the band-edge potential $V_{CB}$ and Poisson's potential $V_\rho$ for single quantum well.

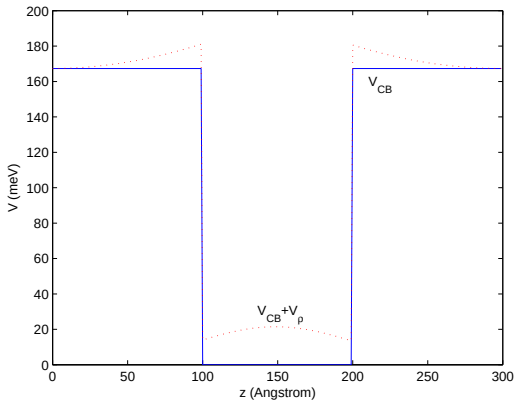


Figure 14: The band-edge potential (solid blue) and the self-consistent potential (dotted red) of a modulation-doped single quantum well.

charge carriers, which collect in a quantum well, quantitative calculations presented thus far have not considered these modulation-doped systems. Fig. 14 shows the band-edge potential, $V_{CB}$, and the self-consistent potential, $V_{CB} + V_\rho$, for a system with. an undoped single quantum well surrounded by doped barriers; with the full layer definition thus being: 100 Å $Ga_{0.8}Al_{0.2}As$ doped n-type to $2 \times 10^{17} cm^{-3}$; 100 Å GaAs undoped; 100 Å $Ga_{0.8}Al_{0.2}As$ doped n-type to $2 \times 10^{17} cm^{-3}$.The electrons introduced into the system are physically separated from the ionised donors, so therefore instead of an ion/charge carrier plasma, the mobile charge in this case is often referred to as a *two-dimensional (2D) electron gas*. The physical separation leads to a reduction in the ionised impurity scattering and hence increased electron mobilities for in-plane $(x - y)$ transport, a feature which is exploited in High-Electron- Mobility Transistors (HEMTs).

Add here the calculation for a delta doped structure

# 3 FREE CARRIERS OPTICAL TRANSITIONS

Absorption and emission of photons in semiconductors and semiconductor nanostructures is the result of the complex interaction between light and condensed matter, i.e. photons, electrons, and ions. In order to capture the physics behind these processes, electromagnetism and quantum mechanics have to be combined, leading to a multitude of physical phenomena. This thesis focuses on the static properties of nanostructures, such as the constant emmision or absorption of light. Therefore, the theory will be treated within the time-independent limit. The theory here is formulated within the classical limit of optical transitions, where the quantum-mechanically treated carriers couple to a classical electromagnetic field. The resulting equations are famous and denoted as *semiconductor-Bloch equations* Haug and Koch [29]. These equations have been used successfully over decades to describe optical properties within semiconductors. A fully consistent treatment of the light-emission would in principle require to work in a fully quantized picture (see the review Kira et al. [33]), leading to the *semiconductor-luminescence equations*. Such a treatment is beyond the scope of this thesis. The derivation presented here serves to illustrate the imposed approximations and to clearly document the implemented equations for nanostructures of any dimensionality using the electronic structure obtained via the $\mathbf{k}\cdot\mathbf{p}$ envelope equations. This theory review is based mainly on Chuang [19], Jackson [30], Chow and Koch [17**?** ], Haug and Koch [29].

The chapter is organized as follows. The first section covers the transformation of the crystal Hamiltonian 2.8 into the second quantization. Then, the representation will be rewritten in terms of the Bloch states, with a particular focus on the details arising when electronic states obtained using the $\mathbf{k}\cdot\mathbf{p}$ envelope function method are used. In the present chapter, the Coulomb interaction will be excluded and thereby, only transitions between free carriers will be considered. Coulomb-correlated transitions will be treated in Chapter 4.

The second section introduces the classical (monochromatic) light field and the self-consistent coupling to the electrons within the semiconductor nanostructure. The resulting equations allow to calculate the optical susceptibility and therefrom absorption, stimulated emission and refractive index change. The third section briefly explains how spontaneous emission can be obtained from optical susceptibility. The fourth section covers the procedure to calculate required matrix elements from wavefunctions obtained using the $\mathbf{k}\cdot\mathbf{p}$ envelope equations.

## 3.1 SECOND QUANTIZATION

### 3.1.1 *Introduction*

The electrons are fermions and consequently their wavefunction must be antisymmetric to obey the Pauli exclusion principle. But instead of using a complicated expression for the antisymmetric wavefunction, restricted to a constant number of particles, the Hamiltonian can be formulated

in the second quantization that allows to include a varying number of particles and maintain the antisymmetry of the wavefunction naturally. Starting with the Hamiltonian 2.8 and separating the interaction with the external electromagnetic field leads to

$$\begin{aligned} H &= \underbrace{\sum_i \left( \frac{\mathbf{p}_i^2}{2m_0} + U(\mathbf{r}_i) \right)}_{H_1} + \underbrace{\sum_i \left( \frac{e}{m_0} \mathbf{A}_i \cdot \mathbf{p}_i + \frac{e^2}{2m_0} \mathbf{A}_i^2 \right)}_{H_{e-EM}} \\ &\quad + \underbrace{\frac{1}{2} \sum_{i,j} \frac{e^2}{4\pi\epsilon_0 \left| \mathbf{r}_i - \mathbf{r}_j \right|}}_{H_2} . \end{aligned} \tag{3.1}$$

Here the pure electro-magnetic Hamiltonian $H_{EM}$ has been dropped as it constitutes within the present theory only an additional energy. Let $\varphi_n$ be the eigenstates of the single particle Hamiltonian $H_1$

$$H_1 \varphi_n = E \varphi_n \tag{3.2}$$

with resulting energies and wavefinctions. Next, the vacuum ground state $|0\rangle$ and creation and annihilation operators $\hat{a}_n^\dagger$ and $\hat{a}_n$ are introduced. These operators create and destroy a particle with $\varphi_n$ and therefore act on the state

$$\hat{a}_n^\dagger |0\rangle = |1_n\rangle , \ \hat{a}_n |1_n\rangle = |0\rangle , \ \hat{a}_n |0\rangle = 0, \ \hat{a}_n^\dagger |1_n\rangle = 0. \tag{3.3}$$

The state span an Hilbert space of varying number of particles termed as the *Fock space*. The Fock space $\mathcal{F}$ can be defined in terms of the direct sum of N-particle Hilbert spaces $\mathcal{H}_N$

$$\mathcal{F} = \mathcal{H}_0 + \mathcal{H}_1 + \mathcal{H}_2 + \dots$$

The antisymmetry of the state is preserved by the fermion commutation rule

$$\left[ \hat{a}_n^\dagger, \hat{a}_{n'} \right]_+ = \hat{a}_n^\dagger \hat{a}_{n'} + \hat{a}_{n'} \hat{a}_n^\dagger = \delta_{nn'} \tag{3.4}$$

and

$$[\hat{a}_n, \hat{a}_{n'}]_+ = \left[ \hat{a}_n^\dagger, \hat{a}_{n'}^\dagger \right]_+ = 0. \tag{3.5}$$

A valuable tool to transfer the Hamiltonian 3.1 (or any other operator) into second quantization representation is given by the electron field operator

$$\hat{\Phi}(\mathbf{r}, t) = \sum_n \varphi_n(\mathbf{r}) \hat{a}_n(t). \tag{3.6}$$

Here, we switch from the Schrödinger to the Heisenberg picture. For an operator $A$ in the Schrödinger picture, the corresponding operator in the Heisenberg picture is given by

$$A_H = e^{iHt/\hbar} A e^{-iHt/\hbar}, \tag{3.7}$$

where $H$ is the Hamilton operator. As the Heisenberg picture will be generally used, the time-dependence of the operators is dropped from now on.

#### 3.1.1.1 *Single Particle Hamiltonian*

Using the field operator $\hat{\Phi}(\mathbf{r})$, the representation of the single-particle Hamiltonian $H_1$ in second quantization is given by

$$\begin{aligned}\hat{H}_1 &= \int d\mathbf{r}\hat{\Phi}^\dagger(\mathbf{r})H_1\hat{\Phi}(\mathbf{r}) \\ &= \sum_{j,k}\hat{a}_j^\dagger\hat{a}_k\int d\mathbf{r}\varphi_j^* H_1\varphi_k \\ &= \sum_j \hat{a}_j^\dagger\hat{a}_j E_j,\end{aligned} \tag{3.8}$$

which is diagonal as $\varphi_n$ is assumed to be an eigenfunction of $H_1$. The representation in terms of second quantization could also be performed using another basis of the single-particle Hilbert space, but then 3.8 would not be diagonal in $jk$. Another detail is that here, the first quasi-particle, a particle occupying the eigenstates of the single particle Hamiltonian $H_1$, has been introduced.

#### 3.1.1.2 *Two Particle Hamiltonian: Coulomb Interaction*

The transformation of the two-particle interaction, the Coulomb term $H_2$, is similar, but more complicated. The result of the expansion is

$$\hat{H}_2 = \frac{1}{2}\sum_{j,k,l,m}\langle jk \mid \nu \mid lm\rangle\,\hat{a}_j^\dagger\hat{a}_k^\dagger\hat{a}_l\hat{a}_m. \tag{3.9}$$

The matrix element $\langle jk \mid \nu \mid lm\rangle$ is given by

$$\langle jk \mid \nu \mid lm\rangle = \int d\mathbf{r}d\mathbf{r}'\varphi_j^*(\mathbf{r})\varphi_k^*(\mathbf{r}')\frac{e^2}{4\pi\epsilon_0|\mathbf{r}-\mathbf{r}'|}\varphi_m(\mathbf{r})\varphi_l(\mathbf{r}'). \tag{3.10}$$

Note that the $m$ and the $l$ are swapped in the integral compared to the annihilation and creation operators and that in $\langle jk \mid \nu \mid lm\rangle$, the spin variable must be included, so

$$\langle jk \mid \nu \mid lm\rangle \to \delta_{s_j s_m}\delta_{s_k s_l}\langle jk \mid \nu \mid lm\rangle.$$

#### 3.1.1.3 *Particle – Electromagnetic Field Interaction Hamiltonian*

The next Hamiltonian to quantize is the electron–EM field interaction Hamiltonian $H_{e=EM}$ defined in 3.1. It is clear that $H_{e=EM}$ is a one-particle Hamiltonian and therefore its representation in the second quantization is obtained by applying the field operators as in 3.8, with the difference that $\varphi_n$ is diagonal in $H_1$ but not in $H_{e=EM}$. The resulting expression reads

$$\hat{H}_{e-EM} = \sum_{j,k}\left(\frac{e}{m_0}\langle j \mid \mathbf{A}\cdot\mathbf{p} \mid k\rangle + \frac{e^2}{2m_0}\left\langle j \mid \mathbf{A}^2 \mid k\right\rangle\right)\hat{a}_j^\dagger\hat{a}_k. \tag{3.11}$$

To simplify the Hamiltonian and in order to get rid of the vector potential $\mathbf{A}$ in favor of the electric field $\mathbf{E} = -\frac{\partial}{\partial t}\mathbf{A}$ (Coulomb gauge

assumed as before), the *dipole approximation* can be applied. As the crystal is a quasi-periodic structure, where the periodicity is much smaller than the photon wavelength of usual electromagnetic fields, the electric field can be assumed to be constant within the range of a lattice cell. This approximation removes the spatial dependence of $\mathbf{A}$ and reduces the second term $\langle j \mid \mathbf{A}^2 \mid k \rangle$ to a contribution diagonal in $j, k$, and is therefore proportional to the number of electrons and does not contribute to any interband transitions. Therefore, it can be treated as an additional energy constant and thus be neglected. The remaining term, $\frac{e}{m_0} \langle j \mid \mathbf{A} \cdot \mathbf{p} \mid k \rangle$ is more difficult to simplify and thus a simplified argument is brought here, while the full justification can be found in **?** ]. The first step is to relate the momentum matrix element $\mathbf{p}$ and the dipole transition matrix element $\mathbf{r}$. The relation is given by

$$[\mathbf{r}, H_1] = \frac{i\hbar}{m_0}\mathbf{p}, \tag{3.12}$$

where $H_1$ is the single particle Hamiltonian. Thus, the second term in 3.11 can transformed into

$$\begin{aligned} \frac{e}{m_0} \langle j \mid \mathbf{A} \cdot \mathbf{p} \mid k \rangle &= \mathbf{A} \cdot \frac{e}{i\hbar} \langle j \mid [\mathbf{r}, H_1(\mathbf{r})] \mid k \rangle \\ &= \mathbf{A} \cdot \frac{e}{i\hbar} \langle j \mid \mathbf{r} H_1(\mathbf{r}) - H_1(\mathbf{r})\mathbf{r} \mid k \rangle \\ &= \mathbf{A} \cdot \frac{e}{i\hbar} \langle j \mid \mathbf{r} \mid k \rangle \left(E_k - E_j\right) \\ &= -\frac{i}{\hbar} \left(E_k - E_j\right) \mathbf{A} \cdot \langle j \mid \mathbf{d} \mid k \rangle , \end{aligned} \tag{3.13}$$

where $\mathbf{d} = -e\mathbf{r}$ is the dipole moment. The last step involved adding the term $\mathbf{d}_{j,k} \cdot \mathbf{E} - \mathbf{d}_{j,k} \cdot \mathbf{E}$, which with the defintion of $\mathbf{E}$ gives

$$\frac{e}{m_0} \langle j \mid \mathbf{A} \cdot \mathbf{p} \mid k \rangle = -\mathbf{d}_{j,k} \cdot \mathbf{E} - \left(\frac{\hbar}{i}\frac{\partial}{\partial t} + E_j - E_k\right) \mathbf{A} \cdot \mathbf{d}_{j,k}. \tag{3.14}$$

If $\mathbf{A}$ is given by a plane wave $\mathbf{A}_0 e^{i(\omega_0 t - k_0 r)}$ with center fraquency $\omega_0$ and the transition energies $E_k - E_j$ are ranged around $\hbar\omega_0$, the expression in the brackets vanished and the sipole approxiamtion for the Hamiltonian is obtained,

$$\hat{H}_{e-EM} = -\sum_{j,k} \langle j \mid \mathbf{d} \cdot \mathbf{E} \mid k \rangle \, \hat{a}_j^\dagger \hat{a}_k. \tag{3.15}$$

The final Hamiltonian for the crystal electrons 3.1, cand therefore be written as

$$\hat{H} = \sum_{j,k} \langle j \mid H_1 \mid k \rangle \, \hat{a}_j^\dagger \hat{a}_k + \frac{1}{2} \sum_{j,k,l,m} \langle jk \mid v \mid lm \rangle \, \hat{a}_j^\dagger \hat{a}_k^\dagger \hat{a}_l \hat{a}_m - \sum_{j,k} \langle j \mid \mathbf{d} \cdot \mathbf{E} \mid k \rangle \, \hat{a}_j^\dagger \hat{a}_k. \tag{3.16}$$

### 3.1.2 *Bloch States Formulation*

Up to now, we have ignored the specific form of the wavefunction $\varphi_n$. Here we consider the wavefunction to be a Bloch function, as presented

in Chapter the electronic states structure . Within a bulk crystal, the Bloch function is given by

$$\varphi_{nk}(\mathbf{r}) = u_{nk}(\mathbf{r})e^{i\mathbf{k}\cdot\mathbf{r}}, \tag{3.17}$$

where $u_{nk}(\mathbf{r})$ is lattice periodic and the exponential term is slowly varying. The current section aims now to transform 3.16 into Bloch states, which needs some clarifications and definitions.

The Bloch-functions are required to be orthonormalized over the crystal domain $\Omega$

$$\int_{\Omega} d\mathbf{r}\varphi^*_{n'\mathbf{k}'}\varphi_{n\mathbf{k}} = \delta_{n',n}\delta_{\mathbf{k}',\mathbf{k}}. \tag{3.18}$$

The goal now is to represent the Hamiltonian 3.16 using the field operator

$$\hat{\Phi}(\mathbf{r},t) = \sum_{n,\mathbf{k}} \varphi_{n\mathbf{k}}\hat{a}_{n\mathbf{k}}(t) \tag{3.19}$$

in terms of the Bloch-functions. As the Bloch-states are not localized, the Fourier transform of certain quantities (such as the electromagnetic field or the Coulomb interaction) in the translational invariant directions will be used to simplify the Hamiltonian. For the spatial Fourier transform, the conventions are given by

$$w(\mathbf{r}) = \sum_{\mathbf{q}} w(\mathbf{q})e^{i\mathbf{q}\cdot\mathbf{r}}, \tag{3.20}$$

$$w(\mathbf{q}) = \frac{1}{\mathcal{A}}\int_{\mathcal{A}} d\mathbf{r}w(\mathbf{r})e^{-i\mathbf{q}\cdot\mathbf{r}}. \tag{3.21}$$

#### 3.1.2.1 *Normalization*

In the case of a quantum nanostructure, the Bloch function loses it's plane wave dependence in the quantized direction and is therefore expressed as

$$\varphi_{n\mathbf{k}}(\mathbf{r},z) = |n\mathbf{k}\rangle = u_{n\mathbf{k}}(\mathbf{r},z)e^{i\mathbf{k}\cdot\mathbf{r}}F_{n\mathbf{k}}(z). \tag{3.22}$$

The free direction is represented by the plane-wave and the symmetry broken part by $F(z)$. The indices $n$ now include the subbands. In the following, the coordinate $z$ will be used for the symmetry broken direction while $\mathbf{r}$ will denote the translational invariant direction.

Regarding the normalization, it is assumed that $\mathcal{A}$ is the volume of the translational invariant direction and $\mathcal{L}$ is the volume of the quantized direction. Obviously, $\Omega = \mathcal{L}\mathcal{A}$. 3.18 is still required to hold, but the normalization over the translational invariant direction is distributed into the lattice periodic part $u_{n\mathbf{k}}(\mathbf{r},z)$. The envelope function $F(z)$ is then normalized over the quantized direction. Therefore, for a system quantized in $d$ dimensions, the units of the wavefunction parts are given by

$$\underbrace{\varphi_{n\mathbf{k}}(\mathbf{r},z)}_{\frac{1}{\sqrt{m^3}}=\frac{1}{\sqrt{\Omega}}} = \underbrace{u_{n\mathbf{k}}(\mathbf{r},z)}_{\frac{1}{\sqrt{m^{3-d}}}=\frac{1}{\sqrt{\mathcal{A}}}} e^{i\mathbf{k}\cdot\mathbf{r}} \underbrace{F_{n\mathbf{k}}(z)}_{\frac{1}{\sqrt{m^d}}=\frac{1}{\sqrt{\mathcal{L}}}}. \tag{3.23}$$

#### 3.1.2.2 *Lattice-Cell Average*

A general problem of the approach using wavefunctions of the $\mathbf{k}\cdot\mathbf{p}$ envelope equation is that the lattice-periodic functions $u_{n\mathbf{k}}(\mathbf{r},z)$ are not given in an explicit form. Only their symmetry properties, the fact that they are orthogonal to each other and some measurable quantities are available. Nevertheless, these properties are sufficient for building the Hamiltonian and calculating desired matrix elements, within the approximation that lattice-cell averaged quantities are used. In the $\mathbf{k}\cdot\mathbf{p}$ method, the envelopes and plane waves are assumed to vary little over a crystal cell. If an operator $A$ mainly acts on the lattice-periodic part, a matrix element between two wavefunctions 3.22 can be simplified as

$$\langle n'\mathbf{k}' \mid A \mid n\mathbf{k}\rangle \approx \frac{\mathcal{A}}{V_c}\langle u_{n'\mathbf{k}'} \mid A \mid u_{n\mathbf{k}}\rangle_{V_c}\,\delta_{k',k}\int dz F^*_{n'\mathbf{k}'}(z)F_{n\mathbf{k}}(z). \tag{3.24}$$

Here the operator $A$ is replaced with it's lattice averaged quantity

$$V_c^{-1}\langle u_{n'\mathbf{k}'} \mid A \mid u_{n\mathbf{k}}\rangle_{V_c}.$$

$V_c$ denotes the crystal cell and $\langle\rangle_{V_c}$ the integration over it. The matrix elements found in the literature are related by

$$\frac{\mathcal{A}}{V_c}\langle u_{n'\mathbf{k}'} \mid A \mid u_{n\mathbf{k}}\rangle_{V_c} = \langle \tilde{u}_{n'\mathbf{k}'} \mid A \mid \tilde{u}_{n\mathbf{k}}\rangle \tag{3.25}$$

where $\tilde{u}_i$ is the Bloch function normalized with respect to a single crystal cell. Therefore to determine values for the short-range operator $\langle n'\mathbf{k}' \mid A \mid n\mathbf{k}\rangle$, only the envelope function $F_{n\mathbf{k}}(z)$ and the experimental value for $\langle \tilde{u}_{n'\mathbf{k}'} \mid A \mid \tilde{u}_{n\mathbf{k}}\rangle$ for the from bulk measurements are required.

The other case is given by the long-range operator $B$, such as the Coulomb potential. In that case, the operator is constant over a lattice cell and the integral of the matrix element can be reduced using the orthogonality of the Bloch functions. The lattice-cell average reads

$$\begin{aligned}\langle n'\mathbf{k}' \mid B \mid n\mathbf{k}\rangle &= \int_\Omega d\mathbf{r}dz u^*_{n'\mathbf{k}'}(\mathbf{r},z)e^{-i\mathbf{k}'\cdot\mathbf{r}}F^*_{n'\mathbf{k}'}(z)Bu_{n\mathbf{k}}(\mathbf{r},z)e^{i\mathbf{k}\cdot\mathbf{r}}F_{n\mathbf{k}}(z)\\ &\approx \int_\Omega d\mathbf{r}dz\frac{1}{V_c}\langle u_{n'\mathbf{k}'} \mid u_{n\mathbf{k}}\rangle_{V_c}\,e^{-i\mathbf{k}'\cdot\mathbf{r}}F^*_{n'\mathbf{k}'}Bu_{n\mathbf{k}}(\mathbf{r},z)e^{i\mathbf{k}\cdot\mathbf{r}}F_{n\mathbf{k}}(z)\end{aligned} \tag{3.26}$$

A further simplification depends on the actual form of the considered operator.

#### 3.1.2.3 *The Kinetic Term*

To transform the kinetic part into the Bloch states, the eigenfunctions $\varphi_{n\mathbf{k}}(\mathbf{r},z)$ of the single particle Hamiltonian are inserted into the field operator. Using that particular field operator, the kinetic term 3.16 is given by

$$\hat{H}_1 = \sum_{n,\mathbf{k}}\hat{a}^\dagger_{n\mathbf{k}}\hat{a}_{n\mathbf{k}}E_{n,\mathbf{k}}. \tag{3.27}$$

#### 3.1.2.4 *The Interaction Term*

The remaining step is to quantize the electron - electromagnetic field interaction Hamiltonian $H_{e-EM}$ within the dipole approximation. The Fourier representation of the electric field $\mathbf{E}(\mathbf{r}, t)$ is given by

$$\mathbf{E}(\mathbf{r}, t) = \sum_{\mathbf{q}} \mathbf{E}(\mathbf{q}, t) e^{i\mathbf{q}\cdot\mathbf{r}}. \tag{3.28}$$

As it is assumed that $\mathbf{E}(\mathbf{r}, t)$ is slowly-varying, the relevant contributions to the sum will be around very small values of $\mathbf{q}$. This allows to pull the $e^{i\mathbf{q}\cdot\mathbf{r}}$ factor out of the dipole integral in the calculation below. The resulting Hamiltonian then reads

$$\begin{aligned}
&\int_{\Omega} d\mathbf{r}dz \hat{\Phi}^{\dagger} H_{e-EM} \hat{\Phi} \\
= & - \sum_{n',\mathbf{k}',n,\mathbf{k}} \hat{a}^{\dagger}_{n'\mathbf{k}'} \hat{a}_{n\mathbf{k}} \int_{\Omega} d\mathbf{r}dz \varphi^{*}_{n'\mathbf{k}'} \mathbf{d} \cdot \left( \sum_{\mathbf{q}} \mathbf{E}(\mathbf{q}, t) e^{i\mathbf{q}\cdot\mathbf{r}} \right) \varphi_{n\mathbf{k}} \\
= & - \sum_{n',\mathbf{k}',n,\mathbf{k}} \sum_{\mathbf{q}} \delta_{\mathbf{k}'\mathbf{k}} \boldsymbol{\mu}_{n'n,\mathbf{k}} \cdot \mathbf{E}(\mathbf{r}, t) e^{i\mathbf{q}\cdot\mathbf{r}},
\end{aligned}$$

where the dipole matrix element between two states $n$ and $nt'$ with same crystal momentum $k$ is given by

$$\boldsymbol{\mu}_{n'n,\mathbf{k}} = \mathcal{A} \int_{\mathcal{L}} dz u^{*}_{n'\mathbf{k}} F^{*}_{n'\mathbf{k}} \mathbf{d} u_{n\mathbf{k}} F_{n\mathbf{k}}. \tag{3.29}$$

The delta function $\delta_{\mathbf{k}'\mathbf{k}}$ results from the plane wave and ensures momentum conservation. In other words, only direct transitions are allowed. Using the dipole matrix element, the Hamiltonian can finally be written as

$$\hat{H}_{e-EM} = -\mathbf{E}(\mathbf{r}, t) \sum_{n',n,\mathbf{k}} \boldsymbol{\mu}_{n',n,\mathbf{k}} \hat{a}^{\dagger}_{n'\mathbf{k}} \hat{a}_{n\mathbf{k}}. \tag{3.30}$$

The transformation of the two particle Hamiltonian $H_2$ is presented in the next chapter. For the moment, it is assumed that the carriers are *uncorrelated* and their coulomb interaction is included in the single particle Hamiltonians. Collecting all single particle interactions, the Hamiltonian in the Bloch basis is given as

$$\hat{H} = \sum_{n} E_n(\mathbf{k}) \hat{a}^{\dagger}_{n\mathbf{k}} \hat{a}_{n\mathbf{k}} - \mathbf{E}(\mathbf{r}, t) \sum_{n',n,\mathbf{k}} \boldsymbol{\mu}_{n',n,\mathbf{k}} \hat{a}^{\dagger}_{n'\mathbf{k}} \hat{a}_{n\mathbf{k}}. \tag{3.31}$$

### 3.1.3 *Holes*

In a semiconductor at $T = 0K$, the valence band is fully occupied while the conduction band is empty. With increasing temperature, electrons in the valence band get excited into the conduction band and leave behind holes. Consequently, it is common to use for the valence band the absence of an electron, the hole, as a quasi particle. Therefore, if an electron with momentum $=\mathbf{k}$ is created ($= \hat{a}^{\dagger}_{-\mathbf{k}}$), a hole with momentum $\mathbf{k}$ is annihilated ($= \hat{b}_{\mathbf{k}}$) and vice versa. The sign is switched by convention. In order to introduce the concept of holes into the Hamiltonian, the commutator rules 3.4 and 3.5 are used to reestablish

the normal ordering of creation and annihilation operators. One obtains for the kinetic and dipole Hamiltonian

$$\begin{aligned}\hat{H} &= \sum_{c,\mathbf{k}} E_c(\mathbf{k})\hat{a}^\dagger_{c\mathbf{k}}\hat{a}_{c\mathbf{k}} - \sum_{v,\mathbf{k}} E_v(\mathbf{k})\hat{b}^\dagger_{b\mathbf{k}}\hat{b}_{b\mathbf{k}} \\ &\quad -\mathbf{E}(\mathbf{r},t)\left(\sum_{c,v,\mathbf{k}} \mu_{cv,\mathbf{k}} \underbrace{\hat{a}^\dagger_{c\mathbf{k}}\hat{b}^\dagger_{v-\mathbf{k}}}_{\hat{p}^\dagger_{vc,\mathbf{k}}} + \mu^*_{cv,\mathbf{k}} \underbrace{\hat{b}_{v-\mathbf{k}}\hat{a}_{c\mathbf{k}}}_{\hat{p}_{vc,\mathbf{k}}}\right). \end{aligned} \tag{3.32}$$

Note that from now on, the summation is distinguished between summation over conduction bands indicated with c and valence bands indicated using the index $v$. In 3.32, transitions between conduction subbands and transitions between valence subbands have been neglected.

One important point is that in the Hamiltonian 3.32, some terms can already be identified: $\hat{n}_{c\mathbf{k}} = \hat{a}^\dagger_{c\mathbf{k}}\hat{a}_{c\mathbf{k}}$ is the number operator counting the number of electrons in the band c with crystal momentum $\mathbf{k}$, while $\hat{n}_{v\mathbf{k}} = \hat{b}^\dagger_{b-\mathbf{k}}\hat{b}_{b-\mathbf{k}}$ is the number operator counting the holes in the valence band $v$. The term $\hat{p}_{vc,\mathbf{k}} = \hat{b}_{v-\mathbf{k}}\hat{a}_{c\mathbf{k}}$ is named *microscopic polarization* and is given by the off-diagonal density matrix element, giving the correlation between a particle in one band and an empty state in the other. In a simplistic view, the dipole matrix element $\mu_{cv,\mathbf{k}}$ gives the coupling strength of such a correlation to an electric field.

### 3.1.4 *Carrier Statistics*

The main interest of the current work is the continuous emission of light of a semiconductor, which is given in the steady state of the system. In the limit of small light intensity and therefore absence of spectral-hole burning, it can be assumed that the carriers relax into their quasi-equilibrium distributions, given by the Fermi distributions for the electrons in the conduction band

$$n_{c\mathbf{k}} = \langle \hat{n}_{c\mathbf{k}} \rangle = f_{c\mathbf{k}} = \frac{1}{1 + e^{(E_c(\mathbf{k}) - E_{F,c})/k_B T}} \tag{3.33}$$

and the holes in the valence band

$$n_{v\mathbf{k}} = \langle \hat{n}_{v\mathbf{k}} \rangle = f_{v\mathbf{k}} = \frac{1}{1 + e^{(E_{F,v} - E_v(\mathbf{k}))/k_B T}}. \tag{3.34}$$

Here, $E_{F,c}$ and $E_{F,v}$ denote the quasi-Fermi levels of the electrons and holes, $k_B$ is Boltzmann's constant and T denotes the temperature. The Fermi levels can be calculated from the 3D carrier density N

$$N = \frac{1}{\Omega}\sum_{c\mathbf{k}} f_{c\mathbf{k}} \tag{3.35}$$

for electrons and P

$$P = \frac{1}{\Omega}\sum_{v\mathbf{k}} f_{v\mathbf{k}} \tag{3.36}$$

for holes. Here $\Omega$ denotes the volume of the system, which is usually unknown. When the sum over $\mathbf{k}$ is transformed into an integral

$$\sum_{\mathbf{k}} \rightarrow \frac{\mathcal{A}}{(2\pi)^d} \int d\mathbf{k} \tag{3.37}$$

the unknown $\Omega$ volume is removed and one ends up with known quantities ($\mathcal{L} = \Omega/\mathcal{A}$). $d$ denotes the dimensionality of the $\mathbf{k}$-space. As the $\mathbf{k}$ dependence of the distributions for general band structures is quite evolved, an analytical inversion of 3.35 and 3.36 is not feasible. Therefore, the simplest way to calculate the quasi-Fermi levels is to perform a numerical Newton procedure to find the roots of $N_0{=}N(E_F) = 0$.

## 3.2 TRANSITIONS CALCULATION

### 3.2.1 *Introduction*

Classically, an electric field $\mathbf{E}$ in a semiconductor induces dipoles. These dipoles create a macroscopic polarization $\mathbf{P}$. The induced polarization $\mathbf{P}(t)$ at time $t$ depends on the electric field $\mathbf{E}(t')$ at time $t' < t$. Their relation is defined in terms of a time-dependent susceptibility $\chi(t-t')$ (in this case a scalar)

$$\mathbf{P}(t) = \epsilon_b \int_{\infty}^{t} \chi(t-t')\mathbf{E}(t')dt'. \tag{3.38}$$

Taking the Fourier transform of 3.38 leads to the more convenient form

$$\mathbf{P}(\omega) = \epsilon_b \chi(\omega)\mathbf{E}(\omega). \tag{3.39}$$

The polarization influences the electric field via the electric displacement

$$\mathbf{D} = \epsilon\mathbf{E} = \epsilon_b\mathbf{E} + \mathbf{P}. \tag{3.40}$$

Therefore, the creation of dipoles and the amplification of an electric field needs to be treated self-consistently. The aim is therefore to calculate the polarization quantum-mechanically in the presence of an electric field and obtain a self-consistent formula for the steady state.

As a first step, Maxwell's equations are rewritten to give a single relation between the electric field E and the macroscopic polarization $\mathbf{P}$. Taking the curl of

$$\nabla \times \mathbf{H} - \frac{\partial \mathbf{D}}{\partial t} = \mathbf{j} \tag{3.41}$$

and using

$$\nabla \times \mathbf{E} = -\frac{\partial \mathbf{B}}{\partial t}, \tag{3.42}$$

ones obtains

$$\nabla \times \nabla \times \mathbf{E} = -\nabla \times \frac{\partial \mu_0 \mathbf{H}}{\partial t}, \tag{3.43}$$

$$\nabla(\nabla \cdot \mathbf{E}) - \nabla^2\mathbf{E} = -\mu_0 \frac{\partial}{\partial t}(\nabla \times \mathbf{H}). \tag{3.44}$$

On the left hand side, the term $\nabla \cdot \mathbf{E} = 0$ vanishes, assuming charge neutrality and homogeneous media. On the right hand side, using 3.41, $\nabla \times \mathbf{H}$ is replaced by the electric displacement $\mathbf{D}$

$$\nabla (\nabla \cdot \mathbf{E}) - \nabla^2 \mathbf{E} \approx -\nabla^2 \mathbf{E} = -\mu_0 \frac{\partial^2 \mathbf{D}}{\partial t^2}, \tag{3.45}$$

which now allows to introduce the macroscopic polarization $\mathbf{P}$ using 3.40

$$-\nabla^2 \mathbf{E} + \mu_0 \epsilon_b \frac{\partial^2 \mathbf{E}}{\partial t^2} = -\mu_0 \frac{\partial^2 \mathbf{P}}{\partial t^2}. \tag{3.46}$$

This equation is the *inhomogeneous Helmholtz equation*. The next step is to assume a monochromatic electrical field $\mathbf{E}$ (traveling into $z$-direction) given by

$$\mathbf{E}(z,t) = \frac{1}{2} \hat{e}_i E(z) e^{i(k_0 z - \nu t - \phi(z))} + \text{c.c}, \tag{3.47}$$

where $k_0 = \nu n/c$ is the photo wavenumber and $\hat{e}_i$is a unit vector orthogonal to $\hat{e}_z$. $\phi(z)$ us the real phase shift and $E(z)$ is the real field amplitude, varying little within an optical wavelength. $\nu$ denotes the field frequency. It is assumed that the spacial strong oscillatory part is properly described by the plane wave. The electric field induces a polarization

$$\mathbf{P}(z,t) = \frac{1}{2} \hat{e}_i P(z) e^{i(k_0 z - \nu t - \phi(z))} + \text{c.c.} \tag{3.48}$$

The next step is to insert 3.47 and 3.48 into 3.46 and neglect all terms containing $\partial_z^2 E(z)$, $\partial_z^2 \phi(z)$ and $\partial_z E(z) \partial_z \phi(z)$. This approach is denoted as the *slowly varying envelope approximation* and one ends up with an equation for the amplitudes $E(z)$ and $P(z)$,

$$\partial_z E(z) - i E(z) \partial_z \phi(z) = i \frac{\mu_0 \nu^2}{2k_0} \chi(z) E(z). \tag{3.49}$$

Splitting into real and imaginary parts and using 3.39, the *self consistent* equations are obtained as

$$\partial_z E(z) = -\frac{\nu}{2\epsilon_0 n c} \mathfrak{I}\{P(z)\} = -\frac{k_0}{2} \chi''(z) E(z) \tag{3.50}$$

$$\partial_z \phi(z) = -\frac{1}{E(z)} \frac{\nu}{2\epsilon_0 n c} \mathfrak{R}\{P(z)\} = -\frac{k_0}{2} \chi'(z) \tag{3.51}$$

where $\chi = \chi' + i\chi''$. Consequently, the intensity gain (amplitude is half of it) is defined by

$$G = -k_0 \chi'' \tag{3.52}$$

and the change of refractive index (via a continuous phase change) is given by the real part of the susceptibility

$$\frac{\delta n}{n} = \frac{\chi'}{2}. \tag{3.53}$$

### 3.2.2 *Quantum Microscopic Polarization*

The second step is to couple quantum mechanical observables to the solids properties. The dipole interaction between electrons and the electric field is given by

$$H_{e-EM} = -V\mathbf{P}\cdot\mathbf{E}, \tag{3.54}$$

where $V$ is the volume of the system and $\mathbf{P}$ is defined as the macroscopic polarization density

$$\mathbf{P} = \frac{1}{V}\sum_{n,n',\mathbf{k}} \mu_{n'n,\mathbf{k}} \left\langle \hat{a}^{\dagger}_{n'\mathbf{k}}\hat{a}_{n\mathbf{k}} \right\rangle = \frac{1}{V}\sum_{c,v,\mathbf{k}} \mu_{cv,\mathbf{k}} p^{\dagger}_{vc,\mathbf{k}} + \mu^{*}_{cv,\mathbf{k}} p_{vc,\mathbf{k}} \tag{3.55}$$

from which the optical properties 3.52 and 3.53 can be obtained. Here, the expectation value $p_{vc,\mathbf{k}} = \left\langle \hat{p}_{vc,\mathbf{k}} \right\rangle$ has been used. The amplitude $P(z)$ of the macroscopic polarization $\mathbf{P}(z,t)$ used for the optical properties is given by

$$P(z) = 2e^{-i(k_0 z - \nu t - \phi(z))}\frac{1}{V}\sum_{c,v,\mathbf{k}} \mu^{*}_{cv,\mathbf{k}} p_{vc,\mathbf{k}} \tag{3.56}$$

The other term of the polarization containing $p^{\dagger}_{vc,\mathbf{k}}$ is related to the complex conjugate part of 3.48 and is not required to determine the macroscopic amplitude $P(z)$.

### 3.2.3 *Heisenberg's Equation of Motion*

In order to calculate the expectation value $p_{nm,\mathbf{k}}$, the equation of motion of the microscopic polarization operator $\hat{p}_{nm,\mathbf{k}}$ has to be solved. Here the index $m$ is used for the conduction band and $n$ for the valence band of interest. The indices $c$ and $v$ will be used for the summation over remaining conduction and valence bands. The Heisenberg equation of motion for a time dependent operator $\hat{O}$ is given by

$$\frac{d}{dt}\hat{O} = \frac{i}{\hbar}\left[\hat{H}, \hat{O}\right]. \tag{3.57}$$

Applying to the microscopic polarization operator, one obtains

$$\frac{d}{dt}\hat{p}_{nm,\mathbf{k}} = \frac{i}{\hbar}\left[\hat{H}_1, \hat{p}_{nm,\mathbf{k}}\right] + \frac{i}{\hbar}\left[\hat{H}_{e-EM}, \hat{p}_{nm,\mathbf{k}}\right]. \tag{3.58}$$

The evaluation of the first commutator gives

$$-\frac{i}{\hbar}\left(E_c(\mathbf{k}) - E_v(\mathbf{k})\right)\hat{p}_{nm,\mathbf{k}}. \tag{3.59}$$

For the second operator

$$\frac{1}{V}\sum_{c,v,\mathbf{k}'} \mu_{cv,\mathbf{k}'}\hat{p}^{\dagger}_{vc,\mathbf{k}'} + \mu^{*}_{cv,\mathbf{k}'}\hat{p}_{vc,\mathbf{k}'}, \tag{3.60}$$

the second term containing $\hat{p}_{vc,\mathbf{k}}$ vanishes because four anticommuting exchanges are required (leading to no sign change) to obtain $\hat{p}_{nm,\mathbf{k}}\hat{H} -$

$\hat{p}_{nm,\mathbf{k}}\hat{H} = 0$. Therefore, one is left with the first term, where operators are exchanged to transform $\hat{H}\hat{p}$ into $\hat{p}\hat{H}$

$$\begin{aligned}\hat{a}^{\dagger}_{c\mathbf{k}'}\hat{b}^{\dagger}_{c-\mathbf{k}'}\hat{b}_{n\mathbf{k}}\hat{a}_{m\mathbf{k}} \quad \rightarrow \quad & \hat{a}^{\dagger}_{c\mathbf{k}'}\hat{a}_{m\mathbf{k}}\delta_{\nu,n}\delta_{\mathbf{k}',\mathbf{k}} \\ & +\hat{b}^{\dagger}_{\nu-\mathbf{k}'}\hat{b}_{n-\mathbf{k}}\delta_{c,m}\delta_{\mathbf{k}',\mathbf{k}} \\ & -\delta_{\mathbf{k}',\mathbf{k}}\delta_{n,\nu}\delta_{m,c} + \hat{p}\hat{H}.\end{aligned} \tag{3.61}$$

The delta functions of the remaining terms lead in the sum over $c, \nu$ and $\mathbf{k}'$ to

$$\sum_{c}\hat{a}^{\dagger}_{c\mathbf{k}}\hat{a}_{m\mathbf{k}} + \sum_{\nu}\hat{b}_{\nu-\mathbf{k}}\hat{b}_{n-\mathbf{k}} - 1. \tag{3.62}$$

Here, the sums over $c$ and $\nu$ except for$c = m$ and $\nu = n$ will vanish when later the expectation value $\left\langle \hat{a}^{\dagger}_{c\mathbf{k}}\hat{a}_{m\mathbf{k}} \right\rangle$ is taken. Therefore, the sums are neglected from now on. This approximation scheme is called the *random phase approximation*. The hand waving argument is that the expectation value $\left\langle \hat{a}^{\dagger}_{n'\mathbf{k}'}\hat{a}_{n\mathbf{k}} \right\rangle$ has a dominant time-dependence

$$\left\langle \hat{a}^{\dagger}_{n'\mathbf{k}'}\hat{a}_{n\mathbf{k}} \right\rangle \propto e^{i(\omega_{n'\mathbf{k}'}-\omega_{n\mathbf{k}})t} \tag{3.63}$$

and therefore rapidly oscillates for $\omega_{n'\mathbf{k}'} \neq \omega_{n\mathbf{k}}$ and then averages out over time.

The terms with $c = m$ and $\nu = n$ are the density operators $\hat{n}_{m\mathbf{k}}$ and $\hat{n}_{n\mathbf{k}}$. Collecting everything and taking the expectation values, the equation of motion of the free carrier microscopic polarization is

$$\begin{aligned}\frac{d}{dt}p_{nm,\mathbf{k}} \quad = \quad & -\frac{i}{\hbar}\left(E_m(\mathbf{k}) - E_n(\mathbf{k})\right)p_{nm,\mathbf{k}} \\ & -\frac{i}{\hbar}\mathbf{E}(z,t)\cdot\boldsymbol{\mu}_{mn,\mathbf{k}}\left(n_{m\mathbf{k}} + n_{n\mathbf{k}} - 1\right) \\ & + \frac{\partial}{\partial t}p_{nm,\mathbf{k}}\Big|_{col.}.\end{aligned} \tag{3.64}$$

This equation is part of the *semiconductor Bloch equations*. The last term is added as an additional term leading to polarization decay, caused by scattering. Scattering here is a electron-phonon or electron-electron process which requires a more sophisticated treatment. For the moment, scattering is approximated using a a simple decay rate model given by

$$\frac{\partial}{\partial t}p_{nm,\mathbf{k}}\Big|_{col.} \approx -\gamma p_{nm,\mathbf{k}}. \tag{3.65}$$

### 3.2.4 *Solving the Free Carrier Equation*

To solve 3.64 one could use the approach given in 17 and formally integrate the differential equation. A simpler way is to replace the oscillating microscopic polarization $p_{nm,\mathbf{k}}$ by its slowly varying envelope

$$s_{nm,\mathbf{k}} = p_{nm,\mathbf{k}}e^{-i(k_0 z - \nu t - \phi(z))} \tag{3.66}$$

and solve for the steady state of

$$\frac{d}{dt}s_{nm,\mathbf{k}} = 0. \tag{3.67}$$

Inserting 3.66 and 3.47 into 3.64, and skipping all fast oscillating parts (as they should average out over time), leads to

$$p_{nm,\mathbf{k}} = -\frac{i}{\hbar}\frac{E(z)}{2}\mu_{mn,\mathbf{k}}\frac{n_{m\mathbf{k}} + n_{n\mathbf{k}} - 1}{i(\omega - \nu) + \gamma}e^{-i(k_0 z - \nu t - \phi(z))}. \quad (3.68)$$

Inserting this equation into 3.52 we obtain the amplification of the light field intensity

$$G = -k_0\chi'' = \frac{\nu}{\epsilon_0 n_b c}\frac{1}{\hbar}\frac{1}{\Omega}\sum_{c,v,\mathbf{k}}\left|\mu_{cv,\mathbf{k}}\right|^2 (n_{c\mathbf{k}} + n_{v\mathbf{k}} - 1)\frac{\gamma}{(\omega - \nu)^2 + \gamma^2}. \quad (3.69)$$

Here, the$\mu_{cv,\mathbf{k}}$ denotes the dipole along the polarization of the light field, resulting from the scalar product between the monochromatic light field $\mathbf{E}$ and the dipole $\boldsymbol{\mu}_{cv,\mathbf{k}}$.

## 3.3 SPONTANEOUS EMISSION

The spontaneous emission within a semiconductor nanostructure can be obtained from the amplification G of the photon field, i.e. the complex part of the optical susceptibility $\chi''$. Using a phenomenological approach, 3.69 can be divided into an emitting and an absorbing part, $G = G_e - G_a$. The term $n_{c\mathbf{k}} + n_{v\mathbf{k}} - 1$ is the inversion of the electron-hole population in the semiconductor, which can be rewritten to

$$n_{c\mathbf{k}} + n_{v\mathbf{k}} - 1 = n_{c\mathbf{k}}n_{v\mathbf{k}} - (1 - n_{c\mathbf{k}})(1 - n_{v\mathbf{k}}). \quad (3.70)$$

The first term on rhs denotes the probability of a photon emission, i.e. electron and hole is occupied, while the second term denotes the probability of a photon absorption. Therefore by evaluating 3.69 including only the emission probability term $G_e \sim n_{c\mathbf{k}}n_{v\mathbf{k}}$, the spontaneous emission probability per unit length is obtained. As the velocity of a photon in the semiconductor is given by $c/n_b$, the spontaneous emission probability per second is given by $G_e c/n_b$. Neglecting the existence of a cavity, the photon density of states (of photons with energy $\hbar\omega$) is given by

$$N(\hbar\omega) = \frac{n_b^3(\hbar\omega)^2}{\pi^2\hbar^3c^3} \quad (3.71)$$

and therefore the spontaneous emission ($s^{=1}m^{=3}eV^{=1}$) per second per unit volume per unit energy is given by

$$r_{sp}(\hbar\omega) = \frac{n_b^3(\hbar\omega)^2}{\pi^2\hbar^3c^2}G_e \quad (3.72)$$

where as the spontaneous emission intensity ($s^{=1}m^{=3}$) is given by

$$I_{sp}(\hbar\omega) = \hbar\omega r_{sp}(\hbar\omega). \quad (3.73)$$

Note that the result can be related to the Kubo-Martin-Schwinger (KMS) 40 relation. The relation between emission and inversion gives

$$\frac{f_{c\mathbf{k}}f_{v\mathbf{k}}}{f_{c\mathbf{k}} + f_{v\mathbf{k}} - 1} = \frac{1}{1 - \exp\left((E_c(\mathbf{k}) - E_v(\mathbf{k}) - (E_{Fc} - E_{Fv}))/k_BT\right)}. \quad (3.74)$$

Due to the Lorentzian in 3.69, the transition energy $E_c(\mathbf{k}) - E_v(\mathbf{k})$ is close to the photon energy. Consequently, it may be replaced with $\hbar\omega$ on the r.h.s of 3.74, which allows to pull the factor 3.74 out of the k-sum in 3.69, leading to the KMS relation

$$r_{sp}(\hbar\omega) = \frac{n_b^2(\hbar\omega)^2}{\pi^2\hbar^3c^2}\frac{1}{1-\exp\left(\left(\hbar\omega-(E_{Fc}-E_{Fv})\right)/k_BT\right)}G(\hbar\omega) \quad (3.75)$$

between gain and spontaneous emission.

Another aspect to consider is the dependence of the dipole matrix element $\mu_{cv,\mathbf{k}}$ on the polarization of the light field. Therefore, the average of all possible transitions is usually taken for the spontaneous emission

$$\mu^{sp}_{cv,\mathbf{k}} = \frac{1}{3}\sum_{i=x,y,z}\mu^{i}_{cv,\mathbf{k}}. \quad (3.76)$$

The spontaneous emission rate per unit volume ($s^{=1}m^{=3}$) is given by integrating $r_{sp}(\hbar\omega)$ over the energy

$$R_{sp} = \int_0^\infty r_{sp}(\hbar\omega)d\hbar\omega = Bnp \quad (3.77)$$

which defines another figure of merit, the spontaneous emission B coefficient ($m^3s^{=1}$).

There is an obvious pathological feature when such a relation is used to obtain the spontaneous emission: if the electric field is zero, then no spontaneous emission would exist. The root of this misbehavior is due to the fact that the quantization of the electro-magnetic field is not included. Including this, spontaneous emission would occur - spontaneously. Nevertheless, the spontaneous emission of a two level system treated using quantized electro-magnetic fields does not differ from dipole radiation, therefore the error of the classical treatment may be small enough for the present purpose.

## 3.4 DIPOLE MATRIX ELEMENT

The evaluation of the interband dipole matrix element $\boldsymbol{\mu}_{mn,\mathbf{k}}$ between the solutions of the $\mathbf{k}\cdot\mathbf{p}$ band structure calculation is not straightforward. In the general case, the envelope functions are given by

$$\varphi_{m\mathbf{k}} = \sum_i F_{m,i\mathbf{k}}u_{i0}, \quad (3.78)$$

where $u_{i0}$ are again zone-center Bloch functions. Using this expansion, the dipole matrix element between two states is given by

$$\boldsymbol{\mu}_{n'n,\mathbf{k}} = \mathcal{A}\int_{\mathcal{L}} dz \sum_{i,j} u^*_{i0}F^*_{m,i\mathbf{k}}\mathbf{d}u_{j0}F_{n,j\mathbf{k}}. \quad (3.79)$$

The question to answer is to whether the dipole operator is acting on the lattice periodic part $u_{j0}$ or on the envelope part $F_i$. The issue has been

addressed by Burt and others 14, 12, concluding that the expression is dominated by

$$\boldsymbol{\mu}_{n'n,\mathbf{k}} \approx \frac{\mathcal{A}}{V_c} \sum_{i,j} \langle u_{i0} \mid u_{j0} \rangle_{V_c} \int_{\mathcal{L}} dz F^*_{m,i\mathbf{k}} \mathbf{d} F_{n,j\mathbf{k}}. \tag{3.80}$$

But, within a $\mathbf{k} \cdot \mathbf{p}$ calculation involving only single-band models for both, conduction and valence band, the last expression evaluates due to the orthogonality of $u_{c0}$ and $u_{v0}$ to zero[1]. Therefore, no transition between conduction and valence subbands in such models would exist. The reason lies in the single-band approximation. While the wavefunction of e.g. conduction subbands is dominated by the envelope modulating $u_{c0}$, the interband dipole moment is dominated by the admixture of $u_{v0}$ into the conduction subbands and $u_{c0}$ into the valence subbands. Working within the $8 \times 8$ model would therefore resolve the problem.

A simpler solution, allowing to use non-$8 \times 8$ models without the pathological feature of vanishing transition probabilities, is to use the momentum- instead of the dipole matrix element. The relation can be derived using the Heisenberg equation of motion for the position operator $r$, given by

$$\frac{\partial}{\partial t}\mathbf{r} = \frac{i}{\hbar} [H, \mathbf{r}] . \tag{3.81}$$

Assuming that $n$ and $m$ are eigenfunctions of the Hamiltonian $H$ with corresponding eigenenergies $E_n$ and $E_m$, replacing the derivative of the position operator by the momentum operator and $H|m\rangle$ by $E_m|m\rangle$ , one obtains

$$\langle n \mid \mathbf{p} \mid m \rangle = \frac{im}{\hbar} (E_n - E_m) \langle n \mid \mathbf{r} \mid m \rangle . \tag{3.82}$$

The electron dipole operator (electrons are negatively charged) is related to the position operator by $\mathbf{d} = e\mathbf{r}$ leading to

$$\langle n \mid \mathbf{d} \mid m \rangle = e \frac{\hbar}{im} \frac{\langle n \mid \mathbf{p} \mid m \rangle}{(E_n - E_m)}. \tag{3.83}$$

Within direct transitions, the energy difference $E_n - E_m$ can be replaced by the photon energy $\hbar\omega$, leading to the simple expression for $\boldsymbol{\mu}_{mn,\mathbf{k}}$ in terms of the momentum matrix element

$$\boldsymbol{\mu}_{mn,\mathbf{k}} = \frac{e}{im\omega} \mathbf{p}_{mn,\mathbf{k}}. \tag{3.84}$$

In the approximation of slowly varying envelopes, the derivatives of the envelopes are small and the momentum matrix element is dominated by

$$\mathbf{p}_{mn,\mathbf{k}} \approx \frac{\mathcal{A}}{V_c} \sum_{i,j} \langle u_{i0} \mid \mathbf{p} \mid u_{j0} \rangle_{V_c} \int_{\mathcal{L}} dz F^*_{m,i\mathbf{k}} F_{n,j\mathbf{k}}. \tag{3.85}$$

The momentum matrix elements are related via 3.25 to band structure parameters $P$, defined e.g. in 2.31. This approximation is commonly applied and is also used in the remainder of the thesis.

1 This fact also applies to $4 \times 4$ and $6 \times 6$ $\mathbf{k} \cdot \mathbf{p}$ valence band models.

Beside the neglected derivatives of the envelopes, the approximation 3.85 neglects the effect of remote bands. 3.85 considers only transitions between zone-center functions $u_{i0}$ included explicitly in the Hamiltonian. In the $\mathbf{k} \cdot \mathbf{p}$ envelope equations, the effect of remote bands is included using Löwdins perturbation theory. Therefore, beside the mixing of the explicitly considered states in the Hamiltonian, the zone-center functions away from k include remote contributions. Consequently, transitions between remote contributions have to be included in a consistent definition of the momentum matrix elements 22.

Put here the momentum matrix calculation in the 2 band model.

# 4 COULOMB CORRELATED OPTICAL TRANSITIONS

The preceding chapter only considered free carriers and omitted their Coulomb interaction. The Coulomb interaction leads to the formation of electron-hole pairs, also denoted as *excitons*. Due to their bound nature, the transition energy is lowered, leading to absorption below the fundamental band gap, while the correlated movement of the electron-hole pair increases the transition probability and consequently the transitions strengths. As in the previous chapter, the theory review is based mainly on Chuang [19], Jackson [30], Chow and Koch [17**?** ], Haug and Koch [29].

The present chapter therefore focuses on the inclusion of such many body effects in the evaluation of optical properties. A large part of the theory presented in the preceding chapter can be recycled. In general, only the omitted two-particle interaction Hamiltonian $H_2$ in 3.9 needs to be added to the equation of motion for the microscopic polarization 3.64. The chapter is therefore structured as follows: first, the Coulomb Hamiltonian is derived for Bloch functions and transformed into the electron-hole picture. Then the Coulomb Hamiltonian is included into the equation of motion, and the so called Hartree-Fock approximation is performed along with the introduction of screening.

## 4.1 SECOND QUANTIZATION

### 4.1.1 *Introduction*

If $n_i, \mathbf{k}_i$ denote the quantum number of a Bloch state, then the Coulomb Hamiltonian 3.9 can be written as

$$\hat{H}_2 = \frac{1}{2} \sum_{n_1\mathbf{k}_1, n_2\mathbf{k}_2, n_3\mathbf{k}_3, n_4\mathbf{k}_4} \langle n_1\mathbf{k}_1 n_2\mathbf{k}_2 \mid v \mid n_3\mathbf{k}_3 n_4\mathbf{k}_4 \rangle \, \hat{a}^\dagger_{n_1\mathbf{k}_1} \hat{a}^\dagger_{n_2\mathbf{k}_2} \hat{a}_{n_3\mathbf{k}_3} \hat{a}_{n_4\mathbf{k}_4} \tag{4.1}$$

and the matrix element of the Coulomb operator reads

$$\begin{aligned} \langle n_1\mathbf{k}_1 n_2\mathbf{k}_2 \mid v \mid n_3\mathbf{k}_3 n_4\mathbf{k}_4 \rangle \quad = \quad & \frac{e^2}{4\pi\epsilon_0} \int_\Omega \int_\Omega d\mathbf{r} dz d\mathbf{r}' dz' \varphi^*_{n_1\mathbf{k}_1}(\mathbf{r}, z) \varphi^*_{n_2\mathbf{k}_2}(\mathbf{r}', z') \\ & \cdot \frac{1}{|(\mathbf{r}, z) - (\mathbf{r}', z')|} \varphi_{n_4\mathbf{k}_4}(\mathbf{r}, z) \varphi_{n_3\mathbf{k}_3}(\mathbf{r}', z'). \end{aligned} \tag{4.2}$$

The Coulomb-potential is mainly long-range and therefore more or less constant within a lattice cell. Consequently, the lattice periodic part can be averaged over a single crystal cell. The integration is then performed over lattice averaged quantities, as suggested in 3.26. Therefore, rewriting 4.2 into a more suitable form including lattice cell averages, yields

$$\begin{aligned} \langle n_1\mathbf{k}_1 n_2\mathbf{k}_2 \mid v \mid n_3\mathbf{k}_3 n_4\mathbf{k}_4 \rangle \quad = \quad & \frac{e^2}{4\pi\epsilon_0} \int_\Omega \int_\Omega d\mathbf{r} dz d\mathbf{r}' dz' \frac{1}{\mathcal{A}^2} e^{i(\mathbf{k}_4 - \mathbf{k}_1)\cdot\mathbf{r}} e^{i(\mathbf{k}_3 - \mathbf{k}_2)\cdot\mathbf{r}'} \\ & \cdot g_{n_1\mathbf{k}_1, n_4\mathbf{k}_4}(z) g_{n_2\mathbf{k}_2, n_3\mathbf{k}_3}(z') \frac{1}{|(\mathbf{r}, z) - (\mathbf{r}', z')|}, \end{aligned} \tag{4.3}$$

where $g_{n_1\mathbf{k}_1,n_4\mathbf{k}_4}(z) \approx \sum_i F^*_{n_1\mathbf{k}_1,i}(z)F_{n_4\mathbf{k}_4,i}(z)$ and $g_{n_2\mathbf{k}_2,n_3\mathbf{k}_3}(z')$ is defined accordingly. The next step is to get rid of the free directions $\mathbf{r}$ and $\mathbf{r}'$, where the slowly varying part of the Bloch-function is given by the plane wave. The first step is to rewrite the term $\frac{1}{|(\mathbf{r},z)-(\mathbf{r}',z')|}$ as $\frac{1}{\sqrt{(\mathbf{r}-\mathbf{r}')^2+(z-z')^2}}$. Then, the integration over $\mathbf{r}'$ is transformed into the integration over the distance between $\mathbf{r}$ and $\mathbf{r}'$, $\mathbf{s} = \mathbf{r}-\mathbf{r}'$. So, instead of performing for every point r the integration over $\mathbf{r}'$, one integrates for every point $\mathbf{r}$ over all possible distances $\mathbf{s}$. This approach leads to several simplifications

$$\begin{aligned}\langle n_1\mathbf{k}_1 n_2\mathbf{k}_2 \mid v \mid n_3\mathbf{k}_3 n_4\mathbf{k}_4\rangle &= \frac{e^2}{4\pi\epsilon_0}\int_{\mathcal{L}}\int_{\mathcal{L}} dz dz' \frac{1}{\mathcal{A}^2} g_{n_1\mathbf{k}_1,n_4\mathbf{k}_4}(z) g_{n_2\mathbf{k}_2,n_3\mathbf{k}_3}(z') \\ &\cdot \int_{\mathcal{A}}\int_{\mathcal{A}} d\mathbf{r} d\mathbf{s} \left[\frac{1}{\sqrt{|\mathbf{s}|^2+(z-z')^2}}\right. \\ &\left.\cdot e^{i(\mathbf{k}_4+\mathbf{k}_3-\mathbf{k}_1-\mathbf{k}_2)\cdot\mathbf{r}} e^{i(\mathbf{k}_2-\mathbf{k}_3)\cdot\mathbf{r}'}\right]. \end{aligned} \tag{4.4}$$

The integration over $\mathbf{r}$ and $\mathbf{s}$ is decoupled and therefore the plane-wave leads to a delta function

$$\int_{\mathcal{A}} d\mathbf{r} e^{i(\mathbf{k}_4+\mathbf{k}_3-\mathbf{k}_1-\mathbf{k}_2)\cdot\mathbf{r}} = \mathcal{A}\delta_{\mathbf{k}_4+\mathbf{k}_3,\mathbf{k}_1+\mathbf{k}_2}. \tag{4.5}$$

The remaining integration over $z, z'$ and $\mathbf{s}$ depends on the dimensionality of the system.

The Fourier transformation along the free direction $\mathcal{A}$ defined in 3.20 is used to expand $\frac{1}{\mathbf{r}}$

$$\vartheta(\mathbf{s},z,z') = \frac{1}{\sqrt{|\mathbf{s}|^2+(z-z')^2}} = \sum_{\mathbf{q}} \vartheta_{\mathbf{q}}(z,z') e^{i\mathbf{q}\cdot\mathbf{s}} \tag{4.6}$$

in terms of its Fourier representation. Taking the integral over $\mathbf{s}$

$$\int_{\mathcal{A}} d\mathbf{s} \sum_{\mathbf{q}} \vartheta_{\mathbf{q}}(z,z') e^{i\mathbf{q}\cdot\mathbf{s}} e^{i(\mathbf{k}_2-\mathbf{k}_3)\cdot\mathbf{s}} = \mathcal{A}\sum_{\mathbf{q}} \vartheta_{\mathbf{q}}(z,z')\delta_{\mathbf{k}_3-\mathbf{k}_2,\mathbf{q}} \tag{4.7}$$

leads to another delta function, which can together with 4.5 be used to simplify 4.1 into

$$\hat{H}_2 = \frac{1}{2}\sum_{n_1,n_2,n_3,n_4}\sum_{\mathbf{k}\mathbf{k}'\mathbf{q}} \Theta^{n_1,n_2,n_3,n_4}_{\mathbf{q},\mathbf{k},\mathbf{k}'} \hat{a}^\dagger_{n_1\mathbf{k}+\mathbf{q}}\hat{a}^\dagger_{n_2\mathbf{k}'-\mathbf{q}}\hat{a}_{n_3\mathbf{k}'}\hat{a}_{n_4\mathbf{k}}. \tag{4.8}$$

Here, $\mathbf{k}_4$ has been relabeled to $\mathbf{k}$ and $\mathbf{k}_3$ to $\mathbf{k}'$. The term $\Theta^{n_1,n_2,n_3,n_4}_{\mathbf{q},\mathbf{k},\mathbf{k}'}$ contains all parts of 4.2 depending on actual wavefunctions and on the dimensionality of the nanostructure. It is given by

$$\Theta^{n_1,n_2,n_3,n_4}_{\mathbf{q},\mathbf{k},\mathbf{k}'} = \frac{e^2}{4\pi\epsilon_0}\int_{\mathcal{L}}\int_{\mathcal{L}} dz dz' g_{n_1\mathbf{k}+\mathbf{q},n_4\mathbf{k}}(z) g_{n_2\mathbf{k}'-\mathbf{q},n_3\mathbf{k}'}(z')\vartheta_{\mathbf{q}}(z,z'). \tag{4.9}$$

In the case of a bulk crystal, there is no integration over $z, z'$. Then, $\vartheta_{\mathbf{q}}^{3D}$ is given by the 3D Fourier transform of the Coulomb potential

$$\vartheta_{\mathbf{q}}^{3D} = \frac{4\pi}{\Omega q^2}. \tag{4.10}$$

The quantum well case has a 2D plane as the translational invariant directions and a 1D axis where symmetry is broken. The 2D Fourier transformation of 4.6 gives

$$\vartheta_{\mathbf{q}}^{2D}(z, z') = \frac{2\pi}{\mathcal{A}q} e^{-q|z-z'|}. \tag{4.11}$$

Hereby, the factor $\frac{2\pi}{\mathcal{A}q}$ denotes the Fourier transform of an ideal quantum well with no extension in the symmetry broken direction, while the exponential factor comprises of the finite extension of the quantum well wavefunctions.

Inspecting the Coulomb terms, it is clear that these terms diverge in the limit of $\mathbf{q} = 0$. The divergence can be resolved within the *Jellium model* **?** ], where the semiconductor is assumed to be intrinsically charge free. As a result, the diverging term of the electron-electron interaction at $\mathbf{q} = 0$ is canceled by the diverging term of the interaction of electrons with the homogeneous positive charge background. Hence, terms $\mathbf{q} = 0$ within the summation over $\mathbf{q}$ are discarded.

### 4.1.2 *Diagonal Approximation*

The next approximation performed aims to remove two of the four subband indices in 4.8 by assuming that Coulomb interactions will not cause interband transitions. Then, $n_1 = n_4$ and $n_2 = n_3$, which is called here diagonal Coulomb approximation. This assumption is for example justified at an approximate level in symmetrical quantum wells, as the diagonal Coulomb matrix elements are due to the symmetry of the wavefunctions, two orders of magnitude larger than the off-diagonal Hader et al. [27]. Also, for single-band effective mass wavefunctions, only the diagonal terms remain, while others vanish due to the orthogonality of the zone-center functions. Using this approximations, the Coulomb Hamiltonian reads

$$\hat{H}_2 = \frac{1}{2} \sum_{m,n} \sum_{\mathbf{k}\mathbf{k}'\mathbf{q}} \Theta_{\mathbf{q},\mathbf{k},\mathbf{k}'}^{m,n,n,m} \hat{a}_{m\mathbf{k}+\mathbf{q}}^{\dagger} \hat{a}_{n\mathbf{k}'-\mathbf{q}}^{\dagger} \hat{a}_{n\mathbf{k}'} \hat{a}_{m\mathbf{k}}. \tag{4.12}$$

Consequently, the notation $\Theta_{\mathbf{q},\mathbf{k},\mathbf{k}'}^{m,n,n,m}$ can be reduced to $\Theta_{\mathbf{q},\mathbf{k},\mathbf{k}'}^{m,n}$.

### 4.1.3 *Holes*

The next step is to transform the Coulomb Hamiltonian into the electron-hole picture. In the diagonal approximation 4.12, one distinguishes between electron states in the conduction bands $c, d$ and hole states in the valence bands $v, w$. Therefore, the following four combinations are possible

$$n = c,\ m = d \quad n = c,\ m = v \quad n = v,\ m = c \quad n = v,\ m = w. \tag{4.13}$$

As next, hole operators are inserted for electrons in the valence band. Further, a natural ordering is reestablished by propagating the creation operators to the left and the annihilation operators to the right and setting the hole creation operator before, the hole annihilation operator after the one of the electron. The terms involving the sum $\sum_{n=c,m=d}$ are already in that ordering. Permuting the hole terms in the sum $\sum_{n=v,m=w}$ introduces a new two-operator term while the sums $\sum_{n=c,m=v}$ and $\sum_{n=v,m=c}$ can be summed together. Hence, the final Hamiltonian which will be used to calculate the microscopic equation of motion is obtained as

$$\begin{aligned}
\hat{H} &= \sum_{c,\mathbf{k}} E_c(\mathbf{k})\hat{a}^\dagger_{c\mathbf{k}}\hat{a}_{c\mathbf{k}} - \sum_{v,\mathbf{k}} E_v(\mathbf{k})\hat{b}^\dagger_{v\mathbf{k}}\hat{b}_{v\mathbf{k}} && (4.14)\\
&\quad -\mathbf{E}(\mathbf{r},t)\cdot\sum_{c,v,\mathbf{k}} \boldsymbol{\mu}_{cv,\mathbf{k}}\hat{a}^\dagger_{c\mathbf{k}}\hat{b}^\dagger_{v-\mathbf{k}} + \boldsymbol{\mu}^*_{cv,\mathbf{k}}\hat{b}_{v-\mathbf{k}}\hat{a}_{c\mathbf{k}} && (4.15)\\
&\quad +\frac{1}{2}\sum_{c,d}\sum_{\mathbf{k}\mathbf{k}'\mathbf{q}} \Theta^{c,d}_{\mathbf{q},\mathbf{k},\mathbf{k}'}\hat{a}^\dagger_{c\mathbf{k}+\mathbf{q}}\hat{a}^\dagger_{d\mathbf{k}'-\mathbf{q}}\hat{a}_{d\mathbf{k}'}\hat{a}_{c\mathbf{k}} && (4.16)\\
&\quad +\frac{1}{2}\sum_{v,w}\sum_{\mathbf{k}\mathbf{k}'\mathbf{q}} \Theta^{w,v}_{-\mathbf{q},-\mathbf{k}'+\mathbf{q},-\mathbf{k}-\mathbf{q}}\hat{b}^\dagger_{v\mathbf{k}+\mathbf{q}}\hat{b}^\dagger_{vk'-\mathbf{q}}\hat{b}_{w\mathbf{k}'}\hat{b}_{v\mathbf{k}} && (4.17)\\
&\quad \sum_{v,\mathbf{k}',\mathbf{q}} \Theta^{v,v}_{-\mathbf{q},-\mathbf{k}'+\mathbf{q},-\mathbf{k}}\hat{b}^\dagger_{v\mathbf{k}'}\hat{b}_{v\mathbf{k}'} && (4.18)\\
&\quad -\frac{1}{2}\sum_{\mathbf{k}\mathbf{k}'\mathbf{q}}\left\{\left(\Theta^{v,c}_{-\mathbf{q},-\mathbf{k}'+\mathbf{q},\mathbf{k}} + \Theta^{c,v}_{\mathbf{q},\mathbf{k},\mathbf{q}-\mathbf{k}'}\right)\hat{a}^\dagger_{c\mathbf{k}+\mathbf{q}}\hat{b}^\dagger_{v\mathbf{k}'-\mathbf{q}}\hat{b}_{v\mathbf{k}'}\hat{a}_{c\mathbf{k}}\right\} && (4.19)
\end{aligned}$$

The indices $\mathbf{k}$ and $\mathbf{k}'$ have in some cases been swapped, shifted by $\mathbf{q}$ and occasionally changed sign.

## 4.2 TRANSITIONS CALCULATION

### 4.2.1 *Equations of Motion*

The next task is to evaluate the equation of motion 3.57 for $\hat{p}_{nm,\mathbf{k}}$, as it has already been done in previous chapter, excluding the Coulomb interaction. Therefore, the remaining task is to evaluate the commutator of the microscopic polarization and the Coulomb Hamiltonian,

$$\frac{d}{dt}\hat{p}_{nm,\mathbf{k}} = \frac{i}{\hbar}\left[\hat{H}_2\hat{p}_{nm,\mathbf{k}}\right] + \text{rest} \tag{4.20}$$

where $\hat{H}_2$ are the Coulomb terms in 4.14. The evaluation is straight forward but lengthy: For each four-operator term, one writes $\hat{H}_2\hat{p}_{nm,\mathbf{k}} - \hat{p}_{nm,\mathbf{k}}\hat{H}_2$ and then permutes $\hat{p}_{nm,\mathbf{k}}$ in the first term to the left to obtain the remaining terms which do not cancel finally. The remaining terms are resorted at the end into the natural ordering. The resulting equation of motion is given by

$$\frac{d}{dt}\hat{p}_{n\,m,\mathbf{k}} = -\frac{i}{\hbar}\left\{E_m(\mathbf{k}) - \left(E_n(\mathbf{k}) - \sum_{\mathbf{q}} \Theta^{n,n}_{-\mathbf{q},-\mathbf{k}+\mathbf{q},\mathbf{k}}\right)\right\}\hat{p}_{n\,m,\mathbf{k}} \tag{4.21}$$

$$-\frac{i}{\hbar}\mathbf{E}(z,t)\cdot\boldsymbol{\mu}_{m\,n,\mathbf{k}}\left(\sum_{c}\hat{a}^{\dagger}_{c\mathbf{k}}\hat{a}_{m\mathbf{k}} + \sum_{\nu}\hat{b}^{\dagger}_{\nu-\mathbf{k}}\hat{b}_{n-\mathbf{k}} - 1\right) \tag{4.22}$$

$$+\frac{i}{2\hbar}\sum_{c,\mathbf{k}',\mathbf{q}}\left(\Theta^{m,c}_{-\mathbf{q},\mathbf{k}+\mathbf{q},\mathbf{k}'} + \Theta^{c,m}_{\mathbf{q},\mathbf{k}',\mathbf{k}+\mathbf{q}}\right)\hat{a}^{\dagger}_{c\mathbf{k}'+\mathbf{q}}\hat{b}_{n-\mathbf{k}}\hat{a}_{c\mathbf{k}'}\hat{a}_{m\mathbf{k}+\mathbf{q}} \tag{4.23}$$

$$+\frac{i}{2\hbar}\sum_{\nu,\mathbf{k}',\mathbf{q}}\left(\Theta^{\nu,n}_{-\mathbf{q},-\mathbf{k}'+\mathbf{q},\mathbf{k}} + \Theta^{n,\nu}_{\mathbf{q},\mathbf{k},-\mathbf{k}'+\mathbf{q}}\right)\hat{b}^{\dagger}_{\nu\mathbf{k}'-\mathbf{q}}\hat{b}_{\nu\mathbf{k}'}\hat{a}_{m\mathbf{k}}\hat{b}_{n-\mathbf{k}-\mathbf{q}} \tag{4.24}$$

$$-\frac{i}{2\hbar}\sum_{c,\mathbf{k}',\mathbf{q}}\left(\Theta^{n,c}_{-\mathbf{q},\mathbf{k},\mathbf{k}'} + \Theta^{c,n}_{\mathbf{q},\mathbf{k}',\mathbf{k}}\right)\hat{a}^{\dagger}_{c\mathbf{k}'+\mathbf{q}}\hat{b}_{n-\mathbf{k}+\mathbf{q}}\hat{a}_{c\mathbf{k}'}\hat{a}_{m\mathbf{k}} \tag{4.25}$$

$$-\frac{i}{2\hbar}\sum_{\nu,\mathbf{k}',\mathbf{q}}\left(\Theta^{\nu,m}_{-\mathbf{q},-\mathbf{k}'+\mathbf{q},\mathbf{k}-\mathbf{q}} + \Theta^{m,\nu}_{\mathbf{q},\mathbf{k}-\mathbf{q},-\mathbf{k}'+\mathbf{q}}\right)\hat{b}^{\dagger}_{\nu\mathbf{k}'-\mathbf{q}}\hat{b}_{n-\mathbf{k}}\hat{b}_{\nu\mathbf{k}'}\hat{a}_{m\mathbf{k}-\mathbf{q}} \tag{4.26}$$

$$+\frac{i}{2\hbar}\sum_{\mathbf{q}}\left(\Theta^{n,m}_{-\mathbf{q},\mathbf{k},\mathbf{k}-\mathbf{q}} + \Theta^{m,n}_{\mathbf{q},\mathbf{k}-\mathbf{q},\mathbf{k}}\right)\hat{b}_{n-\mathbf{k}+\mathbf{q}}\hat{a}_{m\mathbf{k}-\mathbf{q}}. \tag{4.27}$$

Taking the two-band approximation of this particular equation and ignoring the $\mathbf{k}$ dependence of the Coulomb matrix element results in Eq. (3.9) of ref. Chow and Koch [17]. Comparing this equation with the free-carrier result 3.64 reveals that in 4.21, the valence band energy is shifted to

$$E_n(\mathbf{k}) \to E_n(\mathbf{k}) - \sum_{\mathbf{q}} \Theta^{n,n}_{-\mathbf{q},-\mathbf{k}+\mathbf{q},\mathbf{k}}. \tag{4.28}$$

The values usually inserted into $E_\nu(\mathbf{k})$ are results of a preceding band structure calculation, where parameters are obtained from low excitation experiments, where the valence band is full Chow and Koch [17]. Therefore, the $E_\nu(\mathbf{k})$ actually already holds the Coulomb energy of the full valence band. The free-carrier calculation implicitly included this energy within the band structure result, while it appears here explicitly.

The terms 4.23 and 4.24 are the result of the equation of motion of the conduction-conduction and valence-valence terms 4.16, 4.17 and 4.18. The terms 4.25-4.27 are the results of the commutator with the conduction-valence terms 4.19. The term 4.27 is obtained at the end when 4.26 is brought into proper order.

The obtained equation of motion for the two-particle operator term $\hat{p}_{n\,m,\mathbf{k}}$ obviously depends on the four-particle operator terms. Therefore, it would be necessary to calculate the equation of motion of the four-particle operator term which would couple to a six-particle operator term: one obtains an infinite hierarchy of equations, as demonstatred in Fig. 15. For this reason, one usually truncates the hierarchy at a certain order Chow and Koch [17], Koch [34]. Factorizing the four-particle operator into two two-particle operators yields the *Hartree-Fock approximation*, which is considered in the next section.

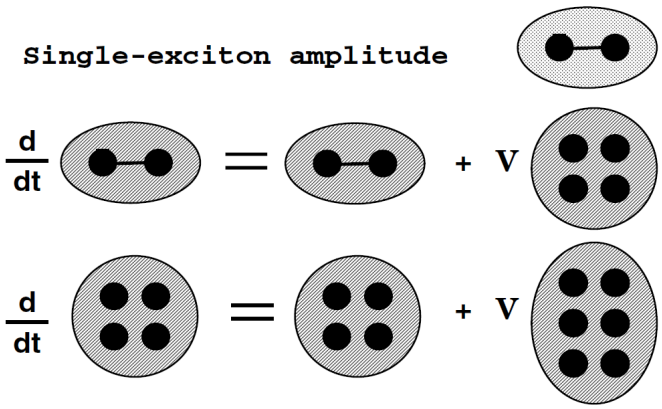


Figure 15: Infinite hierarchy of operator products for the equtions of motion.

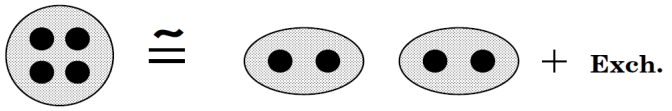


Figure 16: Schematic representation of the Hartree-Fock approximation operator product in the equation of motion.

### 4.2.2 *Hartree-Fock Approximation*

In the next step, all four-particle operators are factorized into all possible products of two-particle operators, of which the expectation values are taken. While permuting these operators, the correct sign due to the anti-commutation relations has to be tracked. Due to the random-phase approximation 3.63, all expectation values of two-particle operators reduce either to microscopic polarizations $p_{nm,\mathbf{k}}$, particle densities $n_{n,\mathbf{k}}$ or to zero. We summarize this approach for a two-operator expectation value

$$\begin{aligned}\frac{d}{dt}\langle AB\rangle &= \frac{d}{dt}\langle AB\rangle_{HF} + \left(\frac{d}{dt}\langle AB\rangle - \frac{d}{dt}\langle AB\rangle_{HF}\right)\\ &= \frac{d}{dt}\langle AB\rangle_{HF} + \frac{d}{dt}\langle AB\rangle_{col.}\end{aligned} \tag{4.29}$$

where $\langle AB\rangle_{HF}$ is the Hartree-Fock contribution to the equation if motion which will be treated in this chapter (see Fig. 16). The term $\langle AB\rangle_{col.}$ us a higher-order contribution containing four-operator expectation values, which is beyond the scope of this thesis. A general explanation of the second born approximation should be adressed.

As an example, the factorization of 4.23 leads to

$$\begin{aligned}\left\langle \hat{a}^\dagger_{c\mathbf{k}'+\mathbf{q}}\hat{b}_{n-\mathbf{k}}\hat{a}_{c\mathbf{k}'}\hat{a}_{m\mathbf{k}+\mathbf{q}}\right\rangle_{HF} &= \left\langle \hat{a}^\dagger_{c\mathbf{k}'+\mathbf{q}}\hat{b}_{n-\mathbf{k}}\right\rangle\langle \hat{a}_{c\mathbf{k}'}\hat{a}_{m\mathbf{k}+\mathbf{q}}\rangle\\ &\quad - \left\langle \hat{a}^\dagger_{c\mathbf{k}'+\mathbf{q}}\hat{a}_{c\mathbf{k}'}\right\rangle\langle \hat{b}_{n-\mathbf{k}}\hat{a}_{m\mathbf{k}+\mathbf{q}}\rangle\\ &\quad + \left\langle \hat{a}^\dagger_{c\mathbf{k}'+\mathbf{q}}\hat{a}_{m\mathbf{k}+\mathbf{q}}\right\rangle\langle \hat{b}_{n-\mathbf{k}}\hat{a}_{c\mathbf{k}'}\rangle\\ &= 0 - \delta_{\mathbf{q}0} + \delta_{\mathbf{k}'\mathbf{k}}\delta_{cm}n_{m,\mathbf{k}+\mathbf{q}}p_{nm,\mathbf{k}}.\end{aligned}$$

Other terms are factorized accordingly. The factorized terms of 4.23 and 4.24 can be added to the transition energy, while the remaining terms are proportional to the inversion factor. Finally, the equation for the

microscopic polarization in the Hartree-Fock approximation is obtained as

$$\begin{aligned}\frac{d}{dt}p_{nm,\mathbf{k}} &= -\frac{i}{\hbar}\hbar\tilde{\omega}_{mn}(\mathbf{k})p_{nm,\mathbf{k}} \\ &\quad -\frac{i}{\hbar}\left\{\mathbf{E}(z,t)\cdot\boldsymbol{\mu}_{mn,\mathbf{k}}+\sum_{\mathbf{q}}\Theta^{n,m}_{-\mathbf{q},\mathbf{k},\mathbf{k}-\mathbf{q}}\right\}(n_{m\mathbf{k}}+n_{n\mathbf{k}}-1) \\ &\quad +\frac{\partial}{\partial t}\,p_{nm,\mathbf{k}}\big|_{col.}, \end{aligned} \tag{4.30}$$

and the renormalized transition energy is given as

$$\begin{aligned}\hbar\tilde{\omega}_{mn}(\mathbf{k}) &= E_m(\mathbf{k})-\left(E_n(\mathbf{k})-\sum_{\mathbf{q}}\Theta^{n,n}_{-\mathbf{q},-\mathbf{k}+\mathbf{q},\mathbf{k}}\right) \\ &\quad -\sum_{\mathbf{q}}\left(\Theta^{m,m}_{\mathbf{q},\mathbf{k},\mathbf{k}+\mathbf{q}}n_{m,\mathbf{k}+\mathbf{q}}+\Theta^{n,n}_{\mathbf{q},\mathbf{k},\mathbf{k}+\mathbf{q}}n_{n,\mathbf{k}+\mathbf{q}}\right). \end{aligned} \tag{4.31}$$

Inspecting 4.30 reveals that the microscopic polarization $p_{nm,\mathbf{k}}$ at $\mathbf{k}$ is now coupled to the one at $\mathbf{k}'$ by the Coulomb interaction, while in the free-carrier expression, the microscopic polarization was entirely determined by the momentum matrix element and the inversion. This coupling introduces the excitonic effects such as enhancing gain or absorption.

### 4.2.3 *Screening*

#### 4.2.3.1 *Background Screening*

In the crystal electron Hamiltonian 2.8, the interaction between ion cores and the interaction between electrons and ion cores is merged into the potential $U(\mathbf{r})$, while the Coulomb energy between electrons has been retained and later transformed into the Bloch states. With the introduction of $\mathbf{k}\cdot\mathbf{p}$ states, only a restricted number of valence electrons are considered, while core electrons are included implicitly. These implicitly included core electrons and ion cores screen the Coulomb interaction between explicitly included electrons. The effect can be considered by replacing the dielectric permittivity of the vacuum $\epsilon_0$ with the static semiconductor crystal background permittivity $\epsilon_b$ in the Coulomb matrix element 4.2.

#### 4.2.3.2 *Plasma Screening*

A profound weakness of the Hartree-Fock approximation is the lack of screening of Coulomb interactions at elevated carrier densities. The presence of unbound carriers of the electron-hole plasma leads to an adjustment of the carriers to a charge, effectively screening it and thereby reducing the Coulomb interaction energy. The lack of screening in the Hartree-Fock equations is caused by the early truncation of the infinite hierarchy of equations of motion. One therefore introduces the screening effect using a dynamic dielectric function $\epsilon(\mathbf{q},\omega)$

$$W_{\mathbf{q}} = \frac{V_{\mathbf{q}}}{\epsilon(\mathbf{q},\omega)}, \tag{4.32}$$

where $W_{\mathbf{q}}$ denotes the screened potential and $V_{\mathbf{q}}$ the unscreened one. There are several model dielectric functions, where all have their strengths, limitations and weaknesses. One standard approach is the *Lindhard formula* Chow and Koch [17], Haug and Koch [29],

$$\epsilon(\mathbf{q},\omega) = 1 - V_{\mathbf{q}} \sum_{n\mathbf{k}} \frac{f_n(\mathbf{k}-\mathbf{q}) - f_n(\mathbf{k})}{E_n(\mathbf{k}-\mathbf{q}) - E_n(\mathbf{k}) + \hbar\omega + \hbar i\delta}, \tag{4.33}$$

also denoted as randomphase approximation. The Lindhard formula can be derived using the self-consistent field (SCF) approach Ehrenreich and Cohen [21], or more profound, by neglecting vertex corrections in the equation of motion for the Green's function Binder and Koch [6] of the designated system and using the Kadanoff-Baym formalism Binder and Koch [6]. The derivation using the SCF approach involves the reaction of a homogeneous electron gas to a test charge. To use the Lindhard formula in optical calculations, the test charge potential $V_{\mathbf{q}}$ is replaced with the Coulomb potential $\Theta^{n_1,n_2,n_3,n_4}_{\mathbf{q},\mathbf{k},\mathbf{k}'}$ defined in 4.9, including the factor due to the finite extend of the wavefunctions.

There are several far better models Mahan [39] for the dielectric screening but the Lindhard formula is still popular and commonly used in optoelectronic modeling Chow and Koch [16] due to its simple structure. For many practical applications, the damped response of the screening is ignored, therefore setting $(w + id)$ to zero. Once $\epsilon(\mathbf{q}, 0)$ is obtained, one replaces the Coulomb potential within all equations with

$$\Theta^{n_1,n_2,n_3,n_4}_{\mathbf{q},\mathbf{k},\mathbf{k}'} \rightarrow \frac{1}{\epsilon(\mathbf{q},0)} \Theta^{n_1,n_2,n_3,n_4}_{\mathbf{q},\mathbf{k},\mathbf{k}'}. \tag{4.34}$$

Beside its physical importance, the screening introduces the desired effect of removing the divergence of the Coulomb potential with $\mathbf{q} \rightarrow 0$, thereby facilitating the numerical evaluation.

#### 4.2.3.3 *Coulomb Hole Seld Energy*

By replacing the electron operators with hole operators in 4.21, the valence band energy was shifted by a constant value,

$$E_n(\mathbf{k}) \rightarrow E_n(\mathbf{k}) - \sum_{\mathbf{q}} \Theta^{n,n}_{-\mathbf{q},-\mathbf{k}+\mathbf{q},\mathbf{k}}. \tag{4.35}$$

This shift is already implicitly included in the band structure. In the high density limit, the Coulomb interaction is screened

$$\frac{\Theta^{n,n}_{-\mathbf{q},-\mathbf{k}+\mathbf{q},\mathbf{k}}}{\epsilon(\mathbf{q},0)} \tag{4.36}$$

and the difference between the unscreened and the screened Coulomb interaction leads to a density dependent shift

$$\Delta E_{CH,n} = \sum_{\mathbf{q}} \Theta^{n,n}_{-\mathbf{q},-\mathbf{k}+\mathbf{q},\mathbf{k}} \left( \frac{1}{\epsilon(\mathbf{q})} - 1 \right). \tag{4.37}$$

The shift is denoted as *Debye shift* or *Coulomb-hole self energy*.

#### 4.2.3.4 *Screened Exchange Energy*

Beside the Coulomb-hole self energy, the transition energy 4.31 is, compared to the free carrier result, reduced by the density dependent *screened exchange shift*,

$$\Delta E_{SX,mn}(\mathbf{k}) = \sum_{\mathbf{q}} \left( \Theta^{m,m}_{\mathbf{q},\mathbf{k},\mathbf{k}+\mathbf{q}} n_{m,\mathbf{k}+\mathbf{q}} + \Theta^{n,n}_{\mathbf{q},\mathbf{k},\mathbf{k}+\mathbf{q}} n_{n,\mathbf{k}+\mathbf{q}} \right). \quad (4.38)$$

where the screened Coulomb potentials are used. Within the screened Hartree-Fock limit, the transition energy is therefore renormalized

$$\hbar\tilde{\omega} = \Delta E_{mn}(\mathbf{k}) + \Delta E_{CH,n} - \Delta E_{SX,mn}(\mathbf{k}). \quad (4.39)$$

Note that both contributions 4.37 and 4.38 reduce the transition energy and can lead to a significant red shift.

### 4.2.4 *Solving the Correlated Equation*

In order to solve the equation of motion 4.30, the collision term is approximated using a decay rate $-\gamma p_{mn,\mathbf{k}}$. As equation 4.30 couples microscopic polarizations $p_{mn,\mathbf{k}}$ of different $\mathbf{k}$ values, the equation system has to be solved self-consistently. Therefore, the equation is transformed using the same ansatz as in Chapter 3. The fast oscillating $p_{mn,\mathbf{k}}$ is replaced with its slowly-varying envelope

$$s_{nm,\mathbf{k}} = p_{mn,\mathbf{k}} e^{-i(k_0 z - \nu t - \phi(z))}. \quad (4.40)$$

Inserting 4.40 into 4.30, taking the time derivative, using the plane wave expression for the electrical field 3.47, skipping the fast oscillating parts (as they should average out to zero) and solving for the steady state leads to

$$\begin{aligned} s_{nm,\mathbf{k}} \quad = \quad & -\frac{1}{i\left(\tilde{\omega}_{mn,\mathbf{k}} - \nu\right) + \gamma} \frac{i}{\hbar} \\ & \cdot \left\{ \mu_{mn,\mathbf{k}} \frac{E(z)}{2} + \sum \Theta^{n,m}_{\mathbf{q},\mathbf{k},\mathbf{k}+\mathbf{q}} s_{nm,\mathbf{k}+\mathbf{q}} \right\} \\ & \cdot \left(n_{m\mathbf{k}} + n_{n\mathbf{k}} - 1\right). \end{aligned} \quad (4.41)$$

The polarization envelope still depends on the intensity of the considered field. Therefore, the field independent solution variable is introduced, given by

$$\lambda_{nm,\mathbf{k}} = \frac{2 s_{nm,\mathbf{k}}}{E(z)}. \quad (4.42)$$

In order to obtain a practicable expression, the lineshape and the inversion factor are combined into

$$\Omega_{nm,\mathbf{k}} = \frac{i}{\hbar} \frac{\left(n_{m\mathbf{k}} + n_{n\mathbf{k}} - 1\right)}{i\left(\tilde{\omega}_{mn,\mathbf{k}} - \nu\right) + \gamma}. \quad (4.43)$$

Inserting 4.42 and 4.43 into 4.41, yields

$$\Omega_{nm,\mathbf{k}} \sum \Theta^{n,m}_{\mathbf{q},\mathbf{k},\mathbf{k}+\mathbf{q}} \lambda_{nm,\mathbf{k}+\mathbf{q}} + \lambda_{nm,\mathbf{k}} = -\mu_{mn,\mathbf{k}} \Omega_{nm,\mathbf{k}}. \quad (4.44)$$

This equation is the self-consistency equation for $\lambda_{nm,\mathbf{k}}$. Once solved, the optical susceptibility is calculated using

$$\chi(\nu) = \frac{1}{n_b^2 \epsilon_0} \frac{P(z)}{E(z)} = \frac{1}{n_b^2 \epsilon_0} \frac{1}{V} \sum_{n,m,\mathbf{k}} \mu^*_{mn,\mathbf{k}} \lambda_{nm,\mathbf{k}}. \tag{4.45}$$

Absorption, refractive index change and spontaneous emission can therefrom be calculated as already presented in the preceding Chapter 3.

# 5 SEMICONDUCTOR MICROCAVITY

Put intro here...

## 5.1 OPTICAL RESONATOR

An optical resonator is a device used for confining light at certain frequencies. The classical resonator (such a the Fabri-Perot etalon seen in Fig. 17) consists of two planar mirrors, separated by a distance $l$. The region between the two mirror is called the spacer layer and its refractove index is denoted by $n$. For now we assume that the medium outside the structure is plain air. The transmitions spectrum of this structure exhibits a pattern of repetative peaks of large transmission corresponding to resonances of the etalon. This varying transmission function is caused by an interference between the multiple reflections of light between the two reflecting surfaces (see Fig. 17). Contructive interference iccurs if the transmitted beams are in phase, which corresponds to a high-transmission peak. for transmitted beams that are out-of-phase a destructive interference occurs, which corresponds to a minimum in the transmission spectrum. The multiple-reflected beams' phase matching depends in the wavelength $\lambda$ of the light, the beam incidence angle $\theta$, the etalon thickness $l$ and the refractive index of the spacer material $n$.

The phase between each successive reflection is Born and Wolf [8]

$$\delta = \left(\frac{2\pi}{\lambda}\right) 2nl\cos(\theta) \tag{5.1}$$

If both surfaces have reflectance $R$, the transmittance function of the entire structure is given by

$$T = \frac{(1-R)^2}{1+R^2-2R\cos(\delta)} = \frac{1}{1+F\sin^2\left(\frac{\delta}{2}\right)}, \tag{5.2}$$

where $F = \frac{4R}{(1-R)^2}$ is the finesse coefficient. Fig. 18 shows the dependence of the trasmittence on the phase parameter $\delta$, for various values of $R$ (or equavalently of $F$). The maximum tranmission occurs when

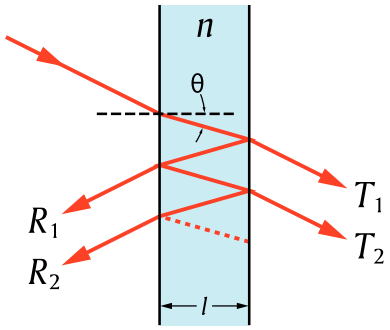


Figure 17: Fabri-Perot etalon multiple reflections.

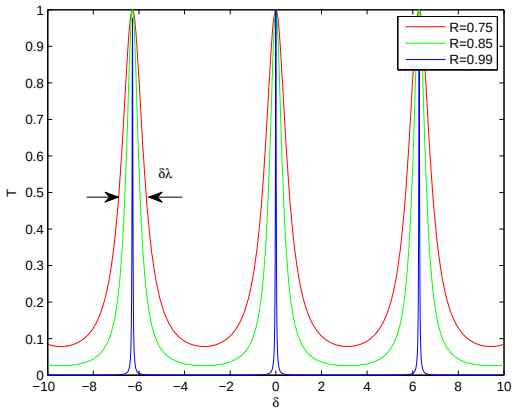


Figure 18: Resonator transmittance function for various values of mirror reflectrance R. $\delta\lambda$ is the full-width half-maximum of the transmission band.

the optical path length difference $2nl\cos(\theta)$ between each transmitted beam is an interger multiple of the wavelength. In the absence of absorption, the reflectance of the structure R is the complement of the transmittence, i.e. $R + T = 1$. The maximum reflectivity is given by

$$R_{max} = 1 - \frac{1}{1+F}, \tag{5.3}$$

which occurs when the path-length difference is equal to half an odd multiple of the wavelength.

The wavelength separation between adjacent transmission peaks or free spectral range (FSR) of the etalon, $Dl$, is given by

$$\Delta\lambda = \frac{\lambda_0^2}{2nl\cos(\theta) + \lambda_0}, \tag{5.4}$$

where $l_0$ is the central wavelength of the nearest transmission peak. The FSR is related to the full-width half-maximum (FWHM) $dl$ of any one transmission band by a quantity known as the *finesse*

$$\mathcal{F} = \frac{\Delta\lambda}{\delta\lambda} = \frac{\pi}{2\arcsin(1/\sqrt{F})} \tag{5.5}$$

## 5.2 DISTRIBUTED BRAGG REFLECTOR

The reflecting surfaces (or mirrors) modeled in previous section by a reflectivity parameter R are realized in practive by a stack of multiple layers of alternating semicondictor materials with varying refractive indices called Distributed Bragg Reflector (DBR) (see Fig. 19). The alternating high and low indices, denoted respectively by $n_H$ and $n_L$, and the semiconductor layer thicknesses satisfy the following condiction

$$n_L l_L = n_H l_H = \frac{\lambda_c}{4}, \tag{5.6}$$

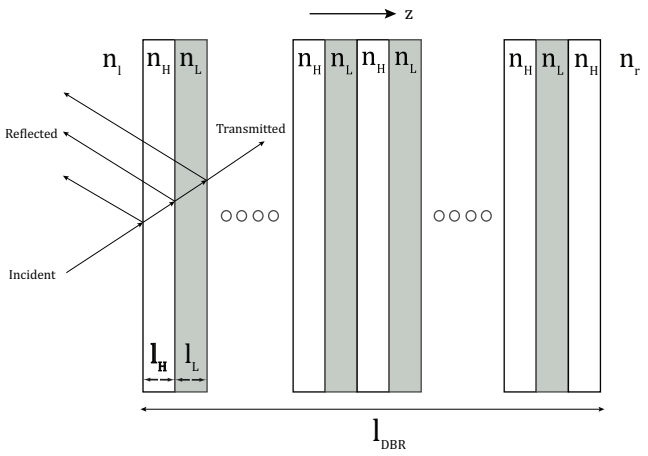


Figure 19: Schematic illustration of a Distributed Bragg Reflector (DBR). $z$ represents the growth direction of the layered structure.

where $\lambda_c$ is the center wavelength of the high reflectevity region of the structure. The two indices $n_l$ and $n_r$ are, respectively, the left- and right-hand cladding material refractive indices.

The principle of operation can be understood as follows. Each interface between the two materials contributes a Fresnel reflection. For the design wavelength $\lambda_c$, the optical path length difference between reflections from subsequent interfaces is half the wavelength; in addition, the reflection coefficients for the interfaces have alternating signs. Therefore, all reflected components from the interfaces interfere constructively, which results in a strong reflection. The reflectivity achieved is determined by the number of layer pairs and by the refractive index contrast between the layer materials. The reflection bandwidth is determined mainly by the index contrast, $n_H - n_L$.

In order to analyze the reflection and transmittance of the DBR, we use the Transfer Matrix formalism **?** ], as is described in the next section.

### 5.2.1 *Transfer Matrix Method (TMM)*

A monochromatic electric field of frequency $\omega$ propagating in a dielecric medium, assuming a frequency independent dielectric function, can be shown to satisfy the following wave eqaution

$$\nabla^2 \mathbf{E}(\mathbf{r}) + \frac{\omega^2}{c^2(r)} \mathbf{E}(\mathbf{r}) = 0, \tag{5.7}$$

where

$$\mathbf{E}(\mathbf{r}, t) = \Re \left\{ \mathbf{E}(\mathbf{r}) e^{i\omega t} \right\},$$

the speed of light in the dielectric $c(r) = c_0/n(r)$, $c_0$ being the speed on light in the vacuum and $n(r)$ the location dependent refractive index.

A medium consisting of pairs of two different dielectric materials with different refraction indices has a growth axis, $\hat{z}$, dependent re-

fraction index, i.e. $n(r) = n(z)$. Therefore equation 5.7 can be written as

$$\nabla^2 \mathbf{E}(\rho, z) + \frac{\omega^2}{c^2(z)} \mathbf{E}(\rho, z) = 0. \tag{5.8}$$

Because of the translational invariance along the in-plane, the solution of Eq. 5.8 consists of plane waves along the in-plane direction. For a given in-plane wave vector $k_{||}$ (parallel to the dielectric layer plane) we can make the following ansatz for the solution

$$\mathbf{E}_{\mathbf{k}_{||}} = E_{\mathbf{k}_{||},\omega}(z) e^{i\mathbf{k}_{||}\cdot\mathbf{J}}. \tag{5.9}$$

Substituting into Eq. 5.8 yields the following one-dimensional equation

$$\frac{d^2 E_{\mathbf{k}_{||},\omega}(z)}{dz^2} + \left( \frac{\omega^2}{c^2(z)} - k_{||}^2 \right) E_{\mathbf{k}_{||},\omega}(z) = 0. \tag{5.10}$$

This equation can be solved separately for each layer of the stack. The solution for a homogeneouos layer with a constant refractive index is of the form

$$\begin{aligned} E_{\mathbf{k}_{||},\omega}(z) &= E^+ e^{ik_z z} + E^- e^{-ik_z z}, \\ k_z &= \sqrt{\frac{\omega^2}{c^2} - \mathbf{k}_{||}^2}. \end{aligned} \tag{5.11}$$

The solution is a linear cobnination of two traveling waves in opposite direction along the $\hat{z}$ axis. A non-evanescent wave solution exist only if $\frac{\omega}{c} > \mathbf{k}_{||}$. The complex amplitudes of the forward ($E^+$) and backward ($E^-$) propagating waves are determined from the boundary cnditions at each interface between two adjacent layers of the stack.

The relation between the two complex amplitudes between two point along the propagation direction, $z_1$ and $z_2$, can be expressed as a $2 \times 2$ matrix transfer matix. From here on we assume the non-unique basis for the transfer matrix is $(E^+, E^-)$. The transfer matrix takes into account the propagation through the deielectric media and the boundary conditions at each interface between two adjacent layers. The boundary conditions resulting from Maxwell's equations Put here the number of Maxwell's equations state that tangential components of the electric and magnetic fields are continuous across the interface. Furhter discuss the boundary conditions here The boundary conditions for the field components can be wtritten as

$$\begin{aligned} D_{\perp 1} &= D_{\perp 2} \\ B_{\perp 1} &= B_{\perp 2} \\ E_{\parallel 1} &= E_{\parallel 2} \\ H_{\parallel 1} &= H_{\parallel 2} \end{aligned} \tag{5.12}$$

For siplicity we assume propagation only in the $\hat{z}$ direction. The boundary conditions for the eletric field become (see Fig. Schematic description of (a) light propagation through an inteface between two andjacent dielectric layers and (b) light propagation in a homogenous medium.

$$E_1^+ + E_1^- = E_2^+ + E_2^- \tag{5.13}$$

$$n_2 \left( E_2^+ - E_2^- \right) = n_1 \left( E_1^+ - E_1^- \right) \tag{5.14}$$

The interface transfer matrix $M_i$, for both linear polarizations of the field, TE and TM, can be written as

$$\begin{pmatrix} E_2^+ \\ E_2^- \end{pmatrix} = \frac{1}{2n_2} \begin{pmatrix} n_2+n_1 & n_2-n_1 \\ n_2-n_1 & n_2+n_1 \end{pmatrix} \begin{pmatrix} E_1^+ \\ E_1^- \end{pmatrix} \equiv M_i \begin{pmatrix} E_1^+ \\ E_1^- \end{pmatrix} \tag{5.15}$$

for a wave propagating from layer 1 to layer 2. The in-layer propagation trasfer matrix $M_p$, which relates different vectors at $z_1$ and $z_2$ in the same layer can be written as (Fig. same figure as above, b )

$$\begin{pmatrix} E_2^+ \\ E_2^- \end{pmatrix} = \begin{pmatrix} e^{ikl} & 0 \\ 0 & e^{-ikl} \end{pmatrix} \begin{pmatrix} E_1^+ \\ E_1^- \end{pmatrix} \equiv M_p \begin{pmatrix} E_1^+ \\ E_1^- \end{pmatrix}, \tag{5.16}$$

where $k = (\omega/c_0)\, n$.

This amplitude propagation approach can be applyed to the entire multilayer structure, for which the transfer matrix is simply the multipliction of $M_i$ and $M_p$ matrices for each boundary and layer

$$M_{DBR} = \prod_m M_{i,m} M_{p,m}, \tag{5.17}$$

where $m$ is the dielectric layer index. The explicit relation between the amplitudes of the incident electric field in the DBR structure and the transmitted field on the other side can be written as

$$\begin{pmatrix} E_{out}^+ \\ 0 \end{pmatrix} = \begin{pmatrix} M_{11} & M_{12} \\ M_{21} & M_{22} \end{pmatrix} \begin{pmatrix} E_{in}^+ \\ E_{in}^- \end{pmatrix}. \tag{5.18}$$

The reflection and tranmission coefficients of the entire structure can thus be written as

$$r_{DBR} = -\frac{M_{21}}{M_{22}} \tag{5.19}$$

$$t_{DBR} = \frac{\det(M_{DBR})}{M_{22}} \tag{5.20}$$

The reflection coefficient can be expressed as $r_{DBR}(\lambda) = |r| e^{i\alpha_r}$. It can be shown that for a structure containing $2N+1$ layers of high and low refractive indices (as in Fig. 19), so that the outermost layers are of high refractive index, $n_H$, and for the case of $k_i l_i = \frac{\pi}{2}$

$$|r| = \left( \frac{1 - \left(\frac{n_H}{n_L}\right)^{2N} \frac{n_H^2}{n_r n_l}}{1 + \left(\frac{n_H}{n_L}\right)^{2N} \frac{n_H^2}{n_r n_l}} \right)^2. \tag{5.21}$$

The phase within the region of high reflectivity (the *stop band*) of the reflector can be expressed as

$$\alpha_r = \frac{n_c L_{DBR}}{c} (\omega - \omega_c), \tag{5.22}$$

where $L_{DBR}$ is the penetration depth into the DBR and is given by **?** ]

$$L_{DBR} = \frac{\lambda_c}{2} \frac{n_L n_H}{n_c (n_H - n_L)}. \tag{5.23}$$

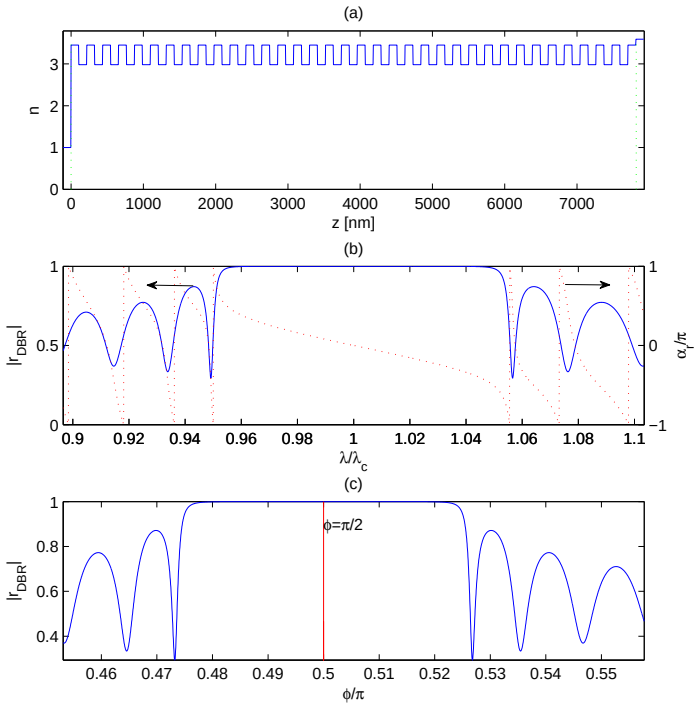


Figure 20: Simulation of a DBR structure with 35 alternating high and low layers, where (a) is the refreactive index profile as a function of the growth axis, (b) the amplitude and phase of the normal incidence reflection function this structure as a fucntion of normalized wavelength, $\lambda/\lambda_c$, and (c) the same amplitude as a function of the phase acquired by the EM field at each layer, $\phi = \frac{2\pi l_i n_i}{\lambda}$.

As an illustration, we present in Fig. 20 an exact calculation of the reflection coefficient of a DBR containing 35 pairs of alternating high and low reflractive index layers. The refractive indices for the simulation are $n_l = 1$ (air), $n_H = 3.45$ ($Al_{0.2}Ga_{0.8}As$), $n_L = 2.98$ ($AlAs$) and $n_r = 3.59$ ($GaAs$) (the structure refractive index profile is presented in (a)). In subplots (b) and (c) we plot the reflection coefficient as a function of the normalized wavelength, $\lambda/\lambda_c$, and the phase acquired by the electromagnetic field at each layer, $\phi = \frac{2\pi l_i n_i}{\lambda}$. The stop-band, as can be clearly seen from these plots, is centered at $\phi = \frac{\pi}{2}$, which corresponds to $\lambda_c$. In subplot (b) we also present the reflectivity phase $\alpha_r$, where the zero-phase crossing is observed at $\lambda_c$ as expected for the left-face reflection.

## 5.3 MICROVITY OPTICAL CHARACTERISTICS

### 5.3.1 *Microcavity Reflection Spectrum*

A microcavity (MC) is a Fabry-Perot resonator, whose mirrors are two DBRs and the spacer material is a semicondictor layer with refractive index $n_c$ and of length $l_c = \frac{\lambda_c}{2n_c}m$ ($m$ is a positive integer). The microcavity can be analyzed similarly to the DBR using the transfer matrix formalism. The MC's transfer matrix for a wave traveling from left to right can be written as

$$M_{MC} = M^r_{DBR} M_c M^l_{DBR}, \tag{5.24}$$

where $M_c$ is the transfer matrix of the spacer (cavity) layer. We can write the these three transfer matrices in their most general form as

$$M^r_{DBR} = \frac{n_c}{n_r}\begin{pmatrix} \frac{1}{t_r^*} & -\frac{r_r^*}{t_r^*} \\ -\frac{r_r}{t_r} & \frac{1}{t_r} \end{pmatrix}, \tag{5.25}$$

$$M^l_{DBR} = \frac{n_l}{n_c}\begin{pmatrix} \frac{1}{t_l^*} & \frac{r_l}{t_l} \\ \frac{r_l^*}{t_l^*} & \frac{1}{t_l} \end{pmatrix}, \tag{5.26}$$

$$M_c = \begin{pmatrix} e^{ikl_c} & 0 \\ 0 & e^{-ikl_c} \end{pmatrix}, \tag{5.27}$$

where $(r_l, t_l)$ and $(r_r, t_r)$ are, respectively, the reflection and transmission coefficients of the left- and right-hand DBR mirrors (see Fig. 21) and $n_l$ and $n_r$ are the left- and right-hand cladding material refractive indices, respecively.

Insering these matrices into Eq. 5.24 yields

$$M_{MC} = \left(\frac{n_L}{n_H}\right)^2 \begin{pmatrix} \frac{e^{ikl_{eff}} - R^* e^{-ikl_{eff}}}{T^*} & \frac{r_l e^{ikl_{eff}} - r_r^* e^{-ikl_{eff}}}{t_l t_r^*} \\ \frac{r_l^* e^{-ikl_{eff}} - r_r e^{ikl_{eff}}}{t_l^* t_r} & \frac{e^{-ikl_{eff}} - R e^{ikl_{eff}}}{T} \end{pmatrix}, \tag{5.28}$$

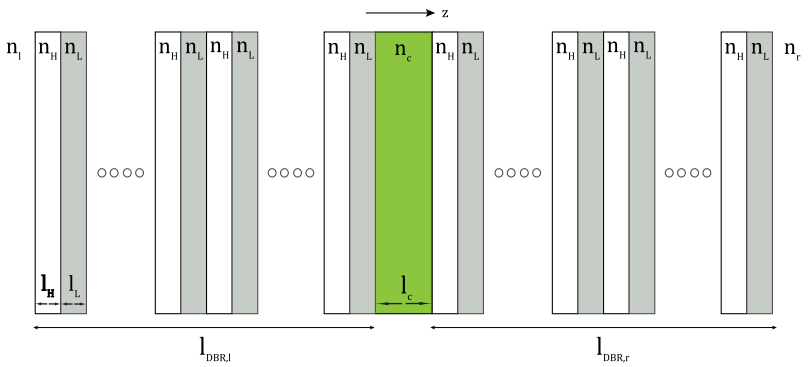


Figure 21: Microcavity schematic structure.

where $T = t_l t_r$ and $R = r_l r_r$. $l_{eff}$ is not equal to $l_c$ but rather to $l_{eff} = l_c + l_p$, where $l_p$ is the penetration depth of the cavity field into the DBR **?** ] and is given by

$$l_p = \frac{\lambda_c}{2} \frac{n_L n_H}{n_c (n_H - n_L)}. \tag{5.29}$$

The reflectance and transmittance of the MC can thus be wtritten as

$$T_{MC} = \frac{1}{\det(M_{MC}) |M^{22}_{MC}|^2} = \frac{T}{(1-R)^2 + 4R\sin^2(k_z l_{eff})} \tag{5.30}$$

$$R_{MC} = \frac{|M^{21}_{MC}|^2}{|M^{22}_{MC}|^2} = \frac{(|r_r| - |r_l|)^2 + 4R\sin^2(k_z l_{eff})}{(1-R)^2 + 4R\sin^2(k_z l_{eff})} \tag{5.31}$$

It is clear that there are several modes which stisfy the condition $k_z l_{eff} = m\pi$. As we increase the number of layers in the DBR mirrors the stop-band reflectivity approaches unity and the cavity field reflection line becomes narrower. Because of the finite transmittion probability of the DBR, the MC mode has a FWHM which can be shown to be **?** ]

$$2\gamma_c = \frac{1 - R_{MC}}{\sqrt{R_{MC}}} \frac{c}{n_c l_{eff}}. \tag{5.32}$$

$\gamma_c$ is a homogenous lifetime broadening of the confined cavity mode, caused by the decay through the mirrors.

As an illustration, we present in Fig. 22 the simulation results of a sample microcavity with two DBR mirrors with 35 alternating layers of high and low refractive index each and cavity length of $l_c = \frac{\lambda_c}{2n_c}$. This calculation was performed using the direct TMM calculation of the entire the structure, similarly to the DBR simulation presented above. The DBR parameters are the same as in Fig. 20, while for the cavity we choose $n_c = n_H = 3.45$ ($Al_{0.2}Ga_{0.8}As$).

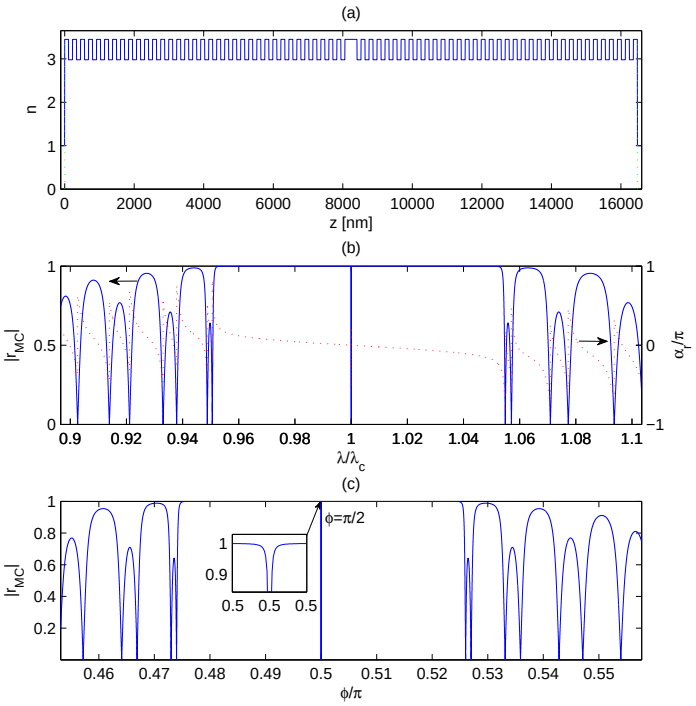


Figure 22: Simulation of a microcavity with two DBR's with 35 alternating high and low refractive index layers each, where (a) is the refreactive index profile as a function of the growth axis, (b) the amplitude and phase of the normal incidence reflection function this structure as a fucntion of normalized wavelength, $\lambda/\lambda_c$, and (c) the same amplitude as a function of the phase acquired by the EM field at each layer, $\phi = \frac{2\pi l_i n_i}{\lambda}$. The inset in (c) shows the reflection profile in the vicinity of $\phi = \frac{\pi}{2}$.

### 5.3.2 *Microcavity Confined Photon*

The photon confinement along the $\hat{z}$ axis leads to the following photon energy dispersion is Skolnick et al. [45]

$$E_{ph}(k_{\parallel}) = \frac{\hbar c k}{n_c} = \frac{\hbar c}{n_c}\sqrt{\left(\frac{2\pi m}{l_c}\right)^2 + k_{\parallel}^2}, \tag{5.33}$$

where $m$ is a positive integer. For small $k_{\parallel}$ we approximate the dispersion relation to a parabola

$$E_{ph}(k_{\parallel}) \cong \frac{2\pi\hbar c}{n_c l_c}\left(1 + \frac{\hbar^2 k_{\parallel}^2}{2m_{ph}}\right). \tag{5.34}$$

Here we define the photon in-plane effective mass $m_{ph} = \frac{\hbar n_c}{c l_c} \approx 10^{-5} m_0$, where $m_0$ is the free electron mass.

Part II

# APPENDICES

# A

# SYMMETRY PROPERTIES OF WAVEFUNCTIONS

Put some intro here...

Let $H(\mathbf{r}) = T + U(\mathbf{r})$ be the Hamiltonian in 2.14 with the kinetic operator $T$ and crystal potential $U(\mathbf{r})$, and let $G$ be the point group[1] of the crystal such that the symmetry operator $g \in G$, the crystal potential is invariant, i.e.

$$\forall g \in G, \;\; U(g^{-1}\mathbf{r}) = U(\mathbf{r}). \tag{A.1}$$

The kinetic operator $T$ is naturally invariant under the action of the elements in the point group $G$. Assuming that $\psi(\mathbf{r})$ is an eigenfunction of $H$ with $H(\mathbf{r})\psi(\mathbf{r}) = E\psi(\mathbf{r})$ and applying the symmetry operator $g$, leads to

$$H(g^{-1}\mathbf{r})\psi(g^{-1}\mathbf{r}) = H(\mathbf{r})\psi(g^{-1}\mathbf{r}) = E\psi(g^{-1}\mathbf{r}). \tag{A.2}$$

Obviously $\psi'(\mathbf{r}) = \psi(g^{-1}\mathbf{r})$ is also an eigenfunction of the Hamiltonian operator $H(\mathbf{r})$ with eigenvalue $E$. The wavefunction $\psi t'(\mathbf{r})$ might be the same wavefunction as $\psi(\mathbf{r})$ or might be linearly independent. Applying all symmetry operations $g \in G$ therefore results in a set of wavefunctions with the same eigenvalue $E$, spanning a function space

$$I_\psi = \left\{ \psi'(\mathbf{r}) | \psi'(\mathbf{r}) = \psi'(g^{-1}\mathbf{r}) \;\; \forall g \in G \right\}. \tag{A.3}$$

Now, the point group $G$ is a closed group, meaning that for $g, f \in G$ : $gf \in G$. Therefore, the function space $I_\psi$ is invariant under the action of $G$,

$$\psi(\mathbf{r}) \in I_\psi \Rightarrow \psi(g^{-1}\mathbf{r}) \in I_\psi. \tag{A.4}$$

Suppose that $\{\psi_0, \psi_1, \ldots, \psi_N\}$ is the basis of the subspace $I_\psi$, which is assumed to be of the demension $N$. The basis is denoted as being the *irreducible representation* of the group $G$. The desirable property deduced from group theory is that for every symmetry group, there are only a few distinct irreducible representations. Every irreducible representation describes an unique way how wavefunctions are transformed under the action of the elements of a symmetry group $G$. Therefore, the eigenfunctions of the crystal Hamiltonian $H$ can be classified according to the irreducible representation they form. It is clear that each eigenfunction does only belong to one irreducible representation and it is clear that eigenfunctions corresponding to different irreducible representations are always orthogonal. In the following, the theory will be focused on the zinc-blende crystal, for which the symmetry group of the Hamiltonian is $T_d$, the tetrahedral group. The elements are given by the 24 symmetry operations mapping a tetrahedron to itself. For an appropriate alignment and orientation, the symmetry operations are

1 A *crystallographic point group* is a set of symmetry operations, like rotations or reflections, that leave a point fixed while moving each atom of the crystal to the position of an atom of the same kind. That is, an infinite crystal would look exactly the same before and after any of the operations in its point group. In the classification of crystals, each point group corresponds to a crystal class.

| **Type** | **Operation** $(xyz) \rightarrow (\ldots)$ |
|---|---|
| E | $(xyz)$ |
| $3C_2$ | $(\bar{x}\bar{y}z), (x y\bar{z}), (\bar{x}y\bar{z})$ |
| $8C_3$ | $(zxy), (yzx), (\bar{y}z\bar{x}), (\bar{z}\bar{x}y), (\bar{y}\bar{z}x), (z\bar{x}\bar{y}), (y\bar{z}\bar{x}), (\bar{z}x\bar{y})$ |
| $6C_4$ | $(\bar{x}z\bar{y}), (\bar{x}\bar{z}y), (z\bar{y}\bar{x}), (\bar{z}\bar{y}x), (\bar{y}x\bar{z}), (y\bar{x}\bar{z})$ |
| $6\sigma$ | $(\bar{y}x\bar{z}), (yxz), (\bar{z}y\bar{x}), (zyx), (xzy), (x\bar{z}\bar{y})$ |

Table 1: Symmetry operations of the group $T_d$ using the Schönflies notation (notations after Yu and Cardona [47]).

listed in Table 1. $T_d$ has in total five distinct irreducible representations, which are commonly labeled as $\Gamma_1$, $\Gamma_2$, $\Gamma_{12}$, $\Gamma_{15}$ and $\Gamma_{25}$. $\Gamma_1$ and $\Gamma_2$ are one dimensional representations, $\Gamma_{12}$ is a two dimensional and $\Gamma_{15}$ and $\Gamma_{25}$ are three dimensional. The basis functions for all irreducible representations are given in Table 2. The representation $\Gamma_1$ is the identity representation, also denoted as trivial representation, leaving the wavefunction invariant. An atomic wavefunction with s-like symmetry transforms accordingly, i.e. is left unchanged under the action of the elements of the group $T_d$. An example of the $\Gamma_1$ representation is given by the conduction band at the $\Gamma$ point of zinc-blende, direct bandgap III-V semiconductors. The conduction band at the $\Gamma$ point is non-degenerate with a wavefunction obeying s-type symmetry. Another important irreducible representation is given by the top of the valence band at the $\Gamma$ point. Neglecting the later considered spin-orbit splitting, the valence band is threefold degenerate, with p-type basis functions $x, y$ and $z$, transforming under the action of $T_d$ according to the elements of a vector. The p-type basis functions correspond to the representation $\Gamma_{15}$. The goal is now to use the introduced group theory to analyze the properties of the momentum matrix elements 2.17. The momentum operator $\mathbf{p}$ is given by a vector of three operators

$$\mathbf{p} = \begin{pmatrix} p_x \\ p_y \\ p_z \end{pmatrix},$$

obviously transforming like the elements of a vector. Therefore, the momentum operator forms an irreducible representation of $\Gamma_{15}$. The action of the momentum operator on wavefunctions of the irreducible representation $\Gamma_j$ leads to a new expression. The corresponding representation is given by the *direct product* $\Gamma_{15} \otimes \Gamma_j$ (see Yu and Cardona [47], p. 46), as one has $p_u$ acting on the basis function $\psi_v$ for $u = x, y, z$ and $v = 1, ..., N$. The direct product is not *irreducible*, but can be decomposed into a *direct sum* of irreducible representations

$$\Gamma_{15} \otimes \Gamma_j = \sum_u \oplus \Gamma_i. \tag{A.5}$$

Recall that functions not belonging to the same irreducible representation are orthogonal. Therefore, the matrix element $\langle \psi^{\Gamma_i} \mid \mathbf{p} \mid \psi^{\Gamma_j} \rangle$ between two wavefunctions belonging to the irreducible representation

| $\Gamma_i$ | Dimension | Basis functions |
|---|---|---|
| $\Gamma_1$ | 1 | $xyz$ |
| $\Gamma_2$ | 1 | $x^4\left(y^2-z^2\right)+y^4\left(z^2-x^2\right)+z^2\left(x^2-y^2\right)$ |
| $\Gamma_{12}$ | 2 | $\left(x^2-y^2\right),\ z^2-\frac{1}{2}\left(x^2+y^2\right)$ |
| $\Gamma_{15}$ | 3 | $x,\ y,\ z$ |
| $\Gamma_{25}$ | 3 | $x\left(y^2-z^2\right),\ y\left(z^2-x^2\right),\ z\left(x^2-y^2\right)$ |

Table 2: Basis functions of the tetrahedral symmetry group $T_d$.

| Direct product | Direct sum |
|---|---|
| $\Gamma_{15}\otimes\Gamma_1$ | $\Gamma_{15}$ |
| $\Gamma_{15}\otimes\Gamma_2$ | $\Gamma_{25}$ |
| $\Gamma_{15}\otimes\Gamma_{12}$ | $\Gamma_{15}\oplus\Gamma_{25}$ |
| $\Gamma_{15}\otimes\Gamma_{15}$ | $\Gamma_{15}\oplus\Gamma_{25}\oplus\Gamma_{12}\oplus\Gamma_1$ |
| $\Gamma_{15}\otimes\Gamma_{25}$ | $\Gamma_{15}\oplus\Gamma_{25}\oplus\Gamma_{12}\oplus\Gamma_2$ |

Table 3: Direct products of the $\Gamma_{15}$ representation with all representations of $T_d$ (after Yu and Cardona [47]).

$\Gamma_i$ and $\Gamma_j$ is nonzero only if the direct sum A.5 of the direct product $\Gamma_{15}\otimes\Gamma_j$ contains $\Gamma_i$. For the tetrahedral symmetry, the decomposition of the direct product into the direct sum is given in Table 3, from which the vanishing momentum matrix elements 2.17 can be calculated. They are given by the matrix in 4. Within the matrix, X denotes a non-vanishing and the 0 denotes a vanishing matrix element. In order to further reduce the number of unknowns, equivalent matrix elements can be determined using the basis functions defined in Table 2 and symmetry operations of G. As an example, for the $\Gamma_1$ type conduction band, the only non-vanishing momentum matrix elements involve - according to Table 4 - only bands belonging to $\Gamma_{15}$. $\Gamma_1$ is represented by the function $xyz$ and $\Gamma_{15}$ by $x, y$ and $z$. The only non-vanishing matrix element is of the type $\langle xyz \mid p_x \mid x\rangle$. For the other, e.g. $\langle xyz \mid p_x \mid z\rangle$, a rotation of the crystal by 180ř around the rotation axis [001] results in

$$\langle xyz \mid p_x \mid x\rangle = -\langle xyz \mid p_x \mid z\rangle ,$$

which can only be met if the matrix element is zero.

| $\mathbf{p}$ | $\left\vert\psi^{\Gamma_1}\right\rangle$ | $\left\vert\psi^{\Gamma_2}\right\rangle$ | $\left\vert\psi^{\Gamma_{12}}\right\rangle$ | $\left\vert\psi^{\Gamma_{15}}\right\rangle$ | $\left\vert\psi^{\Gamma_{25}}\right\rangle$ |
|---|---|---|---|---|---|
| $\left\langle\psi^{\Gamma_1}\right\vert$ | o | o | o | X | o |
| $\left\langle\psi^{\Gamma_2}\right\vert$ | o | o | o | o | X |
| $\left\langle\psi^{\Gamma_{12}}\right\vert$ | o | o | o | X | X |
| $\left\langle\psi^{\Gamma_{15}}\right\vert$ | X | o | X | X | X |
| $\left\langle\psi^{\Gamma_{25}}\right\vert$ | o | X | X | X | X |

Table 4: The non-vanishing momentum matrix elements between the states corresponding to different irreducible representations of the tetrahedral symmetry group. A zero denotes a vanishing and X a non-vanishing element.

# B

## TWO BAND MODEL NUMERICAL IMPLEMENTATION

The method used to solve the Hamiltonian equations in the two-band model is based on the shooting method formulated in 28 for the simple case of the conduction band.

As a starting point, we consider the general one-dimensional form of the Hamiltonian equation 2.76. In order to allow for a location dependent effective mass, we rewrite this equation as

$$\begin{pmatrix} \hat{H}_{hh} + V(z) & \hat{W} \\ \hat{W}^{\dagger} & \hat{H}_{lh} + V(z) \end{pmatrix} \begin{pmatrix} F_{hh} \\ F_{lh} \end{pmatrix} = E(\mathbf{k}) \begin{pmatrix} F_{hh} \\ F_{lh} \end{pmatrix}, \quad \text{(B.1)}$$

with

$$\hat{H}_{lh} = -\frac{\partial}{\partial z}\left(\gamma_1(z) + 2\gamma_2(z)\right)\frac{\partial}{\partial z} + \left(\gamma_1(z) - \gamma_2(z)\right)k_t^2, \quad \text{(B.2)}$$

$$\hat{H}_{hh} = -\frac{\partial}{\partial z}\left(\gamma_1(z) - 2\gamma_2(z)\right)\frac{\partial}{\partial z} + \left(\gamma_1(z) + \gamma_2(z)\right)k_t^2, \quad \text{(B.3)}$$

$$\hat{W} = \begin{cases} \sqrt{3}k_t\left(\gamma_2(z)k_t - 2\gamma_3(z)\frac{\partial}{\partial z}\right) & \text{for [100]} \\ \sqrt{3}k_t\left(\gamma_3(z)k_t - 2\gamma_3(z)\frac{\partial}{\partial z}\right) & \text{for [110]} \end{cases} \quad \text{(B.4)}$$

The potential $V(z)$ describes the valence band edge of the quantum well structure (in terms of hole energy), and $F_{hh}$ and $F_{lh}$ represent the hole wavefunction while under the effective mass and envelope function approximations.

We can rewrite the effective mass equations as

$$\begin{pmatrix} \hat{H}_{hh} + V(z) - E & \hat{W} \\ \hat{W}^{\dagger} & \hat{H}_{lh} + V(z) - E \end{pmatrix} \begin{pmatrix} F_{hh} \\ F_{lh} \end{pmatrix} = 0. \quad \text{(B.5)}$$

The problem now is to find a numerical method for the the solution of both the energy eigenvalues $E$ and the eigenfunctions $F$ for any $V(z)$. For this purpose, we can expand the first and second derivatives in terms of finite differences. The first derivative of a function $f(z)$ can be approximated to

$$\frac{df}{dz} \approx \frac{\Delta f}{\Delta z} = \frac{f(z+\delta z) - f(z-\delta z)}{2\delta z}. \quad \text{(B.6)}$$

The second derivative follows as

$$\begin{aligned} \frac{d^2f}{dz^2} &\approx \frac{\frac{df}{dz}\big|_{z+\delta z} - \frac{df}{dz}\big|_{z-\delta z}}{2\delta z} \\ &= \frac{f(z+2\delta z) - 2f(z) + f(z-2\delta z)}{(2\delta z)^2}. \end{aligned} \quad \text{(B.7)}$$

As $\delta z$ is an, as yet, undefined small step along the $z$-axis, and as it only appears in equation B.7with the factor 2, then we can simplify this expression by substituting $\delta z$ for $2\delta z$

$$\frac{d^2f}{dz^2} \approx \frac{f(z+\delta z) - 2f(z) + f(z-\delta z)}{(\delta z)^2}. \tag{B.8}$$

Let us focus on the term $\hat{H}^0_{lh} = -\frac{\partial}{\partial z}(\gamma_1 + 2\gamma_2)\frac{\partial}{\partial z}$ in the light hole Hamiltonian, and express it in terms of finite differences. We can rewrite this term as

$$\hat{H}^0_{lh} = -\frac{\partial}{\partial z}(\gamma_1(z) + \gamma_2(z))\frac{\partial F_{lh}}{\partial z} + (\gamma_1(z) + \gamma_2(z))\frac{\partial^2 F_{lh}}{\partial z^2}. \tag{B.9}$$

However, the shooting equations derived from this point by expanding the derivatives in terms of finite differences have led to significat computational inaccuracies in systems with a large discountinuous change in the effective mass (the Luttinger parameters), as occurs in the $GaAs/AlGaAs$ system. The source of the inaccuracies is thought to arise from the $\delta$-function nature of the effective mass derivative.

A more robust shceme can be derived by expanding $\hat{H}^0_{lh}$ starting from the left-hand derivative

$$\hat{H}^0_{lh} \approx \frac{(\gamma_1 + \gamma_2)\frac{\partial F_{lh}}{\partial z}\Big|_{z+\delta z} - (\gamma_1 + \gamma_2)\frac{\partial F_{lh}}{\partial z}\Big|_{z-\delta z}}{2\delta z}. \tag{B.10}$$

Recalling the centered finite difference expansion for the first derivative B.6, we can write the numenator of the above expression as

$$\begin{aligned} 2\delta z\hat{H}^0_{lh} &= (\gamma_1 + 2\gamma_2)|_{z+\delta z}\frac{F_{lh}(z+2\delta z) - F_{lh}(z)}{2\delta z} \\ &\quad (\gamma_1 + 2\gamma_2)|_{z-\delta z}\frac{F_{lh}(z) - F_{lh}(z-2\delta z)}{2\delta z}, \end{aligned} \tag{B.11}$$

or

$$\begin{aligned} (2\delta z)^2\hat{H}^0_{lh} &= (\gamma_1 + 2\gamma_2)|_{z+\delta z}\left[F_{lh}(z+2\delta z) - F_{lh}(z)\right] \\ &\quad (\gamma_1 + 2\gamma_2)|_{z-\delta z}\left[F_{lh}(z) - F_{lh}(z-2\delta z)\right]. \end{aligned} \tag{B.12}$$

Making the transformation $2\delta z \to \delta z$ then yields

$$\begin{aligned} \hat{H}^0_{lh} &= \frac{1}{(\delta z)^2}\left[(\gamma_1 - 2\gamma_2)^+ F_{lh}(z+\delta z)\right. \\ &\quad -\left((\gamma_1 - 2\gamma_2)^+ + (\gamma_1 - 2\gamma_2)^-\right)F_{lh}(z) \\ &\quad \left.+(\gamma_1 - 2\gamma_2)^- F_{lh}(z-\delta z)\right], \end{aligned} \tag{B.13}$$

with

$$(\gamma_1 + 2\gamma_2)^+ = (\gamma_1 + 2\gamma_2)|_{z+\delta z/2}, \tag{B.14}$$

$$(\gamma_1 + 2\gamma_2)^- = (\gamma_1 + 2\gamma_2)|_{z-\delta z/2}, \tag{B.15}$$

$$(\gamma_1 - 2\gamma_2)^+ = (\gamma_1 - 2\gamma_2)|_{z+\delta z/2}, \tag{B.16}$$

$$(\gamma_1 - 2\gamma_2)^- = (\gamma_1 - 2\gamma_2)|_{z-\delta z/2}. \tag{B.17}$$

We now substitute the finite difference expressions for $\partial/\partial z$, $\hat{H}^0_{lh}$ and a similar expression for the heavy-hole counterpart into the effective mass equations, and obtain

$$\begin{aligned}
0 &= -\frac{(\gamma_1-2\gamma_2)^+}{(\delta z)^2}F_{hh}(z+\delta z)+\frac{(\gamma_1-2\gamma_2)^++(\gamma_1-2\gamma_2)^-}{(\delta z)^2}F_{hh}(z)\\
&\quad -\frac{(\gamma_1-2\gamma_2)^-}{(\delta z)^2}F_{hh}(z-\delta z)+(\gamma_1+\gamma_2)k_t^2F_{hh}(z)\\
&\quad +(V(z)-E)\,F_{hh}(z)+\sqrt{3}\gamma_2k_t^2F_{lh}(z)-2\sqrt{3}\gamma_3k_t\frac{F_{lh}(z+\delta z)-F_{lh}(z-\delta z)}{2\delta z}, \qquad \text{(B.18)}\\
0 &= \sqrt{3}\gamma_2k_t^2F_{hh}(z)+2\sqrt{3}\gamma_3k_tk_t\frac{F_{hh}(z+\delta z)-F_{hh}(z-\delta z)}{2\delta z}\\
&\quad -\frac{(\gamma_1+2\gamma_2)^+}{(\delta z)^2}F_{lh}(z+\delta z)+\frac{(\gamma_1+2\gamma_2)^++(\gamma_1+2\gamma_2)^-}{(\delta z)^2}F_{lh}(z)\\
&\quad -\frac{(\gamma_1+2\gamma_2)^-}{(\delta z)^2}F_{lh}(z-\delta z)+(\gamma_1-\gamma_2)k_t^2F_{lh}(z)+(V(z)-E)\,F_{lh}(z). \qquad \text{(B.19)}
\end{aligned}$$

The Luttinger parameters $\gamma_i$ can be found at the intermediary points $z\pm\delta z/2$ by taking the mean of the two neighboring points $z$ and $z\pm\delta z$.

It can be seen that we draw up a set of finite difference equations if we map the potential $V(z)$ and the Luttinger parameters $\gamma_i$ to a grid along the $z$-axis. To solve these coupled equations and find the energies $E$ and functions $F$ we assume a equidistant grid $z_i$, with a grid step $\delta z$, we can substitute $z\to z_i$, $z-\delta z\to z_{i-1}$ and $z+\delta z\to z_{i+1}$. If we assume a given energy $E$, we are still left with 6 unknown parameters in the finite difference equations. However, we can rewrite these equations so that we are able to find $F_{lh}(z_{i+1})$ and $F_{hh}(z_{i+1})$ from their values at the two previous nodes, $z_{i-1}$ and $z_i$

$$\begin{aligned}
&F_{hh}(z_{i+1})\left[1+3\frac{\gamma_3^2}{(\gamma_1+2\gamma_2)^+(\gamma_1-2\gamma_2)^-}k_t^2(\delta z)^2\right]=\\
&F_{hh}(z_{i-1})\left[-\frac{(\gamma_1-2\gamma_2)^-}{(\gamma_1-2\gamma_2)^+}+3\frac{\gamma_3^2}{(\gamma_1+2\gamma_2)^+(\gamma_1-2\gamma_2)^+}k_t^2(\delta z)^2\right]\\
&+F_{lh}(z_{i-1})\left[\sqrt{3}\frac{\gamma_3}{(\gamma_1-2\gamma_2)^+}k_t\delta z\left(1+\frac{(\gamma_1+2\gamma_2)^-}{(\gamma_1+2\gamma_2)^+}\right)\right]\\
&F_{hh}(z_i)\left[\frac{(\gamma_1-2\gamma_2)^++(\gamma_1-2\gamma_2)^-}{(\gamma_1-2\gamma_2)^+}+\frac{\gamma_1+\gamma_2}{(\gamma_1-2\gamma_2)^+}k_t^2(\delta z)^2\right.\\
&\left.+\frac{V(z_i)-E}{(\gamma_1-2\gamma_2)^+}(\delta z)^2-3\frac{\gamma_3\gamma_2}{(\gamma_1+2\gamma_2)^+(\gamma_1-2\gamma_2)^+}k_t^3(\delta z)^3\right]\\
&+F_{lh}(z_i)\left[\sqrt{3}\frac{\gamma_2}{(\gamma_1-2\gamma_2)^+}k_t^2(\delta z)^2\right.\\
&-\sqrt{3}\frac{\gamma_3}{(\gamma_1-2\gamma_2)^+}\frac{(\gamma_1+2\gamma_2)^++(\gamma_1+2\gamma_2)^-}{(\gamma_1+2\gamma_2)^+}k_t\delta z\\
&-\sqrt{3}\frac{\gamma_3(\gamma_1-\gamma_2)}{(\gamma_1+2\gamma_2)^+(\gamma_1-2\gamma_2)^+}k_t^3(\delta z)^3\\
&\left.-\sqrt{3}\frac{\gamma_3}{(\gamma_1+2\gamma_2)^+(\gamma_1-2\gamma_2)^+}(V(z_i)-E)\,k_t(\delta z)^3\right], \qquad \text{(B.20)}
\end{aligned}$$

$$
\begin{aligned}
&F_{lh}(z_{i+1})\left[1+3\frac{\gamma_3^2}{(\gamma_1+2\gamma_2)^+(\gamma_1-2\gamma_2)^+}k_t^2(\delta z)^2\right]=\\
&F_{lh}(z_{i-1})\left[-\frac{(\gamma_1+2\gamma_2)^-}{(\gamma_1+2\gamma_2)^+}+3\frac{\gamma_3^2}{(\gamma_1+2\gamma_2)^+(\gamma_1-2\gamma_2)^+}k_t^2(\delta z)^2\right]\\
&+F_{hh}(z_{i-1})\left[\sqrt{3}\frac{\gamma_3}{(\gamma_1+2\gamma_2)^+}k_t\delta z\left(1+\frac{(\gamma_1-2\gamma_2)^-}{(\gamma_1-2\gamma_2)^+}\right)\right]\\
&F_{lh}(z_i)\left[\frac{(\gamma_1+2\gamma_2)^++(\gamma_1+2\gamma_2)^-}{(\gamma_1+2\gamma_2)^+}+\frac{\gamma_1-\gamma_2}{(\gamma_1+2\gamma_2)^+}k_t^2(\delta z)^2\right.\\
&+\frac{V(z_i)-E}{(\gamma_1+2\gamma_2)^+}(\delta z)^2+3\frac{\gamma_3\gamma_2}{(\gamma_1+2\gamma_2)^+(\gamma_1-2\gamma_2)^+}k_t^3(\delta z)^3\Big]\\
&+F_{hh}(z_i)\left[\sqrt{3}\frac{\gamma_2}{(\gamma_1+2\gamma_2)^+}k_t^2(\delta z)^2\right.\\
&+\sqrt{3}\frac{\gamma_3}{(\gamma_1+2\gamma_2)^+}\frac{(\gamma_1-2\gamma_2)^++(\gamma_1-2\gamma_2)^-}{(\gamma_1-2\gamma_2)^+}k_t\delta z\\
&+\sqrt{3}\frac{\gamma_3(\gamma_1+\gamma_2)}{(\gamma_1+2\gamma_2)^+(\gamma_1-2\gamma_2)^+}k_t^3(\delta z)^3\\
&\qquad\left.+\sqrt{3}\frac{\gamma_3}{(\gamma_1+2\gamma_2)^+(\gamma_1-2\gamma_2)^+}(V(z_i)-E)\,k_t(\delta z)^3\right]. \qquad \text{(B.21)}
\end{aligned}
$$

These equations imply that, if the wavefunctions are known at the two points $z-\delta z$ and $z$, then the value at $z+\delta z$ can be determined for any energy $E$. This iterative equation forms the bais of a standard method of solving equations numerically, and is known as the *shooting method*.

The equations can be rewritten in a matrix notation, which allows easy programical implementation. Using a coefficient notation for these two equations of the form

$$
\begin{aligned}
F_{hh}(z_{i+1}) &= a_1F_{hh}(z_{i-1})+a_2F_{lh}(z_{i-1})+a_3F_{lh}(z_i)+a_4F_{hh}(z_i), &\text{(B.22)}\\
F_{lh}(z_{i+1}) &= b_1F_{hh}(z_{i-1})+b_2F_{lh}(z_{i-1})+b_3F_{hh}(z_i)+b_4F_{lh}(z_i), &\text{(B.23)}
\end{aligned}
$$

the effective mass equations can be written in a recursive transfer matrix expression

$$
\begin{pmatrix} 0 & 0 & 1 & 0\\ 0 & 0 & 0 & 1\\ a_1 & a_2 & a_3 & a_4\\ b_1 & b_2 & b_3 & b_4 \end{pmatrix}
\begin{pmatrix} F_{hh}(z_{i-1})\\ F_{lh}(z_{i-1})\\ F_{hh}(z_i)\\ F_{lh}(z_i) \end{pmatrix}=
\begin{pmatrix} F_{hh}(z_i)\\ F_{lh}(z_i)\\ F_{hh}(z_{i+1})\\ F_{lh}(z_{i+1}) \end{pmatrix}. \qquad \text{(B.24)}
$$

Provided that we have intial values for the wave functions at the first and second nodes, we can determine the wavefunction values at any node by an iterative procedure. By multiplying matrices, it is possible to obtain an expression for the wavefunction values at any node (as a function of the intial values)

$$
\begin{pmatrix} F_{hh}(z_n)\\ F_{lh}(z_n)\\ F_{hh}(z_{n+1})\\ F_{lh}(z_{n+1}) \end{pmatrix}=\mathbf{M}_{n+1}\mathbf{M}_n\mathbf{M}_{n-1}\cdots\mathbf{M}_3\mathbf{M}_2
\begin{pmatrix} F_{hh}(z_0)\\ F_{lh}(z_0)\\ F_{hh}(z_1)\\ F_{lh}(z_1) \end{pmatrix}. \qquad \text{(B.25)}
$$

The questions that remain are what is the suitable choise for these initial values, and how to determine whether an energy is an eigenenergy of the system.

Using four known values of the wavefunction components at $z$ and $z+\delta z$, a fifth and sixth values can be predicted. Using the new point togather with the known wavefunction components at $z$, we can subsequently find the wavefunctions at $z+2\delta z$, and so on. Hence the complete wave function solution can be found for any particular energy. The solutions for steady states have wavefunctions that satisfy the standard boundary conditions

$$F \to 0 \text{ and } \frac{\partial}{\partial z}F \to 0, \text{ as } z \to \pm\infty. \tag{B.26}$$

As argued in Harrison [28], in the one-band case of the conduction band only two initial values are required, and the suitable choise is 0 for the first node, and 1 for the second. The 1 can be any arbitrary number, as changing it will only scale the wavefunction (the finite difference equations are linear) and this does not affect the eigenenergy. The valence band case is a bit more complicated, as now there are two coupled wavefunction components, and one cannot be scaled independently from the other. Therefore, we choose the initial values to be 0 and 1 for one subband, and 0 and $c$ for the other. Here $c$ is a parameter, which is to be determined when the equations are solved.

The energy is varied systematically until both wavefunction components switch from diverging to $\pm\infty$ to $\mp\infty$, satisfying the boundary conditions. However, an additional problem araises from the parameter $c$ defined above. On top of that, in many cases one of the wavefunction components exhibit a very sharp sign switching, often twice within a single energy search step. In order to work around these problems, we minimize the amplitude of the wavefunction at the end of the grid. The function to be minimized can be found by generating the transfer matrix which propagates the wavefunction from the first two nodes to the last two nodes

$$\begin{pmatrix} F_{hh}(z_{N-1}) \\ F_{lh}(z_{N-1}) \\ F_{hh}(z_N) \\ F_{lh}(z_N) \end{pmatrix} = \begin{pmatrix} m_{11} & m_{12} & m_{13} & m_{14} \\ m_{21} & m_{22} & m_{23} & m_{24} \\ m_{31} & m_{32} & m_{33} & m_{34} \\ m_{41} & m_{42} & m_{43} & m_{44} \end{pmatrix} \begin{pmatrix} 0 \\ 0 \\ 1 \\ c \end{pmatrix}. \tag{B.27}$$

Minimizing the wavefunction amplitude at the final node leads to

$$(m_{33} + m_{34}c)^2 + (m_{43} + m_{44}c)^2 \to c_{min}, \tag{B.28}$$

and then the minimum of $c_{min}(E)$ is searched to obtain the energy. A solution of the Hamiltonian equations is found when this minimum wavefunction amlitude is smaller than a certain threshold value. This guarantees a converging wavefunction, which can be found by substituting $c_{min}$ into B.25.

Note that the wavefunctions obtained in this procedure are not properly normalized and should be transformed into

$$\begin{pmatrix} F_{hh}(z) \\ F_{lh}(z) \end{pmatrix} \to \begin{pmatrix} F_{hh}(z) \\ F_{lh}(z) \end{pmatrix} \frac{1}{\sqrt{\int \left(F_{hh}^2(z) + F_{lh}^2(z)\right) dz}} \tag{B.29}$$

# C

# SELF-CONSISTENT SOLUTION OF SCHRÖDINGER -POISSON MODEL

For a quantitative discussion of carriers that are strongly confined to a small area, it is necessary to consider not only the band-edge and external potential, but also the carrier-carrier electrostatic potential. We start by considering the Schrödinger equation in the slowly varying envelope approximation in one dimension

$$\frac{\hbar^2}{2}\frac{d}{dz}\left(\frac{1}{m^*(z)}\frac{d}{dz}\right)\varphi(z) + V(z)\varphi(z) = E\varphi(z) \tag{C.1}$$

where $V(z)$ is the overall potential and $\varphi(z)$ is the slowly varying envelope. The Poisson equation 2.89 can be formulated as

$$\frac{d}{dz}\left(\epsilon(z)\frac{d}{dz}\right)V_\rho(z) = -e[N_D^+(z) - n(z) - N_A^-(z) + p(z)], \tag{C.2}$$

where $\epsilon(z)$ is the position dependent dielectric constant, $V_\rho(z)$ is the electrostatic potential and $e$ denotes the elementary charge. N. $N_D^+(z)$ represents the ionized donor distribution and $n(z)$ is the electron distribution. For now, we only consider the conduction-band, so we set $N_A^-(z) = p(z) = 0$.

The first coupling term between these two equations is the overall potential

$$V(z) = V_{CB}(z) - eV_\rho(z) \tag{C.3}$$

where $V_{CB}(z)$ represents the conduction-band profile given by the material composition. The second coupling term is the electron concentration $n(z)$, which is calculated from the envelope fucntion $\varphi$and the Fermi level $E_F$

$$n(z) = \frac{m^*(z)k_BT}{\pi\mathcal{L}\hbar^2}\sum_{\mathbf{k}}|\varphi_{\mathbf{k}}(z)|^2 \ln\left(1 + e^{\frac{E_F - E_{\mathbf{k}}}{k_BT}}\right), \tag{C.4}$$

where $k_B$ is the Boltzmann constant, $T$ is the temperature, $\mathcal{L}$ is the length of the heterostructure and $E$ is the eigenenergy. The summation over $\mathbf{k}$ represents the summation over all eigenstates (including spin). As a consequence, we have to solve for a given heterostructure with given donor concentration C.1 and C.2 self-consistently. We restrict ourselves to model only the mesoscopic part and not the whole device, so we have to define appropriate boundary conditions for the envelope function and the electrostatic potential. The boundary conditions for the envelope function are given by B.26, whereas we set the electrostatic potential $V_\rho$ to zero at the boundaries Chuang [19], which is equivalent to assume the device in equilibrium.

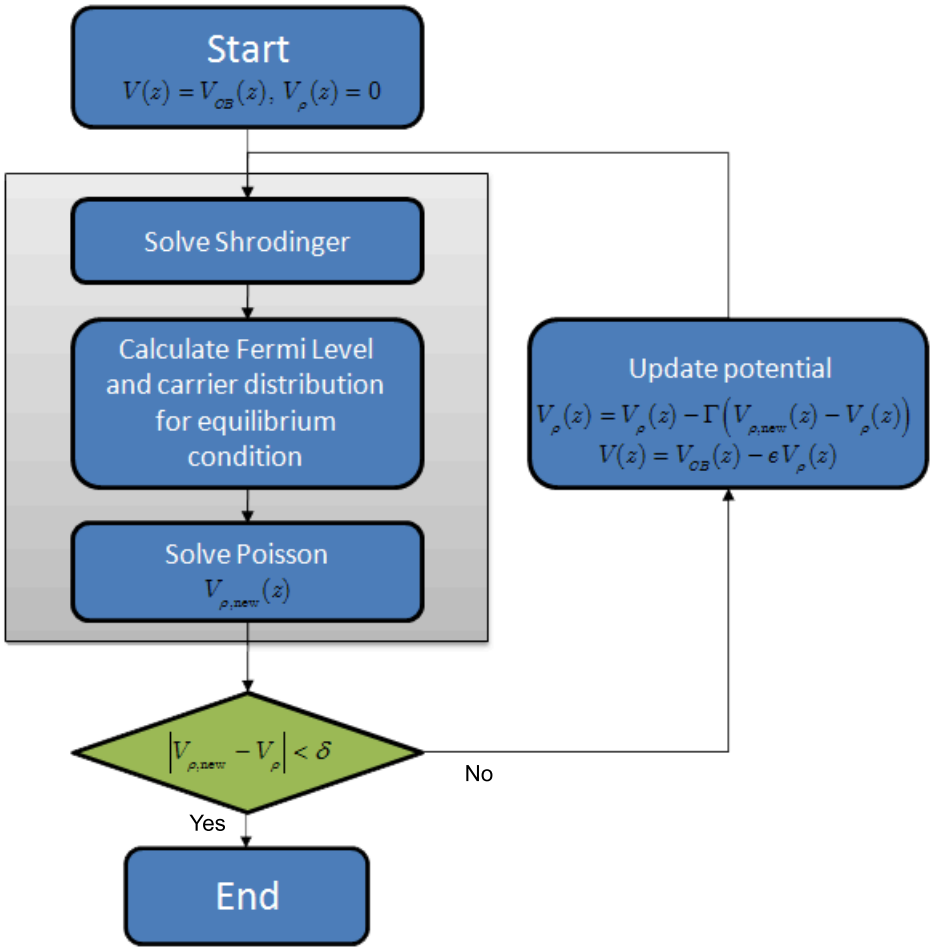


Figure 23: Program flow for self-consistent solution of Schrödinger -Poisson under equilibrium condition with given donator concentration.

To solve C.1 and C.2 numerically, we apply the shooting method from Appendix B to the Schrödinger equation and to the Poisson equation a finite-difference scheme, which reads

$$\begin{aligned} 0 &= \frac{1}{2\,(\delta z)^2}\left((\epsilon_i + \epsilon_{i-1})V_{\rho,i-1} - (\epsilon_{i-1} + 2\epsilon_i + \epsilon_{i+1})V_{\rho,i} + (\epsilon_i + \epsilon_{i+1})V_{\rho,i+1}\right) \\ &\quad + e(N^+_{D,i} - n_i), \end{aligned} \tag{C.5}$$

where $\delta z$ is the spatial discretization. Equilibrium conditions require us to choose the Fermi level appropriate to allow that

$$\int_{-\infty}^{\infty} N_D^+(z)\,dz = \int_{-\infty}^{\infty} n(z)\,dz. \tag{C.6}$$

To ensure this equilibrium condition, we solve C.4 with the constraint C.6 to obtain the Fermi level $E_F$ .

Figure 23 shows the program flow to obtain the self-consistent solution of the Schrödinger -Poisson system under equilibrium condition. First, Schrödinger 's equation is solved assuming an initial potential $V(z) = V_{CB}(z)$, $V_\rho(z) = 0$. Next, the Fermi level $E_F$ and the carrier distribution $n(z)$ are obtained by solving C.4 with respect to C.6. Then, the Poisson equation is solved resulting in a new electrostatic potential $V_{\rho,new}(z)$. If $|V_{\rho,new}(z) - V_\rho(z)|$ is smaller than a pre-defined value d,

we obtain the converged solution. Otherwise, the electrostatic potential is updated $V_\rho(z)(z) = V_\rho(z) + G(V_{\rho,new}(z) - V_\rho(z))$, where $0 < G < 1$ is a damping parameter used to improve convergence.

# BIBLIOGRAPHY


[1] M. Altarelli. Electronic structure and semiconductor-semimetal transition in InAs-GaSb superlattices. *Physical Review B*, 28 (2):842, July 1983. doi: 10.1103/PhysRevB.28.842. URL http://link.aps.org/doi/10.1103/PhysRevB.28.842. Copyright (C) 2010 The American Physical Society; Please report any problems to prola@aps.org. (Cited on page 12.)

[2] L. C. Andreani, A. Pasquarello, and F. Bassani. Hole subbands in strained GaAs-Ga1-xAlxAs quantum wells: Exact solution of the effective-mass equation. *Physical Review B*, 36(11):5887, October 1987. doi: 10.1103/PhysRevB.36.5887. URL http://link.aps.org/doi/10.1103/PhysRevB.36.5887. Copyright (C) 2010 The American Physical Society; Please report any problems to prola@aps.org. (Cited on page 21.)

[3] G. Bastard. Superlattice band structure in the envelope-function approximation. *Physical Review B*, 24(10):5693, November 1981. doi: 10.1103/PhysRevB.24.5693. URL http://link.aps.org/doi/10.1103/PhysRevB.24.5693. Copyright (C) 2010 The American Physical Society; Please report any problems to prola@aps.org. (Cited on page 12.)

[4] G. Bastard. Theoretical investigations of superlattice band structure in the envelope-function approximation. *Physical Review B*, 25 (12):7584, June 1982. doi: 10.1103/PhysRevB.25.7584. URL http://link.aps.org/doi/10.1103/PhysRevB.25.7584. Copyright (C) 2010 The American Physical Society; Please report any problems to prola@aps.org. (Cited on page 12.)

[5] D. J. BenDaniel and C. B. Duke. Space-Charge effects on electron tunneling. *Physical Review*, 152(2):683, December 1966. doi: 10.1103/PhysRev.152.683. URL http://link.aps.org/doi/10.1103/PhysRev.152.683. Copyright (C) 2010 The American Physical Society; Please report any problems to prola@aps.org. (Cited on page 12.)

[6] R. Binder and S. W. Koch. Nonequilibrium semiconductor dynamics. *Progress in Quantum Electronics*, 19(4-5):307–462, 1995. ISSN 0079-6727. doi: 10.1016/0079-6727(95)00001-S. URL http://www.sciencedirect.com/science/article/B6TJD-3YB518G-1/2/20e5c9ce4d3726ceaa95c0943f28056f. (Cited on page 56.)

[7] G. L. Bir, G. E. Pikus, P. Shelnitz, and D. Louvish. *Symmetry and strain-induced effects in semiconductors*. Israel Program for Scientific Translations, 1976. ISBN 0706513673, 9780706513677. (Cited on page 9.)

[8] M. Born and E. Wolf. *Principles of Optics: Electromagnetic Theory of Propagation, Interference and Diffraction of Light*. Cambridge University Press, 7th edition, 2002. (Cited on page 59.)

[9] D. A. Broido and L. J. Sham. Effective masses of holes at GaAs-AlGaAs heterojunctions. *Physical Review B*, 31(2):888, 1985. doi: 10.1103/PhysRevB.31.888. URL http://link.aps.org/doi/10.1103/PhysRevB.31.888. Copyright (C) 2010 The American Physical Society; Please report any problems to prola@aps.org. (Cited on page 21.)

[10] M. G. Burt. A new effective-mass equation for microstructures. *Semiconductor Science and Technology*, 3(12):1224–1226, 1988. (Cited on page 13.)

[11] M. G. Burt. The justification for applying the effective-mass approximation to microstructures. *Journal of Physics: Condensed Matter*, 4 (32):6651–6690, 1992. (Cited on page 13.)

[12] M. G. Burt. The evaluation of the matrix element for interband optical transitions in quantum wells using envelope functions. *Journal of Physics: Condensed Matter*, 5(24):4091, 1993. (Cited on page 47.)

[13] M. G. Burt. Direct derivation of effective-mass equations for microstructures with atomically abrupt boundaries. *Physical Review B*, 50(11):7518, 1994. doi: 10.1103/PhysRevB.50.7518. URL http://link.aps.org/doi/10.1103/PhysRevB.50.7518. Copyright (C) 2010 The American Physical Society; Please report any problems to prola@aps.org. (Cited on page 13.)

[14] M. G. Burt. Breakdown of the atomic dipole approximation for the quantum well interband dipole matrix element. *Semiconductor Science and Technology*, 10(4):412, 1995. (Cited on page 47.)

[15] M. G. Burt. Fundamentals of envelope function theory for electronic states and photonic modes in nanostructures. *Journal of Physics: Condensed Matter*, 11(9):R53–R83, 1999. (Cited on page 13.)

[16] W. W. Chow and S. W. Koch. *Semiconductor-Laser Physics*. Springer Verlag, 1994. (Cited on page 56.)

[17] W. W. Chow and S. W. Koch. *Semiconductor-Laser Fundamentals*. Springer, 1999. (Cited on pages 33, 44, 49, 53, and 56.)

[18] S. L. Chuang. Efficient band-structure calculations of strained quantum wells. *Physical Review B*, 43(12):9649, April 1991. doi: 10.1103/PhysRevB.43.9649. URL http://link.aps.org/doi/10.1103/PhysRevB.43.9649. Copyright (C) 2010 The American Physical Society; Please report any problems to prola@aps.org. (Cited on page 12.)

[19] S. L. Chuang. *Physics of Optoelectronic Devices*. Wiley-Interscience, 1995. (Cited on pages 8, 12, 20, 21, 33, 49, and 81.)

[20] G. Dresselhaus. Spin-Orbit coupling effects in zinc blende structures. *Physical Review*, 100(2):580, October 1955. doi: 10.1103/PhysRev.100.580. URL http://link.aps.org/doi/10.1103/PhysRev.100.580. Copyright (C) 2010 The American Physical Society; Please report any problems to prola@aps.org. (Cited on page 14.)

[21] H. Ehrenreich and M. H. Cohen. Self-Consistent field approach to the Many-Electron problem. *Physical Review*, 115(4):786, 1959. doi: 10.1103/PhysRev.115.786. URL http://link.aps.org/doi/10.1103/PhysRev.115.786. (Cited on page 56.)

[22] P. Enders, A. Borwolff, M. Woerner, and D. Suisky. kÂ·p theory of energy bands, wave functions, and optical selection rules in strained tetrahedral semiconductors. *Physical Review B*, 51(23): 16695, June 1995. doi: 10.1103/PhysRevB.51.16695. URL http://link.aps.org/doi/10.1103/PhysRevB.51.16695. Copyright (C) 2010 The American Physical Society; Please report any problems to prola@aps.org. (Cited on pages 18 and 48.)

[23] R. Eppenga, M. F. H. Schuurmans, and S. Colak. New kÂ·p theory for GaAs/Ga1-xA1xAs-type quantum wells. *Physical Review B*, 36 (3):1554, July 1987. doi: 10.1103/PhysRevB.36.1554. URL http://link.aps.org/doi/10.1103/PhysRevB.36.1554. Copyright (C) 2010 The American Physical Society; Please report any problems to prola@aps.org. (Cited on page 12.)

[24] B. A. Foreman. Effective-mass hamiltonian and boundary conditions for the valence bands of semiconductor microstructures. *Physical Review B*, 48(7):4964, 1993. doi: 10.1103/PhysRevB.48.4964. URL http://link.aps.org/doi/10.1103/PhysRevB.48.4964. Copyright (C) 2010 The American Physical Society; Please report any problems to prola@aps.org. (Cited on pages 13 and 15.)

[25] B. A. Foreman. Exact effective-mass theory for heterostructures. *Physical Review B*, 52(16):12241, October 1995. doi: 10.1103/PhysRevB.52.12241. URL http://link.aps.org/doi/10.1103/PhysRevB.52.12241. Copyright (C) 2010 The American Physical Society; Please report any problems to prola@aps.org. (Cited on pages 13, 14, and 15.)

[26] B. A. Foreman. Analytical Envelope-Function theory of interface band mixing. *Physical Review Letters*, 81(2):425, July 1998. doi: 10.1103/PhysRevLett.81.425. URL http://link.aps.org/doi/10.1103/PhysRevLett.81.425. Copyright (C) 2010 The American Physical Society; Please report any problems to prola@aps.org. (Cited on page 13.)

[27] J. Hader, J. V. Moloney, and S. W. Koch. Microscopic theory of gain, absorbtion, and refractive index in semiconductor laser Materials-Influence of Conduction-Band nonparabolicity and Coulomb-Induced intersubband coupling. *IEEE Journal of Quantum Electronics*, 35:1878–1886, 1999. (Cited on page 51.)

[28] P. Harrison. *Quantum Wells, Wires and Dots Theoretical and Computational Physics*. John Wiley & Sons Canada, Ltd., 2000. (Cited on pages x, 27, 75, and 79.)

[29] H. Haug and S. W. Koch. *Quantum Theory of the Optical and Electronic Properties of Semiconductors*. World Scientific, 4 edition, 1994. (Cited on pages 33, 49, and 56.)

[30] J. D. Jackson. *Classical Electrodynamics*. John Wiley and Sons, Inc., 3rd edition, 1998. (Cited on pages 5, 6, 27, 33, and 49.)

[31] E. O. Kane. Band structure of indium antimonide. *Journal of Physics and Chemistry of Solids*, 1(4):249–261, 1957. ISSN 0022-3697. doi: 10.1016/0022-3697(57)90013-6. URL http://www.sciencedirect.com/science/article/B6TXR-46MF59X-8N/2/bef159baa98d883244251c3b38c88fbd. (Cited on page 9.)

[32] E. O. Kane. *Handbook on semiconductors*, volume 1. W.Paul, 1982. (Cited on pages 8, 13, and 18.)

[33] M. Kira, F. Jahnke, W. Hoyer, and S. W. Koch. Quantum theory of spontaneous emission and coherent effects in semiconductor microstructures. *Progress in Quantum Electronics*, 23(6):189–279, November 1999. ISSN 0079-6727. doi: 10.1016/S0079-6727(99)00008-7. URL http://www.sciencedirect.com/science/article/B6TJD-3YF44VC-1/2/871827e2264fddc1b8f01ca83ab0b786. (Cited on page 33.)

[34] S. W. Koch. Semiconductor laser theory with many-body effects. *Physical Review A*, 39:1887–1898, 1989. (Cited on page 53.)

[35] O. Krebs and P. Voisin. Krebs and voisin reply:. *Physical Review Letters*, 82(6):1340, February 1999. doi: 10.1103/PhysRevLett.82.1340. URL http://link.aps.org/doi/10.1103/PhysRevLett.82.1340. Copyright (C) 2010 The American Physical Society; Please report any problems to prola@aps.org. (Cited on page 13.)

[36] P. Lowdin. A note on the Quantum-Mechanical perturbation theory. *The Journal of Chemical Physics*, 19(11):1396–1401, November 1951. doi: 10.1063/1.1748067. URL http://link.aip.org/link/?JCP/19/1396/1. (Cited on page 9.)

[37] J. M. Luttinger. Quantum theory of cyclotron resonance in semiconductors: General theory. *Physical Review*, 102(4):1030, May 1956. doi: 10.1103/PhysRev.102.1030. URL http://link.aps.org/doi/10.1103/PhysRev.102.1030. Copyright (C) 2010 The American Physical Society; Please report any problems to prola@aps.org. (Cited on pages 19 and 20.)

[38] J. M. Luttinger and W. Kohn. Motion of electrons and holes in perturbed periodic fields. *Physical Review*, 97(4):869, February 1955. doi: 10.1103/PhysRev.97.869. URL http://link.aps.org/doi/10.1103/PhysRev.97.869. Copyright (C) 2010 The American Physical Society; Please report any problems to prola@aps.org. (Cited on pages 9 and 20.)

[39] G. D. Mahan. *Many-Particle Physics*. New York, Plenum, 1997. (Cited on page 56.)

[40] P. C. Martin and J. Schwinger. Theory of Many-Particle systems. i. *Physical Review*, 115(6):1342, 1959. doi: 10.1103/PhysRev.115.1342. URL http://link.aps.org/doi/10.1103/PhysRev.115.1342. Copyright (C) 2010 The American Physical Society; Please report any problems to prola@aps.org. (Cited on page 45.)

[41] R. A. Morrow and K. R. Brownstein. Model effective-mass hamiltonians for abrupt heterojunctions and the associated wave-function-matching conditions. *Physical Review B*, 30(2):678, July

1984. doi: 10.1103/PhysRevB.30.678. URL http://link.aps.org/doi/10.1103/PhysRevB.30.678. Copyright (C) 2010 The American Physical Society; Please report any problems to prola@aps.org. (Cited on page 12.)

[42] J. Piprek. *Semiconductor Optoelectronic Devices: Introduction to Physics and Simulation*. Academic Press, 2003. ISBN 0125571909. (Cited on pages ix and 7.)

[43] G. B. Ren, Y. M. Liu, and P. Blood. Valence-band structure of wurtzite GaN including the spin-orbit interaction. *Applied Physics Letters*, 74(8):1117, 1999. ISSN 00036951. doi: 10.1063/1.123461. URL http://adsabs.harvard.edu/abs/1999ApPhL..74.1117R. (Cited on page 14.)

[44] A. V. Rodina and A. Y. Alekseev. Least-action principle for envelope functions in abrupt heterostructures. *Physical Review B*, 73 (11):115312, March 2006. doi: 10.1103/PhysRevB.73.115312. URL http://link.aps.org/doi/10.1103/PhysRevB.73.115312. Copyright (C) 2010 The American Physical Society; Please report any problems to prola@aps.org. (Cited on page 13.)

[45] M. S. Skolnick, T. A. Fisher, and D. M. Whittaker. Strong coupling phenomena in quantum microcavity structures. *Semicond. Sci. Technol.*, 13:645–669, 1998. URL http://iopscience.iop.org/0268-1242/13/7/003/pdf/0268-1242_13_7_003.pdf. (Cited on page 68.)

[46] R. G. Veprek, S. Steiger, and B. Witzigmann. Ellipticity and the spurious solution problem of kbullp envelope equations. *Physical Review B*, 76(16):165320, October 2007. doi: 10.1103/PhysRevB.76.165320. URL http://link.aps.org/doi/10.1103/PhysRevB.76.165320. Copyright (C) 2010 The American Physical Society; Please report any problems to prola@aps.org. (Cited on page 13.)

[47] P. Y. Yu and M. Cardona. *Fundamentals of Semiconductors: Physics and Materials Properties*. Springer-Verlag Telos, 2nd edition, May 1999. ISBN 354065352X. (Cited on pages xi, 6, 7, 8, 9, 14, 72, and 73.)

[48] P. S. Zory, P. F. Liao, and P. Kelley. *Quantum Well Lasers*. Academic Press, April 1993. ISBN 0127818901. (Cited on pages ix, 23, and 24.)